

# Solar fusion cross sections II: the pp chain and CNO cycles

E. G. Adelberger, A. García, R. G. Hamish Robertson, and K. A. Snover

*Department of Physics and Center for Experimental Nuclear Physics and Astrophysics,  
University of Washington, Seattle, WA 98195 USA*

A. B. Balantekin, K. Heeger, and M. J. Ramsey-Musolf

*Department of Physics, University of Wisconsin, Madison, WI 53706 USA*

D. Bemmerer and A. Junghans

*Forschungszentrum Dresden-Rossendorf, D-01314 Dresden, Germany*

C. A. Bertulani

*Department of Physics and Astronomy, Texas A&M University, Commerce, TX 75429 USA*

J.-W. Chen

*Department of Physics and Center for Theoretical Sciences, National Taiwan University, Taipei 10617, Taiwan*

H. Costantini and P. Prati

*Università di Genova and INFN Sezione di Genova, Genova, Italy*

M. Couder, E. Uberseder, and M. Wiescher

*Department of Physics and JINA, University of Notre Dame, Notre Dame, IN 46556 USA*

R. Cyburt

*JINA and National Superconducting Cyclotron Laboratory, Michigan State University, East Lansing, MI 48824 USA*

B. Davids

*TRIUMF, 4004 Wesbrook Mall, Vancouver, BC, Canada V6T 2A3*

S. J. Freedman

*Department of Physics, University of California, Berkeley, and  
Lawrence Berkeley National Laboratory, Berkeley, CA 94720 USA*

M. Gai

*Laboratory for Nuclear Sciences at Avery Point, University of Connecticut, CT 06340-6097 and  
Department of Physics, Yale University, New Haven, CT 06520-8124 USA*

D. Gazit

*Institute for Nuclear Theory, University of Washington, Seattle, WA 98195 USA and  
Racah Institute of Physics, The Hebrew University, Jerusalem, 91904, Israel*

L. Gialanella and G. Imbriani

*Dipartimento di Scienze Fisiche, Università di Napoli, and INFN Sezione di Napoli, Napoli, Italy*

U. Greife

*Department of Physics, Colorado School of Mines, Golden, CO 80401 USA*

M. Hass

*Department of Particle Physics and Astrophysics, The Weizmann Institute, Rehovot, Israel*

W. C. Haxton

*Department of Physics, University of California, Berkeley, and Lawrence Berkeley National Laboratory,  
Berkeley, CA 94720 and Institute for Nuclear Theory, University of Washington, Seattle, WA 98195 USA*

T. Itahashi

*Research Center for Nuclear Physics, Osaka University, Ibaraki, Osaka 567-0047 Japan*

K. Kubodera

*Department of Physics and Astronomy, University of South Carolina, Columbia, SC 29208 USA*

K. Langanke

*GSI Helmholtzzentrum für Schwerionenforschung, D-64291 Darmstadt, Germany, Institut für Kernphysik, Universität Darmstadt, Germany and Frankfurt Institute for Advanced Studies, Frankfurt, Germany*

D. Leitner, M. Leitner, P. Vetter, and L. Winslow

*Lawrence Berkeley National Laboratory, Berkeley, CA 94720 USA*

L. E. Marcucci

*Department of Physics "E. Fermi", University of Pisa, and INFN Sezione di Pisa, Largo B. Pontecorvo 3, I-56127, Pisa, Italy*

T. Motobayashi

*The Institute of Physical and Chemical Research (RIKEN), 2-1 Hirosawa, Wako, Saitama 351-0198, Japan*

A. Mukhamedzhanov and R. E. Tribble

*Cyclotron Institute, Texas A&M University, College Station, TX 77843 USA*

Kenneth M. Nollett

*Physics Division, Argonne National Laboratory, 9700 S. Cass Ave., Argonne, IL 60439 USA*

F. M. Nunes

*National Superconducting Cyclotron Laboratory and Department of Physics and Astronomy, Michigan State University, East Lansing, MI 48824 USA*

T.-S. Park

*Department of Physics and BAERI, Sungkyunkwan University, Suwon 440-746 Korea*

P. D. Parker

*Wright Nuclear Structure Laboratory, Yale University, New Haven, CT 06520 USA*

R. Schiavilla

*Department of Physics, Old Dominion University, Norfolk, VA 23529 and Jefferson Laboratory, Newport News, VA 23606 USA*

E. C. Simpson

*Department of Physics, University of Surrey, Guildford, Surrey GU2 7XH, United Kingdom*

C. Spitaleri

*INFN Laboratori Nazionali del Sud & DMFCI, Università di Catania, Catania, Italy*

F. Strieder and H.-P. Trautvetter

*Institut für Experimentalphysik III, Ruhr-Universität Bochum, Bochum, Germany*

K. Suemmerer

*GSI Helmholtzzentrum für Schwerionenforschung GmbH, Planckstraße 1, D-64291 Darmstadt, Germany*

S. Typel

*Excellence Cluster Universe, Technische Universität München, Boltzmannstraße 2, D-85748 Garching and GSI Helmholtzzentrum für Schwerionenforschung GmbH, Planckstraße 1, D-64291 Darmstadt, Germany*

We summarize and critically evaluate the available data on nuclear fusion cross sections important to energy generation in the Sun and other hydrogen-burning stars and to solar neutrino production. Recommended values and uncertainties are provided for key cross sections, and a recommended spectrum is given for  $^8\text{B}$  solar neutrinos. We also discuss opportunities for further increasing the precision of key rates, including new facilities, new experimental techniques, and improvements in theory. This review, which summarizes the conclusions of a workshop held at the Institute

for Nuclear Theory, Seattle, in January 2009, is intended as a 10-year update and supplement to Reviews of Modern Physics **70** (1998) 1265.

## Contents

<b>I. INTRODUCTION</b>	3	3. Transition to the ground state and 6.79 MeV in $^{15}\text{O}$	36
A. Solar Fusion II: the 2009/10 effort	4	4. Transition to the 6.17 MeV state	38
B. Contents of this review	5	5. Total $S_{14}(0)$ and conclusions	39
<b>II. NUCLEAR REACTIONS IN HYDROGEN-BURNING STARS</b>	6	B. Other CNO-cycle reactions	40
A. Rates and S-factors	7	1. $^{12}\text{C}(p,\gamma)^{13}\text{N}$	40
B. Screening of stellar and laboratory reactions	9	2. $^{15}\text{N}(p,\alpha)^{12}\text{C}$	40
C. Fitting and extrapolating S-factors	10	3. $^{15}\text{N}(p,\gamma)^{16}\text{O}$	41
1. Theory constraints: model-based methods	11	4. $^{16}\text{O}(p,\gamma)^{17}\text{F}$	42
2. Theory constraints: <i>ab initio</i> methods	12	5. $^{17}\text{O}(p,\alpha)^{14}\text{N}$	42
3. Adopted procedures	13	6. $^{17}\text{O}(p,\gamma)^{18}\text{F}$	42
D. Treatment of uncertainties	14	7. $^{18}\text{O}(p,\alpha)^{15}\text{N}$	42
<b>III. THE <math>pp</math> REACTION</b>	14	<b>XII. INDIRECT METHODS AND THEIR VALIDATION</b>	42
A. Progress in potential models	15	A. The asymptotic normalization coefficient method	43
B. Progress in effective field theory (EFT)	15	B. The Coulomb dissociation method	44
1. Hybrid EFT (EFT*)	15	C. The Trojan Horse method	45
2. Pionless EFT	16	D. Summary	45
3. Comment on Mosconi <i>et al.</i>	16	<b>XIII. FUTURE FACILITIES AND CURRENT CAPABILITIES</b>	46
C. Summary	16	A. Inverse kinematics measurements using recoil separators	46
<b>IV. THE <math>d(p,\gamma)^3\text{He}</math> RADIATIVE CAPTURE REACTION</b>	17	B. Underground facilities	47
A. Data sets	17	<b>Acknowledgments and Dedication</b>	50
B. Theoretical studies	18	<b>Appendix: Treating Uncertainties</b>	50
C. Summary	18	A. Introduction	50
<b>V. THE <math>^3\text{He}(^3\text{He},2p)^4\text{He}</math> REACTION</b>	18	B. The inflation factor method	51
A. Data sets and fitting	19	C. Application of the inflation factor method	52
<b>VI. THE <math>^3\text{He}(\alpha,\gamma)^7\text{Be}</math> REACTION</b>	20	D. Other methods	52
A. Experimental measurements	20	<b>References</b>	52
B. Theory	21	<b>I. INTRODUCTION</b>	
1. Model selection for $S_{34}(0)$ determination	22		
2. Region of $S_{34}(E)$ fitting	22	In 1998 the Reviews of Modern Physics published a summary and critical analysis of the nuclear reaction cross sections important to solar burning. That effort, Adelberger <i>et al.</i> (1998) and denoted here as Solar Fusion I, began with a meeting hosted by the Institute for Nuclear Theory, University of Washington, 17-20 February 1997. A group of international experts in the nuclear physics and astrophysics of hydrogen-burning stars met to begin critical discussions of the existing data on relevant nuclear reactions, with the aim of determining “best values” and uncertainties for the contributing low-energy S-factors. The group also considered opportunities for further improvements in both measurements and theory.	
3. Theoretical uncertainty in the $S_{34}(0)$ determination	22	Such data and related nuclear theory have been crucial to the standard solar model (SSM) and the neutrino fluxes it predicts. Indeed, measurements of nuclear reactions gave the field its start. In 1958 Holmgren and Johnston (1958, 1959) showed that the rate for $^3\text{He}+^4\text{He} \rightarrow ^7\text{Be} + \gamma$ was $\sim 1000$ times larger than expected, and thus that the pp chain for $^4\text{He}$ synthesis would have additional terminations beyond $^3\text{He}+^3\text{He} \rightarrow ^4\text{He} + 2p$ . This result led Davis to recognize that his chlorine detector	
4. S-factor derivatives	22		
5. Comment on phase shifts	22		
C. $S_{34}(0)$ determination	23		
<b>VII. THE <math>^3\text{He}(p,e^+\nu_e)^4\text{He}</math> REACTION</b>	24		
A. hep calculations	24		
B. Summary	25		
<b>VIII. ELECTRON CAPTURE BY <math>^7\text{Be}</math>, <math>pp</math>, and CNO NUCLEI</b>	26		
<b>IX. THE <math>^7\text{Be}(p,\gamma)^8\text{B}</math> REACTION</b>	28		
A. The direct $^7\text{Be}(p,\gamma)^8\text{B}$ reaction	28		
1. Beam-target overlap	28		
2. $^8\text{B}$ backscattering	29		
3. Proton energy loss corrections	29		
B. Theory	29		
C. $^8\text{B}$ Coulomb dissociation measurements	31		
D. Direct $^7\text{Be}(p,\gamma)^8\text{B}$ analysis and $S_{17}(0)$ determination	32		
<b>X. THE SPECTRUM OF <math>^8\text{B}</math> NEUTRINOS</b>	34		
<b>XI. THE CNO CYCLES</b>	35		
A. The reaction $^{14}\text{N}(p,\gamma)^{15}\text{O}$	35		
1. Current status and results	35		
2. R-matrix analysis and normalization	36		

might be able to see the higher energy neutrinos from these other terminations, and spurred Bahcall and others to develop a quantitative model of the Sun capable of predicting those fluxes (Bahcall and Davis Jr., 1982).

At the time of the 1997 meeting, three decades of effort in solar neutrino physics had produced four measurements that were at variance with the SSM and the standard model of electroweak interactions. The measurements came from the pioneering work of Ray Davis, Jr. (Davis Jr., 1994; Davis Jr. *et al.*, 1968); the observation of  $^8\text{B}$  neutrinos in the Kamiokande water Cerenkov detector (Fukuda *et al.*, 1996); and the GALLEX (Kirsten *et al.*, 2003) and SAGE (Gavrin *et al.*, 2003) radiochemical detectors sensitive primarily to pp and  $^7\text{Be}$  neutrinos. The resulting pattern of fluxes that emerged from these experiments was difficult to reconcile with any plausible variation in the SSM, requiring a much sharper reduction in the  $^7\text{Be}$  neutrino flux than in the  $^8\text{B}$  flux, despite the greater sensitivity of the latter to changes in the solar core temperature.

For this reason it was argued in Solar Fusion I that the measurements provided evidence for new physics beyond the standard model. New solar neutrino experiments that promised much more precise data – the 50-kiloton successor to Kamiokande, Super-Kamiokande, and the heavy-water-based Sudbury Neutrino Observatory (SNO), with sensitivity to both electron and heavy-flavor neutrinos – were then underway. The authors of Solar Fusion I, recognizing that the impact of these new experiments would depend in part on the quality of the nuclear microphysics input to the SSM, thus undertook an extended study of the key reaction rates for the pp chain and CNO bi-cycle. The effort appears to have been of some value to the community, as Solar Fusion I has become one of the most heavily cited papers in nuclear astrophysics.

### A. Solar Fusion II: the 2009/10 effort

Ten years after publication of Solar Fusion I a proposal was made to the INT to revisit this process, in order to produce a new evaluation that would reflect the considerable progress made in the past decade, as well as new motivations for further constraining the SSM. Examples of advances in the nuclear physics include the LUNA II program at Gran Sasso (Costantini *et al.*, 2009), which has provided remarkable low-energy measurements of key reactions such as  $^3\text{He}(\alpha,\gamma)^7\text{Be}$  and  $^{14}\text{N}(\text{p},\gamma)^{15}\text{O}$ ; several high-precision measurements addressing the key pp-chain uncertainty identified in Solar Fusion I,  $^7\text{Be}(\text{p},\gamma)^8\text{B}$ ; the application of new theoretical techniques to the p+p and hep neutrino reactions; and the resolution of several unresolved questions about screening corrections in plasmas.

The context for these measurements has also changed. In 1997 the field’s central concern was, in some sense, a qualitative one, the origin of the solar neutrino problem. This question was answered in spectacular fashion by

the dual discoveries of Super-Kamiokande (Fukuda *et al.*, 2001) and SNO (Ahmad *et al.*, 2001) – two distinct neutrino oscillations responsible for the missing atmospheric and solar neutrinos, largely determining the pattern of the light neutrino masses. But issues remain, and most of these require precision. There is intense interest in extending direct measurements to the low-energy portion of the solar neutrino spectrum ( $\lesssim 2$  MeV), where experiments with good energy resolution can determine the separate contributions of pep, CNO,  $^7\text{Be}$ , and pp neutrinos. There is the potential to further constrain the solar neutrino mixing angle  $\theta_{12}$ : the solar luminosity determines the pp flux to high accuracy, and the low-energy spectrum lies in the vacuum region of the MSW triangle, in contrast to the high-energy  $^8\text{B}$  neutrinos, where matter effects are significant. Thus precise low-energy measurements have considerable “leverage” to test  $\theta_{12}$  and the consistency of the conclusions we have drawn from SNO, Super-Kamiokande, and the KamLAND reactor neutrino experiment. Borexino, now entering its calibration phase, is the first effort in this program of high-precision spectroscopy of low-energy solar neutrinos.

But the resolution of the solar neutrino problem has also returned the field to its roots: Davis built the chlorine detector to probe the interior of the Sun and thereby test directly the theory of stellar evolution and nuclear energy generation (Bahcall and Davis Jr., 1982). Davis was diverted from that goal by the missing solar neutrinos. But as the weak interaction effects responsible for that anomaly are now reasonably well understood, solar neutrinos again have become a quantitative tool for astronomy. Indeed, the program carried out by SNO and Super-Kamiokande has already yielded one remarkable constraint on the Sun, a direct determination of the core temperature to high precision, through measurement of the  $^8\text{B}$  neutrino flux ( $\phi(^8\text{B}) \propto T_c^{22}$ ). The 8.6% precision of the SNO NCD-phase results (Aharmim *et al.*, 2008),  $\phi(^8\text{B}) = (5.54^{+0.33+0.36}_{-0.31-0.34}) \times 10^6/\text{cm}^2/\text{s}$ , implies a sensitivity to core temperature of  $\sim 0.5\%$ .

New questions have arisen about the Sun that neutrinos could potentially address, provided the associated laboratory astrophysics has been done. One important success of the SSM in the 1990s was in predicting the local sound speed  $c(r)$ . Comparisons between  $c(r)$  deduced from helioseismology and the predictions of the SSM yielded agreement at  $\sim 0.2\%$  throughout much of the Sun. Bahcall and others argued (Bahcall *et al.*, 2001) that helioseismology is a more severe and detailed test of the SSM than neutrino production, so that SSM success in reproducing  $c(r)$  made a particle-physics resolution of the solar neutrino problem more likely.

The sound speed is a function of the Sun’s interior pressure and density profiles, which in turn reflect thermal transport properties that depend on the Sun’s metal content, through the opacity. Thus the comparison between helioseismology and the SSM tests a key assumption of the SSM, that the metals are distributed uniformly throughout the Sun, apart from small corrections

due to diffusion. This assumption allows one to equate SSM interior metal abundances to convective-zone abundances deduced from analyses of photospheric absorption lines. Such analyses had been based on 1D models of the photosphere. Recently *ab initio* 3D analyses have been developed, yielding significant improvements in predicted line shapes and in the consistency of metal abundance determinations from various atomic and molecular lines. However, this work also reduced metallicity estimates from  $Z \sim 0.0169$  to  $\sim 0.0122$  (Asplund *et al.*, 2005), destroying the once excellent agreement between helioseismology and the SSM.

It has been suggested that this difficulty may reflect, contrary to the SSM, differences in solar core and convective-zone metallicities that could have arisen from the late-stage evolution of the solar disk: as a great deal of metal was scoured out of the disk by the formation of the giant planets, the last few percent of gas deposited onto the Sun could have been depleted of metals (Haxton and Serenelli, 2008). Indeed, recent studies of “solar twins” show abundance trends that correlate with the existence of planets (Israelian *et al.*, 2009; Ramírez *et al.*, 2009). Haxton and Serenelli (2008) argued that a direct measurement of solar core metallicity could be made by observing CNO solar neutrinos.

In both of the above examples – using neutrinos to determine the solar core temperature and metallicity – nuclear physics uncertainties remain one of the limiting factors in the analyses.

The proposal to revisit in 2009 the deliberations of 1997 thus had several motivations:

- providing a set of standard S-factors and uncertainties that reflect the progress made in laboratory and theoretical nuclear astrophysics over the last decade;
- enabling more precise analyses of solar neutrino experiments designed to constrain neutrino oscillations and other new physics, e.g., future pp and pep neutrino experiments that exploit these well understood fluxes; and
- enabling analyses in which solar neutrinos are used as a probe of the solar core.

The 2009 INT workshop<sup>1</sup> was modeled after that of 1997, with invitations extended to and accepted by representa-

tives from most of the experimental groups active in the nuclear physics of hydrogen burning stars. There was also active involvement of theorists, reflecting the progress that has been made in *ab initio* calculations. The workshop participants are the authors of this manuscript. As in 1997, early organizing included the selection of working group leaders who identified key papers, which were then entered in a database for review, prior to the start of the workshop. These materials were then summarized and discussed during the workshop, as the various working groups considered the state of the data and outlined any additional work that would be needed for this review. The process of critically analyzing both new and older data and working toward a consensus on best-value cross sections and uncertainties continued throughout 2009. A few new topics not considered in 1997 but now recognized to be quite important, such as the shape of the  ${}^8\text{B}$  neutrino spectrum, were addressed. (The  ${}^8\text{B}$  neutrino spectrum is one of the inputs to SNO and Super-Kamiokande analyses.) The workshop included working groups on indirect techniques for constraining cross sections, to summarize the progress that has been made in validating such approaches, and on new facilities and instrumentation, in view of the facility investments that are being considered in laboratory nuclear astrophysics (above and below ground).

## B. Contents of this review

The review begins in Section II with a description of hydrogen burning by the pp chain and CNO bi-cycle, and the neutrino byproducts of these reaction chains. The role of S-factors and the associated questions of screening and of extrapolating data to the solar Gamow peak are discussed. We provide a fairly complete overview of progress in theory, which in some cases provides our only estimate of S-factors, and in other cases determines the forms of the functions that are needed for data extrapolations.

Discussions of individual reactions are organized by chapter: Secs. III-IX discuss the pp chain reactions  $p+p \rightarrow d+e^++\nu_e$ ;  $d+p \rightarrow {}^3\text{He}+\gamma$ ;  ${}^3\text{He}+{}^3\text{He} \rightarrow {}^4\text{He}+p+p$ ;  ${}^3\text{He}+{}^4\text{He} \rightarrow {}^7\text{Be}+\gamma$ ;  ${}^3\text{He}+p \rightarrow {}^4\text{He}+e^++\nu_e$ ;  ${}^7\text{Be}$ , pp, and CNO nuclei electron capture; and  ${}^7\text{Be}+p \rightarrow {}^8\text{B}+\gamma$ . Sec. X discusses the spectrum of  ${}^8\text{B}$  neutrinos produced in the  $\beta$  decay to a broad resonance in  ${}^8\text{Be}$ . Sec. XI discusses  ${}^{14}\text{N}+p \rightarrow {}^{15}\text{O}+\gamma$  and other reactions contribut-

<sup>1</sup> The workshop was proposed in a letter to the Institute for Nuclear Theory’s National Advisory Committee (NAC) and approved by the NAC and INT Director at the time of the NAC’s August 2008 annual meeting. Wick Haxton (lead), Eric Adelberger, Heide Costantini, Peter Parker, R. G. Hamish Robertson, Kurt Snover, Frank Strieder, and Michael Wiescher formed the organizing committee and served as co-editors of this paper. Additional community members joined this group to act as working group heads: Jiunn-Wei Chen, Barry Davids, Stuart Freedman, Alejandro Garcia, Uwe Greife, Michael Hass, Gianluca Imbriani, Kuniharu Kubodera, Daniela Leitner, Laura Marcucci,

Filomena Nunes, Tae-Sun Park, Paolo Prati, Hanns-Peter Trautvetter, and Stefan Typel. The working group heads were responsible for organizing discussions, creating section drafts, and responding to subsequent criticisms of the drafts. Organizing committee members, in their capacity as co-editors, were responsible for creating from the drafts a coherent document, and for addressing any issues unresolved by the working groups. Workshop presentations are archived on the INT’s web site, [http://www.int.washington.edu/PROGRAMS/solar\\_fusion.html](http://www.int.washington.edu/PROGRAMS/solar_fusion.html).

ing to the CNO cycles. Sec. XII describes the progress that has been made in developing and validating indirect methods, while Sec. XIII describes future facilities and instrumentation that could further advance the field.

The conclusions of this review, in some cases, required the working groups to make some judgments. There are discrepant data sets, and there are cases where data extrapolations have some dependence on models. We have tried to treat such questions as consistently as possible, aware that excessively optimistic treatments of uncertainties could be misleading, while excessively conservative treatments would degrade the value of the best experiments done in the field. In most cases our working groups were able to reach consensus. In cases where significant differences remained among the experts, we have tried to identify the source of the disagreement, so that “consumers” will be aware that full consensus may have to await future measurements.

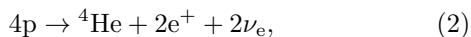
Table I summarizes the conclusions of this review.

## II. NUCLEAR REACTIONS IN HYDROGEN-BURNING STARS

Observations of stars reveal a wide variety of stellar conditions, with luminosities relative to solar spanning a range  $L \sim 10^{-4}$  to  $10^6 L_\odot$  and surface temperatures  $T_s \sim 2000$ – $50000$  K. The simplest relation one could propose between luminosity  $L$  and  $T_s$  is

$$L = 4\pi R^2 \sigma_{\text{SB}} T_s^4 \Rightarrow L/L_\odot = (R/R_\odot)^2 (T_s/T_\odot)^4, \quad (1)$$

where  $\sigma_{\text{SB}}$  is the Stefan-Boltzmann constant, and  $L_\odot$ ,  $T_\odot$ , and  $R_\odot$  are the solar values. This relation suggests that stars of a similar structure might lie along a one-parameter path (in this simplified example, defined by a function of the blackbody radii,  $(R/R_\odot)^2$ ) in the luminosity (or magnitude) vs. temperature (or color) plane. In fact, there is a dominant path in the Hertzsprung–Russell color–magnitude diagram along which roughly 80% of the stars reside. This is the main sequence, those stars supporting themselves by hydrogen burning through the pp chain,



or CNO cycles. The laboratory nuclear astrophysics of hydrostatic hydrogen burning is the focus of this review.

As one such star, the Sun is an important test of our theory of main sequence stellar evolution: its properties – age, mass, surface composition, luminosity, and helioseismology – are by far the most accurately known among the stars. The SSM traces the evolution of the Sun over the past 4.6 Gyr of main sequence burning, thereby predicting the present-day temperature and composition profiles, the relative strengths of competing nuclear reaction chains, and the neutrino fluxes resulting from those chains. The SSM makes four basic assumptions:

- The Sun evolves in hydrostatic equilibrium, maintaining a local balance between the gravitational force and the pressure gradient. Knowledge of the equation of state as a function of temperature, density, and composition allows one to implement this condition in the SSM.
- Energy is transported by radiation and convection. The solar envelope, about 2.6% of the Sun by mass, is convective. Radiative transport dominates in the interior,  $r \lesssim 0.72R_\odot$ , and thus in the core region where thermonuclear reactions take place. The opacity is sensitive to composition.
- The Sun generates energy through hydrogen burning, Eq. (2). Figure 1 shows the competition between the pp chain and CNO cycles as a function of temperature: the relatively cool temperatures of the solar core favor the pp chain, which in the SSM produces  $\sim 99\%$  of the Sun’s energy. The reactions contributing to the pp chain and CNO bi-cycle are shown in Fig. 2. The SSM requires as input rates for each of the contributing reactions, which are customarily provided as S-factors, defined below. Typically cross sections are measured at somewhat higher energies, where rates are larger, then extrapolated to the solar energies of interest. Corrections also must be made for the differences in the screening environments of terrestrial targets and the solar plasma.
- The model is constrained to produce today’s solar radius, mass, and luminosity. The primordial Sun’s metal abundances are generally determined from a combination of photospheric and meteoritic abundances, while the initial  ${}^4\text{He}/\text{H}$  ratio is adjusted to reproduce, after 4.6 Gyr of evolution, the modern Sun’s luminosity.

The SSM predicts that, as the Sun evolves, the core He abundance increases, the opacity and core temperature rise, and the luminosity increases (by a total of  $\sim 44\%$  over 4.6 Gyr). The details of this evolution depend on a variety of model input parameters and their uncertainties: the photon luminosity  $L_\odot$ , the mean radiative opacity, the solar age, the diffusion coefficients describing the gravitational settling of He and metals, the abundances of the key metals, and the rates of the nuclear reactions.

If the various nuclear rates are precisely known, the competition between burning paths can be used as a sensitive diagnostic of the central temperature of the Sun. Neutrinos probe this competition, as the relative rates of the ppI, ppII, and ppIII cycles comprising the pp chain can be determined from the fluxes of the pp/pep,  ${}^7\text{Be}$ , and  ${}^8\text{B}$  neutrinos. This is one of the reasons that laboratory astrophysics efforts to provide precise nuclear cross section data have been so closely connected with solar neutrino detection.

Helioseismology provides a second way to probe the solar interior, and thus the physics of the radiative zone

TABLE I The Solar Fusion II recommended values for  $S(0)$ , its derivatives, and related quantities, and for the resulting uncertainties on  $S(E)$  in the region of the solar Gamow peak – the most probable reaction energy – defined for a temperature of  $1.55 \times 10^7$  K characteristic of the Sun’s center. See the text for detailed discussions of the range of validity for each  $S(E)$ . Also see Sec. VIII for recommended values of CNO electron capture rates, Sec. XI.B for other CNO S-factors, and Sec. X for the  $^8\text{B}$  neutrino spectral shape. Quoted uncertainties are  $1\sigma$ .

Reaction	Section	$S(0)$ (keV-b)	$S'(0)$ (b)	$S''(0)$ (b/keV)	Gamow peak uncertainty (%)
$p(p, e^+ \nu_e) d$	III	$(4.01 \pm 0.04) \times 10^{-22}$	$(4.49 \pm 0.05) \times 10^{-24}$	–	$\pm 0.7$
$d(p, \gamma) ^3\text{He}$	IV	$(2.14^{+0.17}_{-0.16}) \times 10^{-4}$	$(5.56^{+0.18}_{-0.20}) \times 10^{-6}$	$(9.3^{+3.9}_{-3.4}) \times 10^{-9}$	$\pm 7.1^a$
$^3\text{He}(^3\text{He}, 2p) ^4\text{He}$	V	$(5.21 \pm 0.27) \times 10^3$	$-4.9 \pm 3.2$	$(2.2 \pm 1.7) \times 10^{-2}$	$\pm 4.3^a$
$^3\text{He}(^4\text{He}, \gamma) ^7\text{Be}$	VI	$0.56 \pm 0.03$	$(-3.6 \pm 0.2) \times 10^{-4}^b$	$(0.151 \pm 0.008) \times 10^{-6}^c$	$\pm 5.1$
$^3\text{He}(p, e^+ \nu_e) ^4\text{He}$	VII	$(8.6 \pm 2.6) \times 10^{-20}$	–	–	$\pm 30$
$^7\text{Be}(e^-, \nu_e) ^7\text{Li}$	VIII	See Eq. (40)	–	–	$\pm 2.0$
$p(pe^-, \nu_e) d$	VIII	See Eq. (46)	–	–	$\pm 1.0^d$
$^7\text{Be}(p, \gamma) ^8\text{B}$	IX	$(2.08 \pm 0.16) \times 10^{-2}^e$	$(-3.1 \pm 0.3) \times 10^{-5}$	$(2.3 \pm 0.8) \times 10^{-7}$	$\pm 7.5$
$^{14}\text{N}(p, \gamma) ^{15}\text{O}$	XI.A	$1.66 \pm 0.12$	$(-3.3 \pm 0.2) \times 10^{-3}^b$	$(4.4 \pm 0.3) \times 10^{-5}^c$	$\pm 7.2$

<sup>a</sup>Error from phenomenological quadratic fit. See text.

<sup>b</sup> $S'(0)/S(0)$  taken from theory; error is that due to  $S(0)$ . See text.

<sup>c</sup> $S''(0)/S(0)$  taken from theory; error is that due to  $S(0)$ . See text.

<sup>d</sup>Estimated error in the pep/pp rate ratio. See Eq. (46)

<sup>e</sup>Error dominated by theory.

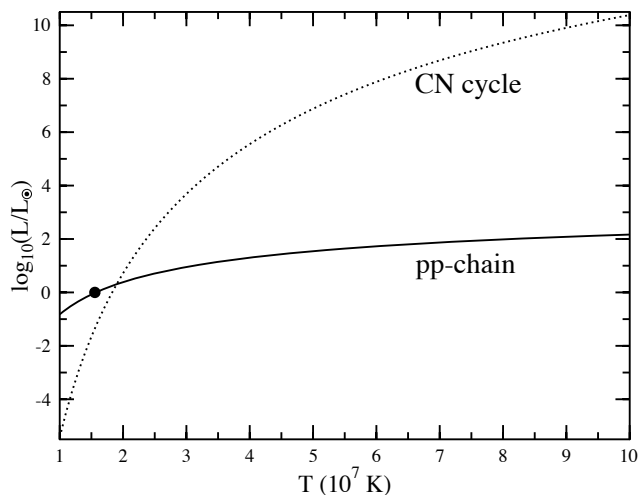


FIG. 1 The stellar energy production as a function of temperature for the pp chain and CN cycle, showing the dominance of the former at solar temperatures. Solar metallicity has been assumed. The dot denotes conditions in the solar core: the Sun is powered dominantly by the pp chain.

that the SSM was designed to describe. The sound speed profile  $c(r)$  has been determined rather precisely over the outer 90% of the Sun and, as previously discussed, is now in conflict with the SSM, when recent abundance determinations from 3D photospheric absorption line analyses are used.

## A. Rates and S-factors

The SSM requires a quantitative description of relevant nuclear reactions. Both careful laboratory measurements constraining rates at near-solar energies and a supporting theory of sub-barrier fusion reactions are needed.

At the temperatures and densities in the solar interior (e.g.,  $T_c \sim 15.5 \times 10^6$  K and  $\rho_c \sim 153$  g/cm<sup>3</sup> at the Sun’s center), interacting nuclei reach a Maxwellian equilibrium distribution in a time that is infinitesimal compared to nuclear reaction time scales. Therefore, the reaction rate between two nuclei can be written (Burbidge *et al.*, 1957; Clayton, 1968)

$$r_{12} = \frac{n_1 n_2}{1 + \delta_{12}} \langle \sigma v \rangle_{12}. \quad (3)$$

Here the Kronecker delta prevents double counting in the case of identical particles,  $n_1$  and  $n_2$  are the number densities of nuclei of type 1 and type 2 (with atomic numbers  $Z_1$  and  $Z_2$ , and mass numbers  $A_1$  and  $A_2$ ), and  $\langle \sigma v \rangle_{12}$  denotes the product of the reaction cross section  $\sigma$  and the relative velocity  $v$  of the interacting nuclei, averaged over the collisions in the stellar gas,

$$\langle \sigma v \rangle_{12} = \int_0^\infty \sigma(v) v \Phi(v) dv. \quad (4)$$

Under solar conditions nuclear velocities are very well approximated by a Maxwell–Boltzmann distribution. It follows that the relative velocity distribution is also a Maxwell–Boltzmann, governed by the reduced mass  $\mu$  of the colliding nuclei,

$$\Phi(v) dv = \left( \frac{\mu}{2\pi kT} \right)^{3/2} \exp\left( -\frac{\mu v^2}{2kT} \right) 4\pi v^2 dv. \quad (5)$$

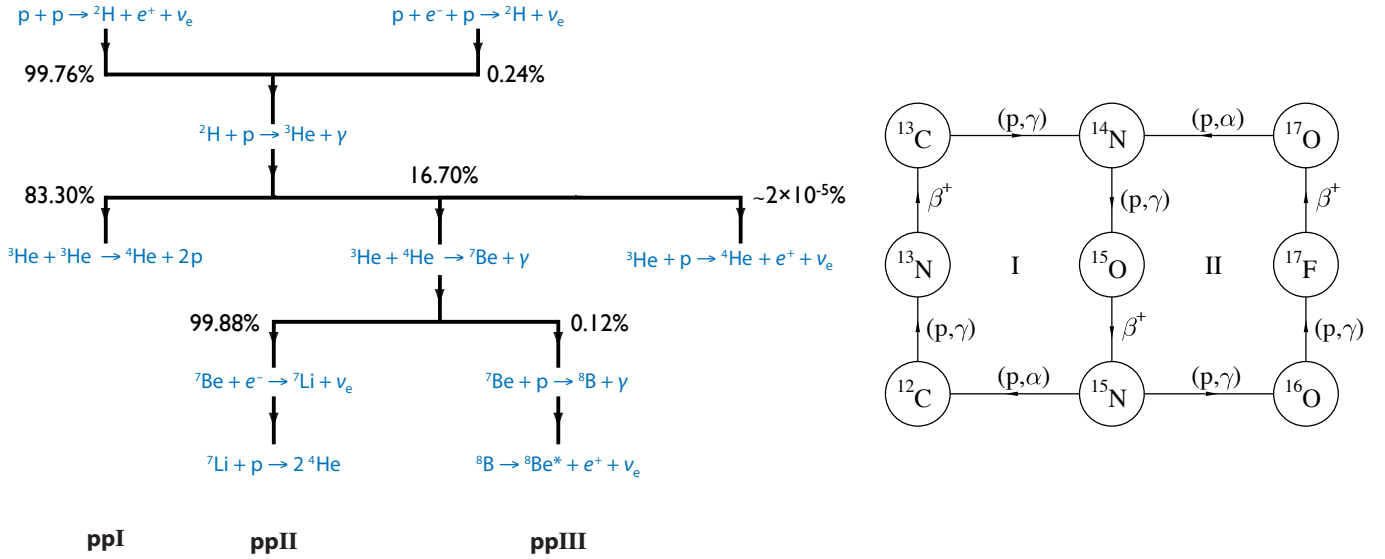


FIG. 2 The left frame shows the three principal cycles comprising the pp chain (ppI, ppII, and ppIII), with branching percentages indicated, each of which is “tagged” by a distinctive neutrino. Also shown is the minor branch  ${}^3\text{He} + p \rightarrow {}^4\text{He} + e^+ + \nu_e$ , which burns only  $\sim 10^{-7}$  of  ${}^3\text{He}$ , but produces the most energetic neutrinos. The right frame shows the CNO bi-cycle. The CN cycle, marked I, produces about 1% of solar energy and significant fluxes of solar neutrinos.

Therefore,

$$\langle \sigma v \rangle_{12} = \sqrt{\frac{8}{\pi \mu (kT)^3}} \int_0^\infty E \sigma(E) \exp\left(-\frac{E}{kT}\right) dE, \quad (6)$$

where  $E$  is the relative kinetic energy and  $k$  is the Boltzmann constant. In order to evaluate  $\langle \sigma v \rangle_{12}$  the energy dependence of the reaction cross section must be determined.

Almost all of the nuclear reactions relevant to solar energy generation are nonresonant and charged-particle induced. For such reactions it is helpful to remove much of the rapid energy dependence associated with the Coulomb barrier, by evaluating the probability of s-wave scattering off a point charge. The nuclear physics (including effects of finite nuclear size, higher partial waves, antisymmetrization, and any atomic screening effects not otherwise explicitly treated) is then isolated in the S-factor, defined by

$$\sigma(E) = \frac{S(E)}{E} \exp[-2\pi\eta(E)], \quad (7)$$

with the Sommerfeld parameter  $\eta(E) = Z_1 Z_2 \alpha / v$ , where  $v = \sqrt{2E/\mu}$  is the relative velocity and  $\alpha$  the fine structure constant ( $\hbar = c = 1$ ). Because the S-factor is slowly varying, one can extrapolate  $S(E)$  more reliably from the range of energies spanned by data to the lower energies characterizing the Gamow peak.

A substitution of Eq. (7) into Eq. (6) followed by a Taylor expansion of the argument of the exponentials then

yields (Bahcall, 1989)

$$\begin{aligned} \langle \sigma v \rangle_{12} &= \sqrt{\frac{2}{\mu kT}} \frac{\Delta E_0}{kT} f_0 S_{\text{eff}} \exp[-3E_0/(kT)] \\ &= 1.301 \times 10^{-14} \text{ cm}^3/\text{s} \left(\frac{Z_1 Z_2}{A}\right)^{1/3} \\ &\times f_0 \frac{S_{\text{eff}}}{\text{MeV b}} T_9^{-2/3} \exp[-3E_0/(kT)], \quad (8) \end{aligned}$$

where

$$\frac{E_0}{kT} = (\pi Z_1 Z_2 \alpha / \sqrt{2})^{2/3} [\mu / (kT)]^{1/3},$$

$$\frac{\Delta E_0}{kT} = 4\sqrt{\frac{E_0}{3kT}}, \quad A = \frac{A_1 A_2}{A_1 + A_2},$$

and

$$\begin{aligned} S_{\text{eff}} &= S(0) \left(1 + \frac{5kT}{36E_0}\right) + S'(0)E_0 \left(1 + \frac{35kT}{36E_0}\right) \\ &+ \frac{1}{2}S''(0)E_0^2 \left(1 + \frac{89kT}{36E_0}\right). \end{aligned}$$

$E_0$ , the Gamow peak energy where the integrand of Eq. (6) takes on its maximum value, is the most probable energy of reacting nuclei.  $\Delta E_0$  corresponds to the full width of the integrand at  $1/e$  of its maximum value, when approximated as a Gaussian. Equation (8) includes a factor  $f_0$ , discussed below, to correct for the effects of electronic screening on nuclear reactions occurring in the solar plasma.



Rates in an astrophysical plasma can be calculated given  $S(E)$  which by virtue of its slow energy dependence, in the case of non-resonant reactions, can be approximated by its zero-energy value  $S(0)$  and possible corrections determined by its first and second derivatives,  $S'(0)$  and  $S''(0)$ . It is these quantities that we need to determine by fitting laboratory data, or in cases where such data cannot be obtained, through theory. For most of the reactions contributing to the pp chain and CNO bicycle, data have been obtained only for energies in regions above the Gamow peak, e.g., typically  $E \gtrsim 100$  keV, so that extrapolations to lower energies depend on the quality of the fit to higher energy data. Ideally one desires a fitting function that is well motivated theoretically and tightly constrained by the existing, higher-energy data. The purpose of this review is to provide current best values and uncertainties for  $S(0)$  and, if feasible, its derivatives.

S-factor uncertainties, when folded into SSM calculations, then limit the extent to which that model can predict observables, such as the depth of the convective zone, the sound speed profile, and the neutrino fluxes. It has become customary in the SSM to parameterize the consequences of input uncertainties on observables through logarithmic partial derivatives, determined by calculating the SSM response to variations in individual input parameters. SSM compilations of the logarithmic partial derivatives provide, for example, a way to assess the importance of each S-factor uncertainty on neutrino flux predictions.

The partial derivatives  $\alpha(i, j)$  for each neutrino flux  $\phi_i$  and SSM input parameter  $\beta_j$  are defined by

$$\alpha(i, j) \equiv \frac{\partial \ln [\phi_i / \phi_i(0)]}{\partial \ln [\beta_j / \beta_j(0)]} \quad (9)$$

where  $\phi_i(0)$  and  $\beta_j(0)$  denote the SSM best values. The  $\alpha(i, j)$  for 19 SSM input parameters  $\beta_j$  are given by Peña-Garay and Serenelli (2008) in their 2008 SSM update. The  $\beta_j$  include parameters such as the Sun's age and luminosity, the abundances of important metals, and S-factors.

The partial derivatives define the power-law dependencies of neutrino fluxes with respect to the SSM best-value prediction  $\phi_i(0)$ ,

$$\phi_i = \phi_i(0) \prod_{j=1}^N \left[ \frac{\beta_j}{\beta_j(0)} \right]^{\alpha(i, j)} = \phi_i(0) \prod_{j=1}^N [1 + \delta\beta_j]^{\alpha(i, j)}, \quad (10)$$

where the product extends over  $N$  SSM input parameters, and where  $\delta\beta_j \equiv \Delta\beta_j / \beta_j(0)$  is the fractional uncertainty of input parameter  $\beta_j$  with respect to its SSM best value. This expression separates the impact of SSM parameter variations on  $\phi_i$  into a solar piece – the infinitesimal SSM response described by  $\alpha(i, j)$  – and a laboratory or theory piece – the estimated uncertainty  $\delta\beta_j$  of an input parameter (in our case, that of an S-factor). From SSM tabulations of the  $\alpha(i, j)$ , one can

estimate the change in a SSM flux prediction  $\phi_i$ , when a given SSM parameter  $\beta_j$  is perturbed away from its SSM best value by an amount  $\delta\beta_j$ , without redoing the SSM calculation. For example, to assess the impact of an improved nuclear cross section measurement on  $\phi_i$ , one sets  $\delta\beta_j$  to the estimated uncertainty of the corresponding S-factor, to obtain the corresponding variation in  $\phi_i$ . In this way one can identify nuclear physics improvements that will have the most impact on reducing flux uncertainties. Alternatively, the process can be inverted: a flux measurement could in principle be used to constrain an uncertain input parameter.

For example, Peña-Garay and Serenelli (2008) define the dependence of  $\phi(^8\text{B})$  on the S-factors under discussion here,

$$\phi(^8\text{B}) \propto (1 + \delta S_{11})^{-2.73} (1 + \delta S_{33})^{-0.43} (1 + \delta S_{34})^{0.85} \times (1 + \delta S_{17})^{1.0} (1 + \delta S_{e7})^{-1.0} (1 + \delta S_{14})^{-0.02}, \quad (11)$$

where  $S_{11}$  denotes the S-factor for p+p reaction, etc., and  $\delta S_{11} \equiv \Delta S_{11} / S_{11}(0)$  denotes its fractional uncertainty. This review gives the best current values for the needed  $\delta S$ s.

## B. Screening of stellar and laboratory reactions

One must take into account differences in the atomic environments to correctly relate screened laboratory and solar cross sections,  $\sigma_s^{\text{lab}}(E)$  and  $\sigma_s^{\text{solar}}(E)$ , to each other or to the underlying bare cross section  $\sigma_b(E)$ . Screening enhances solar cross sections by reducing the Coulomb barrier that reacting ions must overcome. As light nuclei in the solar core are almost completely ionized, the solar electron screening correction  $f_0$ ,

$$f_0(E) \equiv \frac{\sigma_s^{\text{solar}}(E)}{\sigma_b(E)}, \quad (12)$$

can be treated in a weak-screening approximation (Salpeter, 1954). The impact of the modified potential,

$$V(r) = \frac{\alpha Z_1 Z_2}{r} \exp\left(-\frac{r}{R_D}\right), \quad (13)$$

on reactions depends on the ratio of the Coulomb potential at the Debye radius  $R_D$  to the temperature,

$$f_0 \sim \exp\left(\frac{Z_1 Z_2 \alpha}{R_D kT}\right) = \exp\left(0.188 Z_1 Z_2 \zeta \rho_0^{1/2} T_6^{-3/2}\right), \quad (14)$$

where  $\zeta R_D = [kT / (4\pi\alpha\rho)]^{1/2}$ ,  $\rho$  is the number density of nucleons,  $\rho_0$  is a dimensionless density measured in  $\text{g}/\text{cm}^3$ ,  $\zeta = \left[ \sum_i X_i (Z_i^2 / A_i) + (f'_0 / f_0) \sum_i X_i (Z_i / A_i) \right]^{1/2}$ ,  $X_i$  is the mass fraction of nuclei of type  $i$ , and  $T_6$  is the dimensionless temperature in units of  $10^6$  K. The

factor  $f_0'/f_0 \sim 0.92$  corrects for the effects of electron degeneracy in the solar core (Salpeter, 1954).

The weak-screening approximation requires the average interaction energy between particles to be smaller than the average particle kinetic energy (Baimbetov *et al.*, 1995; Kobzev *et al.*, 1995). This places a constraint on the argument of Eq. (14),  $Z_1 Z_2 \alpha / (R_D kT) \ll 1$ , that is satisfied in the solar core if  $Z_1 Z_2 \lesssim 10$  (Gruzinov, 1998), a condition met by the low- $Z$  reactions of the pp chain and CNO bi-cycle. However corrections to the Salpeter formula are expected at some level. Nonadiabatic effects have been suggested as one source, e.g., when a high Gamow energy guarantees reacting nuclei having velocities significantly higher than the typical ion velocity, so that the response of slower plasma ions might be suppressed. At the time of Solar Fusion I such dynamic corrections were a source of controversy. Dynamic corrections were first discussed by Mitler (1977) and later studied by Carraro *et al.* (1988). Subsequent work showed that Salpeter's formula would be valid independent of the Gamow energy due to the nearly precise thermodynamic equilibrium of the solar plasma (Brown and Sawyer, 1997; Gruzinov, 1998; Gruzinov and Bahcall, 1998). The arguments, summarized in Solar Fusion I, were significantly extended in 2002 by Bahcall *et al.* (2002), who pointed out a number of contradictions in investigations claiming larger corrections, and showed that a field theoretic approach led to the expectation of only small ( $\sim 4\%$ ) corrections to the standard formula, for solar conditions. However controversies have not entirely died out (Mao *et al.*, 2009).

The Salpeter correction relates the solar and bare cross sections,  $\sigma_s^{\text{solar}}(E)$  and  $\sigma_b(E)$ . As the reactions studied in the laboratory generally involve target nuclei bound in neutral atoms and molecules, not bare ions, a second step is needed to extract  $\sigma_b(E)$  from laboratory data. As in the Sun, electrons in the laboratory target tend to reduce the barrier, so that the screened cross section  $\sigma_s^{\text{lab}}(E)$  will exceed that for bare ions  $\sigma_b(E)$ . The enhancement is given by (Assenbaum *et al.*, 1987)

$$f_{\text{lab}}(E) \equiv \frac{\sigma_s^{\text{lab}}(E)}{\sigma_b(E)} \sim \exp \left[ \frac{\pi \eta(E) U_e}{E} \right] \geq 1 \quad \text{for } U_e \ll E, \quad (15)$$

where  $U_e$  is an electron-screening potential energy. This energy can be estimated from the difference in atomic binding energies between the compound atom and the projectile plus target atoms of the entrance channel. Because the correction depends on the ratio  $U_e/E$ , one expects screening corrections to be most important for very low projectile energy.

In contrast with the case of solar screening, a great deal can be done experimentally (Angulo *et al.*, 1993; Assenbaum *et al.*, 1987; Engstler *et al.*, 1988, 1992; Greife *et al.*, 1995; Prati *et al.*, 1994; Rolfs, 2001; Rolfs and Somorjai, 1995) to test our understanding of electron screening in terrestrial targets. Studies of reactions involving light nuclei (Engstler *et al.*, 1988; Strieder *et al.*, 2001) revealed

an upturn in cross section at low energies, as predicted by Eq. (15). For example, results for  ${}^3\text{He}(\text{d,p}){}^4\text{He}$  (Aliotta *et al.*, 2001) could be represented by Eq. (15) for a screening potential  $U_e = 219 \pm 15$  eV. While this potential is significantly larger than the one obtained from the adiabatic approximation,  $U_{ad} = 119$  eV, the analysis requires one to assume an energy dependence of the bare cross section  $\sigma_b(E)$ . This adds a difficult-to-quantify theoretical uncertainty to the extracted potential. It may be possible to remove much of this uncertainty through an indirect measurement of  $\sigma_b(E)$  by the Trojan Horse Method (Lattuada *et al.*, 2001; Spitaleri *et al.*, 2001; Strieder *et al.*, 2001; Tumino *et al.*, 2003).

There exist various surrogate environments that have been exploited by experimentalists to test our understanding of plasma screening effects. Screening in d(d,p)t has been studied for gaseous targets and for deuterated metals, insulators, and semiconductors (Raiola *et al.*, 2004). For a summary of the results see Haxton *et al.* (2006): it is believed that the quasi-free valence electrons in metals create a screening environment quite similar to that found in stellar plasmas. Experiments in metals have confirmed important predictions of the Debye model, such as the temperature dependence  $U_e(T) \propto T^{-1/2}$ .

The tendency of experimentally determined values of  $U_e$  to exceed theoretical estimates by a factor  $\sim 2$  has been noted by Assenbaum *et al.* (1987); Rolfs (2001); Rolfs and Somorjai (1995). Various possible explanations have been considered (Balantekin *et al.*, 1997; Fiorentini *et al.*, 2003; Flambaum and Zelevinsky, 1999; Hagino and Balantekin, 2002; Shoppa *et al.*, 1993). A possible solution of the laboratory screening problem was proposed in Langanke *et al.* (1996) and in Bang *et al.* (1996), that the stopping of ions in matter differs at low energy from that obtained by extrapolating from stopping power tables at higher energies (Andersen and Ziegler, 1977). Smaller stopping powers were indeed verified experimentally (Golser and Semrad, 1991; Rolfs, 2001) and explained theoretically (Bertulani, 2004; Bertulani and de Paula, 2000).

Screening corrections for laboratory reactions are important in extracting S-factors in cases where data extend to very low energies. In this review two cases of interest are  ${}^3\text{He}+{}^3\text{He} \rightarrow \text{p}+\text{p}+{}^4\text{He}$ , where the lowest data point is at  $E = 16$  keV, and  ${}^{14}\text{N}(\text{p},\gamma){}^{15}\text{O}$ , where measurements extend down to 70 keV.

### C. Fitting and extrapolating S-factors

$S(0)$  (and its derivatives  $S'(0)$  and  $S''(0)$ ) needed in Eq. (8) could be taken from a polynomial fit to data. A quadratic form often provides an excellent representation of the data up to a few hundred keV. However, as the procedure is purely empirical, it provides no theoretical justification for extrapolating beyond the last known data point. For example, a quadratic fit to the labora-

tory data for  ${}^7\text{Be}(p,\gamma){}^8\text{B}$  would miss the upturn in the S-factor at low energy expected from theory, as this increase occurs beyond the range of existing data. For this reason, we restrict our use of empirical fitting functions to cases where the data sets encompass the full range of energies relevant to astrophysics.

### 1. Theory constraints: model-based methods

One class of important theoretical constraints makes use of the peripheral nature of non-resonant radiative capture reactions close to the threshold. If the reaction occurs at separations much larger than the sum of the nuclear radii, one can derive the coefficients for the Taylor series for  $S(E)$  independent of models, as only the asymptotic forms of the bound and scattering initial- and final-state wave functions are relevant. This idea has been exploited in several ways.

Williams and Koonin (1981) used Bessel function expansions of Coulomb wave functions and a hard-sphere approximation to derive an expansion of the low-energy logarithmic derivative,

$$\frac{1}{S(E)} \frac{dS(E)}{dE} = a + bE. \quad (16)$$

This approach was further developed by Mukhamedzhanov and Nunes (2002), who considered variables such as the remnant Coulomb barrier, the initial and final centrifugal barriers, and the binding energy (but not the interactions of the colliding nuclei in the entrance channel). They found that the near-threshold behavior of  $S(E)$  could be sensitive to such parameters. Baye and collaborators, employing zero-energy solutions of the Schrödinger equation and their energy derivatives, showed that model-independent values for the coefficients in the Taylor expansion for  $S(E)$  around  $E = 0$  could be extracted from the asymptotic normalization coefficient (ANC) of the bound state wave function and the scattering lengths of the scattering states, thus including effects from interactions in the continuum (Baye, 2000, 2004, 2005; Baye and Brainis, 2000).

Despite the successful application of the Taylor series expansion for  $S(E)$ , it was noticed that the series has a restricted domain of convergence, determined by the binding energy  $E_B$  of the final state. This is a consequence of a pole in the relevant radial integral at  $E = -E_B$  (Baye, 2000; Jennings *et al.*, 1998a,b). This limitation becomes particularly severe for weakly bound nuclei: for  ${}^7\text{Be}(p,\gamma){}^8\text{B}$ ,  $|E_B| \sim 138$  keV barely reaches the domain of experimental data. Thus the alternatives of a Laurent expansion of the S-factor in the photon energy  $E_\gamma = E + E_B$ , an expansion of  $(E + E_B)S(E)$ , and the explicit treatment of the pole have been explored as alternatives in the analysis of experimental data (Cyburt and Davids, 2008; Cyburt *et al.*, 2004). See also Typel

and Baur (2005) for explicit expressions of the cross sections without the convergence limitation.

Model-based calculations of fusion cross sections also provide a template for fitting and extrapolating experimental data. Models can be constrained by the known properties of the system under study and can be applied over a wide range of energies. While they often predict the energy dependence of  $S(E)$  accurately, in many cases an overall renormalization is needed to give the correct magnitude of the S-factor. The need for this scaling is qualitatively understood, as model calculations of interior wave functions are generally done in restricted spaces, and thus lack high-momentum (and certain low-momentum) components of the true wave function, with consequences for the normalization. (The goal of predicting both the shape and normalization of S-factors is motivating the development of quasi-exact *ab initio* methods, as discussed below.)

Modeling approaches involve various levels of complexity. The simplest microscopic reaction theories are the potential models, in which the internal structure of the colliding nuclei is ignored. The dynamics of the process is reduced to a single coordinate, the distance vector between the two nuclei. The potential-model Hamiltonian is typically a phenomenological one, e.g., a Woods-Saxon potential, with parameters that can be determined by fitting data, such as the elastic cross section.

More realism is provided by cluster models like the resonating group method (RGM) or the generator-coordinate method (GCM), which take into account the many-body substructure of the reacting nuclei. These models employ fully antisymmetrized many-body wave functions of the compound system, though constructed in a restricted model space. The full wave function is described as a superposition of many-body cluster wave functions of fixed internal structure moving against each other. The interaction is described by phenomenological nucleon-nucleon potentials with parameters that are adjusted for each reaction under consideration.

Another description of fusion reaction cross sections comes from the R-matrix. Space is divided into two regions, the interior where nuclear forces are important, and the exterior where the interaction between the nuclei is assumed to be only Coulombic. The full scattering wave function connecting different channels  $i$  is expanded in partial waves with total angular momentum  $J$ . The Schrödinger equation for the interior Hamiltonian is solved, with boundary conditions at the channel radii  $a_i$  encoding the correct asymptotic behavior. The solutions of the Schrödinger equation determine the level energies  $E_\lambda$  and reduced widths  $\gamma_{\lambda i}$  that appear in the expression for the R-matrix

$$R_{ij}(E) = \sum_{\lambda=1}^N \frac{\gamma_{\lambda i} \gamma_{\lambda j}}{E - E_\lambda}, \quad (17)$$

for each  $J$ , in the standard approach of Lane and Thomas (1958). Simple expressions relate the reaction cross sections at energy  $E$  to the R-matrix. The cross section

should be insensitive to the choice of the channel radii. In most applications the R-matrix is viewed as a parameterization of measured reaction cross sections in terms of fitted level energies and reduced widths. A connection to an underlying reaction model is not required. The R-matrix allows one to properly account for penetrability effects, and to adjust the complexity of the fitting in response to various practical considerations, such as the energy range of interest.

R-matrix resonance parameters (level energies and reduced widths) are not directly comparable to the experimental quantities due to level shifts associated with the chosen boundary conditions. Generalizing earlier ideas of Barker (1971) and Angulo and Descouvemont (2000), an alternative parametrization of R-matrix theory has been developed by Brune (2002) where all level shifts vanish and the partial widths and level energies are identical to the observed parameters. This approach simplifies the incorporation of known nuclear properties in the fitting procedure and the comparison with experimental resonance properties.

## 2. Theory constraints: *ab initio* methods

*Ab initio* methods – defined here as methods that provide a quasi-exact solution to the many-body Schrödinger equation, such as the hyperspherical harmonic expansion (HH) and Green’s function Monte Carlo (GFMC) methods, or that express observables in terms of a controlled expansion, such as effective field theory – play two critical roles. Two reactions discussed in this review,  $p+p \rightarrow d+e^++\nu_e$  and  ${}^3\text{He}+p \rightarrow {}^4\text{He}+e^++\nu_e$ , are presently beyond the reach of experiment. Thus we are entirely dependent on theory for the corresponding S-factors. The convincing demonstration that the rate for  $p+p \rightarrow d+e^++\nu_e$  can be calculated to a precision of  $\lesssim 1\%$  is one of the important achievements of *ab initio* nuclear theory, as described in Sec. III.

Furthermore, *ab initio* methods potentially could be applied to all other reactions in the pp chain (and, farther in the future, to the CNO bi-cycle) to provide a more reliable basis for extrapolating data. One of the impressive examples of progress to date, the agreement between data for  $d(p,\gamma){}^3\text{He}$  and theory (calculations employing variational HH wave functions in combination with an electromagnetic current operator with both one- and two-body components), is discussed in Sec. IV and illustrated in Fig. 3.

*Ab initio* methods break into two broad categories, potential-based calculations and effective field theory expansions. The former are distinguished from model-based methods discussed in Sec. II.C.1 in two regards. First, they use a realistic interaction that fits two-body scattering data in detail, as well as certain bound-state properties of the lightest nuclei. Thus the interaction has both a rich operator structure and an explicit treatment of the short-distance repulsive core. Second, they

combine this potential,

$$H_A = \sum_{i=1}^A t_i + \sum_{i<j}^A v_{ij}^{\text{phen}} + \sum_{i<j<k}^A v_{ijk}^{\text{phen}}, \quad (18)$$

with numerical techniques that can accurately treat an interaction of such complexity and with such disparate spatial scales, producing a quasi-exact solution of the many-body Schrödinger equation. The form of the three-body potential in Eq. (18), which contributes for  $A \geq 3$  but plays a less important role than the dominant two-body potential, is typically taken from theory. Once the wave functions are obtained, they can be combined with electroweak transition operators to produce estimates of observables. The transition operators include both one-body terms determined from the coupling of the single nucleon to the electroweak current, and two-body corrections, typically derived from one-boson-exchange diagrams. Examples of the potential approach, including discussions of the associated issue of transition operators, are found in Secs. III, IV, and VII.

The second approach is based on effective field theory (EFT). EFTs exploit the gap between the long-wavelength properties of nuclei that govern nuclear reactions near threshold, and the short-range interactions in the NN potential that make an exact solution of the Schrödinger equation technically difficult. The calculations are restricted to a limited basis describing the long-wavelength behavior, and the omitted degrees of freedom are absorbed into effective operators that can be organized in powers of  $Q/\Lambda_{\text{cut}}$ , where  $Q$  is the momentum characterizing the physics of interest and  $\Lambda_{\text{cut}}$  is the momentum characterizing the omitted physics. If carried out completely, no simplification is achieved, because the low-momentum EFT Lagrangian has an infinite number of such operators. EFT becomes useful when there is a significant gap between  $Q$  and  $\Lambda_{\text{cut}}$ , so that only a small number of the effective operators corresponding to the leading powers in  $Q/\Lambda_{\text{cut}}$  must be retained, to reproduce long-wavelength observables to a specified accuracy. The coefficients of the leading operators can then be determined by fitting data: if enough constraints exist to fix all of the needed low-energy constants, then accurate predictions can be made about new processes. The application of this method to  $p+p \rightarrow d+e^++\nu_e$  and  ${}^3\text{He} + p \rightarrow {}^4\text{He} + e^+ + \nu_e$  is described in some detail in Secs. III and VII, respectively. This approach can also be applied to  $d(p,\gamma){}^3\text{He}$ .

One of the potential-based methods now being developed for reactions should be highlighted because of its established success in predicting bound-state properties throughout most of the  $1p$  shell. The quantum Monte Carlo (QMC) approach combines the variational Monte Carlo (VMC) and GFMC methods (Pieper, 2008). The VMC calculation produces an approximate wave function by minimizing the energy of a variational wave function including elaborate two- and three-body correlations. The GFMC method is then employed to make the

needed small improvements to the VMC result required for a true solution to the Schrödinger equation.

The GFMC method requires a local potential, so its use has been restricted to the Argonne  $v_{18}$  NN potential (Wiringa *et al.*, 1995), denoted AV18. There is also an important three-nucleon interaction, determined by fitting 17 bound- and narrow-state energies for  $A \leq 8$  (Pieper *et al.*, 2001). The high quality of the QMC predictions for energies of bound states and sharp resonances in nuclei with  $A \leq 12$ , and for charge radii, electromagnetic moments, and other observables, has been thoroughly established (Pieper *et al.*, 2001, 2002, 2004).

Recent VMC-based calculations of capture cross sections using realistic potentials (Marcucci *et al.*, 2006; Nollett, 2001; Nollett *et al.*, 2001) represent a first step in extending the QMC program to reactions. These calculations used VMC wave functions for bound states in  $^3\text{H}$ ,  $^3\text{He}$ ,  $^4\text{He}$ ,  $^6\text{Li}$ ,  $^7\text{Li}$ , and  $^7\text{Be}$ , as well as an exact deuteron. Initial states in the reactions  $d(\alpha, \gamma)^6\text{Li}$ ,  $^3\text{H}(\alpha, \gamma)^7\text{Li}$ , and  $^3\text{He}(\alpha, \gamma)^7\text{Be}$  were computed as products of the reactant VMC wave functions and a correlation, matched to experimental phase shifts, to describe the relative motion of the interacting nuclei. Work has focused, in particular, on building in the proper long-range clustering of the final states, as this is important in reproducing the proper energy dependence of S-factors. Results for  $^3\text{H}(\alpha, \gamma)^7\text{Li}$  closely match the measured absolute S-factor. However, the prediction for  $^3\text{He}(\alpha, \gamma)^7\text{Be}$  lies below the data by about a factor of 1.3 to 1.45.

Better QMC calculations of those and other cross sections are possible. VMC wave functions were used partly because of the technical difficulty of computing quantities off-diagonal in the energy eigenstates using GFMC; this problem has now been solved, and electroweak matrix elements between discrete levels have been computed (Marcucci *et al.*, 2008; Pervin *et al.*, 2007). Scattering wave functions are also now being computed directly from the NN+NNN potential, with successful calculations of low-energy neutron- $^4\text{He}$  scattering wave functions reported by Nollett *et al.* (2007) using particle-in-a-box formulations of the QMC methods.

While we have used the QMC approach to illustrate the progress in quasi-exact approaches, there are other important efforts underway to compute cross sections beyond  $A=4$  from realistic NN potentials. Examples include the *ab initio* no-core shell model both alone (Navrátil *et al.*, 2006a,b) and in combination with the resonating group method (Quaglioni and Navrátil, 2009); the Lorentz integral transform method (Efros *et al.*, 2007); and the unitary correlation operator method (Neff and Feldmeier, 2008). The hyperspherical harmonics method, which will be discussed in connection with the  $d(p, \gamma)^3\text{He}$  and hep reactions, is also being extended to heavier systems.

We anticipate that quasi-exact methods will soon be practical for many scattering and capture processes in light nuclei. Calculations based on exact solutions of accurate interactions will predict not only the energy de-

pendences of solar fusion reactions but also absolute cross sections. Theory may thus provide a firm basis for validating and extrapolating data and for resolving systematic differences between measured data sets.

### 3. Adopted procedures

These are the procedures we adopt for fitting and extrapolating data:

- In two cases,  $p+p \rightarrow d+e^++\nu_e$  and  $^3\text{He}+p \rightarrow ^4\text{He}+e^++\nu_e$ , S-factor estimates depend entirely on theory. The goal in such cases should be the application of both potential and EFT or EFT-inspired methods, yielding consistent results with quantified uncertainties. As detailed in Sec. III, one is close to achieving this for  $S_{11}$ , with two methods providing consistent answers and uncertainties of  $\lesssim 1\%$ , and with a third method (EFT) potentially reaching similar precision, if ancillary measurements can better determine the needed low-energy constant. In the case of  $S_{\text{hep}}$ , a less critical cross section, the further developments of methods like Green's function Monte Carlo will provide an important check on the current state-of-the-art, a variational calculation in which a correlated hyperspherical harmonics expansion was used.
- In cases where data exist through the energy range of astrophysical interest, much can be done independent of theory. A polynomial representation of  $S(E)$ , e.g., values for  $S(0)$ ,  $S'(0)$ , and  $S''(0)$ , could be obtained by directly fitting the data. However, as  $S(E)$  represents the bare cross section, theory may still be needed to remove the effects of screening in the terrestrial target. As detailed above, there is some confidence that theory determines the functional form of the screening (Eq. (15)), so that such effects can be subtracted given sufficient low-energy data to fix the numerical value of the screening potential (which theory appears to predict less reliably). This issue arises in  $S_{33}$ .
- In cases where data exist but are not adequate to fully characterize the cross section in the region of astrophysical interest, we advocate the use of fitting functions motivated by theory to extrapolate data, with data determining the normalization. To the extent that well-justified models differ in their predictions, additional uncertainties must be assigned to  $S(0)$  and its derivatives. Judgment is required in assessing the models and determining how they should be applied, e.g., the range in  $E$  over which a given model is likely to be valid. Each working group was asked to consider such issues, and to present and justify the procedures it followed to assess associated fitting uncertainties.

#### D. Treatment of uncertainties

The treatment of uncertainties – the statistical and systematic errors in data and the impact of imperfect theory in fitting and extrapolating data – is discussed in some detail in the Appendix. There are cases where several high-quality data sets exist, each with errors that presumably reflect both the statistical and evaluated systematic uncertainties of the experiment, that disagree by more than the error bars would indicate. In treating such cases, an error-bar “inflation factor” is commonly introduced, to account for the apparent underestimation of systematic errors. We have done so following Particle Data Group (PDG) conventions (Amsler *et al.*, 2008), with one minor modification described in the Appendix. Uncertainties quoted in this review correspond to one standard deviation (68% confidence level).

As discussed in the Appendix, there are alternative prescriptions for apportioning the unidentified systematics – and thus the inflations – among the experiments that disagree. However our group concluded that the PDG procedure was the best choice both for technical reasons and because the procedure is widely used in the physics community.

### III. THE pp REACTION

The rate for the initial reaction in the pp chain,  $p+p \rightarrow d + e^+ + \nu_e$ , is too small to be measured in the laboratory. Instead, this cross section must be calculated from standard weak interaction theory.

As in Solar Fusion I, the adopted value and range for the logarithmic derivative is taken from Bahcall and May (1969),

$$S'_{11}(0) = S_{11}(0) (11.2 \pm 0.1) \text{ MeV}^{-1}. \quad (19)$$

This result is in excellent agreement with those obtained from linear fits to the modern potential-model calculations of Schiavilla *et al.* (1998), which yield values of  $11.14 \text{ MeV}^{-1}$  and  $11.16 \text{ MeV}^{-1}$  for the full and impulse-approximation calculations. As the Gamow peak energy is  $\sim 6 \text{ keV}$  for temperatures characteristic of the Sun’s center, the linear term generates a  $\lesssim 8\%$  correction to the  $E = 0$  value. The 1% uncertainty in Eq. (19) corresponds to a  $\lesssim 0.1\%$  uncertainty in the total reaction rate. This is negligible compared to other uncertainties described below. Therefore, in the following, we focus on  $S_{11}(0)$ .

At zero relative energy  $S_{11}(0)$  can be written (Bahcall and May, 1968, 1969),

$$S_{11}(0) = 6\pi^2 m_p \alpha \ln 2 \frac{\bar{\Lambda}^2}{\gamma^3} \left( \frac{G_A}{G_V} \right)^2 \frac{f_{pp}^R}{(ft)_{0^+ \rightarrow 0^+}}, \quad (20)$$

where  $\alpha$  is the fine-structure constant;  $m_p$  is the proton mass;  $G_V$  and  $G_A$  are the usual Fermi and axial-vector weak coupling constants;  $\gamma = (2\mu B_d)^{1/2} = 0.23161 \text{ fm}^{-1}$

is the deuteron binding wave number;  $\mu$  is the proton-neutron reduced mass;  $B_d$  is the deuteron binding energy;  $f_{pp}^R$  is the phase-space factor for the pp reaction with radiative corrections;  $(ft)_{0^+ \rightarrow 0^+}$  is the  $ft$  value for superallowed  $0^+ \rightarrow 0^+$  transitions; and  $\bar{\Lambda}$  is proportional to the transition matrix element connecting the pp and deuteron states.

Inserting the current best values, we find

$$S_{11}(0) = 4.01 \times 10^{-25} \text{ MeV b} \left( \frac{(ft)_{0^+ \rightarrow 0^+}}{3071 \text{ s}} \right)^{-1} \times \left( \frac{G_A/G_V}{1.2695} \right)^2 \left( \frac{f_{pp}^R}{0.144} \right) \left( \frac{\bar{\Lambda}^2}{7.035} \right). \quad (21)$$

We now discuss the best estimates and the uncertainties for each of the factors appearing in Eq. (21).

We take  $(ft)_{0^+ \rightarrow 0^+} = (3071.4 \pm 0.8) \text{ s}$ , the value for superallowed  $0^+ \rightarrow 0^+$  transitions that has been determined from a comprehensive analysis of experimental rates corrected for radiative and Coulomb effects (Hardy and Towner, 2009). This value determines the weak mixing matrix element  $|V_{ud}| = 0.97418(27)$ , the value adopted by the PDG (Amsler *et al.*, 2008). This  $ft$  value is also consistent with  $(3073.1 \pm 3.1) \text{ s}$  used in Solar Fusion I.

For  $G_A/G_V$ , we use the PDG value  $G_A/G_V = 1.2695 \pm 0.0029$  which is consistent with  $1.2654 \pm 0.0042$  used in Solar Fusion I.

For the phase-space factor  $f_{pp}^R$ , we have taken the value without radiative corrections,  $f_{pp} = 0.142$  (Bahcall and May, 1969) and increased it by 1.62% to take into account radiative corrections to the cross section (Kurylov *et al.*, 2003). The main source of error is from neglected diagrams in which the lepton exchanges a weak boson and a photon with different nucleons. These diagrams are estimated to modify  $f_{pp}^R$  by  $\sim 0.1\%$ , based on scaling the similar nucleus-dependent correction in superallowed  $\beta$  decay (Kurylov *et al.*, 2003). It would be useful to check this estimate through direct computations. We adopt  $f_{pp}^R = 0.144(1 \pm 0.001)$ , which is consistent with  $0.144(1 \pm 0.005)$  used in Solar Fusion I.

The dominant uncertainty in  $S_{11}(0)$  comes from the normalized Gamow-Teller (GT) matrix element  $\bar{\Lambda}$ . A great deal of theoretical work since Solar Fusion I has focused on reducing this uncertainty. In Solar Fusion I  $\bar{\Lambda}$  was decomposed into  $\bar{\Lambda} = \Lambda(1 + \delta)$ , where  $\Lambda$  represents the contribution of the one-body transition operator and  $\Lambda\delta$  that from two-body corrections.  $\Lambda$  thus involves an evaluation of the Gamow-Teller operator between the initial-state pp wave function and the final-state deuteron wave function.  $\Lambda^2 = 6.92(1 \pm 0.002^{+0.014}_{-0.009})$  was adopted, where the first and second uncertainties reflect, respectively, variations in empirical values of the deuteron and low-energy pp scattering parameters, and the model dependence of the nuclear potential (Kamionkowski and Bahcall, 1994). The value and uncertainty of the exchange current contribution,  $\delta = 0.01^{+0.02}_{-0.01}$ , was determined from the range of values of published calculations,

following the conservative recommendation of Bahcall and Pinsonneault (1992).

Two major steps have contributed to reducing the uncertainty on  $\bar{\Lambda}$  since Solar Fusion I. The first is a much deeper understanding of the correlation between the uncertainties in  $\Lambda$  and  $\delta\Lambda$ : the overall uncertainty in  $\bar{\Lambda}$  can be described by a universal parameter that can be fixed by a single measurement. The study of Schiavilla *et al.* (1998) demonstrated this phenomenologically in the context of potential-model approaches, while later analysis via EFT provided a more formal justification (Butler *et al.*, 2001; Park *et al.*, 2003). The second step is the use of the precisely known tritium  $\beta$  decay rate  $\Gamma_\beta^T$ , as first proposed by Carlson *et al.* (1991), to fix this universal parameter. This has been done in both potential models (Schiavilla *et al.*, 1998) and in the hybrid EFT approach (Park *et al.*, 2003). We briefly describe these developments.

### A. Progress in potential models

The most elaborate calculation for the pp fusion process in the potential-model approach (see Sec. II.C.2) was carried out by Schiavilla *et al.* (1998). A comparison of the results for five representative modern potentials – potentials designed to accurately reproduce nucleon-nucleon scattering data – yielded  $\Lambda^2 = 6.975 \pm 0.010$ . This study demonstrated the importance of using the tritium  $\beta$  decay rate to constrain the two-body GT transition operator. (Both the Fermi and GT operators contribute to tritium  $\beta$  decay, but the former can be reliably calculated because of the conserved vector current and the smallness of isospin breaking effects,  $\sim 0.06\%$ .) If one adjusts the uncertain strength of the exchange current so that the tritium  $\beta$  decay rate is reproduced, the variation in  $S_{11}(0)$  that otherwise would come from the choice of the phenomenological potential is largely removed. Predictions for five representative high-precision phenomenological potentials fall in a narrow interval  $7.03 \lesssim \bar{\Lambda}^2 \lesssim 7.04$  (Schiavilla *et al.*, 1998).

We note two other sources of model dependence that contribute to the overall uncertainty in  $\bar{\Lambda}$ . First, as three-body potentials and currents contribute to the tritium  $\beta$  decay rate, uncertainties in modeling such effects will influence the extracted constraint on the two-body currents needed for  $S_{11}(0)$ . The best estimate of the consequences of this uncertainty for  $S_{11}(0)$ ,  $\sim 0.8\%$ , comes from the chiral (or pionful) EFT\* approach described below. Second, the experimental uncertainties in the effective range parameters for nucleon-nucleon scattering will propagate to  $\bar{\Lambda}$ . We have assigned a 0.5% uncertainty in  $\bar{\Lambda}^2$  to this source, pending future work in EFT to better quantify this uncertainty. By adding in quadrature these uncertainties of 0.8% and 0.5% and the smaller uncertainty associated with the above potential range,  $\bar{\Lambda}^2 = 7.035 \pm 0.005$ , we obtain the potential model esti-

mate

$$\bar{\Lambda}^2 = 7.035(1 \pm 0.009). \quad (22)$$

### B. Progress in effective field theory (EFT)

The application of EFT, described in Sec. II.C.2, to the calculation of the pp fusion rate (and several other electroweak processes in light nuclei) is one of the notable developments since Solar Fusion I. There have been two lines of EFT calculations of pp fusion, described below.

#### 1. Hybrid EFT (EFT\*)

Electroweak nuclear transitions in EFT

$$\mathcal{M}^{\text{EFT}} = \langle \Psi_f^{\text{EFT}} | \sum_i^A \mathcal{O}_i^{\text{EFT}} + \sum_{i<j}^A \mathcal{O}_{ij}^{\text{EFT}} | \Psi_i^{\text{EFT}} \rangle, \quad (23)$$

require initial and final nuclear wave functions and the transition operators to be derived from EFT. However, this has not yet been achieved in EFT with dynamical pions for pp fusion. Instead, a hybrid approach (Park *et al.*, 2003) called EFT\* (or MEEFT) has been developed in which transition operators are taken from chiral perturbation theory ( $\chi$ PT), but sandwiched between phenomenological wave functions,  $\Psi_i^{\text{phen}}$  and  $\Psi_f^{\text{phen}}$ , generated by a potential model. As discussed below, this approach is a substantial improvement over the earlier calculation of Park *et al.* (1998).

For the low-energy GT transition that governs pp fusion, the one-body transition operators  $\mathcal{O}_i^{\text{EFT}}$  are well known, while the two-body operators  $\mathcal{O}_{ij}^{\text{EFT}}$  contain only one unknown low-energy constant (LEC). This LEC, denoted by  $\hat{d}^R$ , parameterizes the strength of contact-type four-nucleon coupling to the axial current. Park *et al.* (2003) chose to determine  $\hat{d}^R$  from the tritium  $\beta$ -decay rate  $\Gamma_\beta^T$ . The fact that  $\Psi^{\text{phen}}$  is not exactly an eigenstate of the EFT Hamiltonian can in principle be a source of concern, but it is plausible that the mismatch affects primarily the short-distance behavior of the wave function, so that the procedure of fixing the relevant LEC(s) to data can remove most of the inconsistency: While  $\mathcal{L}_{\chi\text{PT}}$  by construction is valid only well below  $\Lambda_{\text{QCD}}$ , the use of the phenomenological Hamiltonian, Eq. (18), introduces high momentum components above  $\Lambda_{\text{QCD}}$ . To test this procedure, one can introduce a cutoff  $\Lambda_{\text{NN}}$  to eliminate high-momentum components in the two-nucleon relative wave function, fitting the LEC as a function of this parameter. One expects, if the fitting of the LEC reasonably accounts for missing or inconsistent short-distance physics, little  $\Lambda_{\text{NN}}$  dependence would be found in the calculated pp fusion rate. The residual dependence on  $\Lambda_{\text{NN}}$ , when this cutoff is varied over a physically reasonable range, provides a measure of the model independence of an EFT\* calculation.

The Park *et al.* (2003) calculation included up to next-to-next-to-next-to-leading order ( $N^3LO$ ) terms in chiral expansion, and after fitting  $\hat{d}^R$  to  $\Gamma_\beta^T$ , yielded  $\bar{\Lambda}^2 = 7.03(1 \pm 0.008)$ . The uncertainty was estimated from the changes in  $\bar{\Lambda}^2$  when  $\Lambda_{NN}$  is varied over an energy range typical of vector meson masses, 500 to 800 MeV. A rough estimate based on higher order chiral contributions was also made. Specifically, the contributions of the first four chiral orders to  $\bar{\Lambda}$  follow the pattern (1+0.0%+0.1%+0.9%), while the fifth-order term is estimated to be  $\sim 0.4\%$ . We assume that the second- and third-order terms are accidentally small, while the fourth- and fifth-order terms reflect the convergence of the expansion in  $m_\pi/\Lambda_{QCD} \sim 1/7$ . Three-body currents contribute in sixth order. We therefore use the size of the fifth-order term, 0.4%, as a measure of the uncertainty due to neglected higher order contributions (including three-body currents).

Full EFT calculations that use  $\Psi^{EFT}$  instead of  $\Psi^{phen}$ , thus eliminating operator-wave function inconsistencies, are an important goal. Progress toward this goal includes recent constructions of EFT-based nuclear interactions; see, *e.g.*, Epelbaum (2006) and Gazit *et al.* (2009).

## 2. Pionless EFT

This approach can be applied to processes where the characteristic momentum  $p$  is much smaller than the pion mass  $m_\pi$  (Bedaque *et al.*, 1999; Chen *et al.*, 1999; Kaplan *et al.*, 1996), which is the case for solar pp fusion. Pions can then be integrated out, so that all nucleon-nucleon interactions and two-body currents are described by point-like contact interactions with a systematic expansion in powers of  $p/m_\pi$ . The one- and two-body contributions individually depend on the momentum cut-off but the sum does not. Thus,  $\Lambda$  and  $\Lambda\delta$  in pp fusion are correlated. In pionless EFT only one two-body current (with coupling  $L_{1,A}$ ) is needed in the description of deuteron weak breakup processes, through next-to-next-to-leading order (NNLO) in the  $p/m_\pi$  expansion (Butler *et al.*, 2001). This two-body current is a GT operator. Other two-body currents are either missing due to conservation of the vector current, or involve matrix elements suppressed due to the pseudo-orthogonality of the initial- and final-state wave functions. This means the universal number  $L_{1,A}$  encodes the two-body contributions for all low-energy weak deuteron breakup processes, so that a single measurement will fix the rates of all such processes. The other approaches discussed above share this feature.

The computation of  $\bar{\Lambda}$  in pionless EFT was carried out to the second order by Kong and Ravndal (2001) and Ando *et al.* (2008) and then to the fifth order by Butler and Chen (2001). Constraints on  $L_{1,A}$  from two nucleon systems (Butler *et al.*, 2002; Chen *et al.*, 2003) yield  $\bar{\Lambda}^2 = 6.99 \pm 0.21$ . The MuSun experiment (Andreev *et al.*, 2008) is taking data on  $\mu$  capture on deuterium.

The experimental goal is to constrain  $\bar{\Lambda}^2$  to  $\lesssim 1.5\%$  for pionless EFT (Chen *et al.*, 2005) and chiral EFT\* (Ando *et al.*, 2002).

## 3. Comment on Mosconi *et al.*

Mosconi *et al.* (2007) have compared  $\nu$ -d reaction cross sections for various models that differ in their treatments of two-body transition operators, concluding from this comparison that the results obtained in potential models, EFT\*, and pionless EFT have uncertainties as large as 2-3%. Although they address only  $\nu$ -d cross sections, a comment is in order here because this process is closely related to that for pp fusion. Mosconi *et al.* (2007) reach their conclusions by examining the scatter of unconstrained calculations of the  $\nu$ -d cross section. However, all state-of-the-art calculations use  $\Gamma_\beta^T$  to reduce two-body current and other uncertainties, as we have detailed here. Once this requirement is imposed, the scatter in the calculated value of  $\nu$ -d cross sections is significantly reduced.

## C. Summary

We have seen that the various approaches discussed above yield accurate and very consistent values for  $\bar{\Lambda}^2$ . The remaining factors in Eq (18) also have uncertainties, but these are common to all the calculations. Adding all the uncertainties in quadrature, we find that the current best estimates for  $S_{11}(0)$  are

$$\begin{aligned} 4.01(1 \pm 0.009) \times 10^{-25} \text{ MeV b} & \quad \text{potential models} \\ 4.01(1 \pm 0.009) \times 10^{-25} \text{ MeV b} & \quad \text{EFT*} \\ 3.99(1 \pm 0.030) \times 10^{-25} \text{ MeV b} & \quad \text{pionless EFT.} \end{aligned} \quad (24)$$

The larger uncertainty in the pionless EFT result is due to the relatively weak constraints on  $L_{1,A}$  that can be imposed within two-nucleon systems but, as mentioned, this situation will soon be improved. The agreement of the central values obtained in the potential model and EFT\* indicates the robustness of the results as long as the two-body current is constrained by tritium  $\beta$  decay. Meanwhile, the agreement of the error estimates in the two approaches is primarily due to the fact that, as explained above, the dominant part of the uncertainty has been estimated using the same argument. Based on the result obtained in the potential model and EFT\*, we adopt as the recommended value

$$S_{11}(0) = 4.01(1 \pm 0.009) \times 10^{-25} \text{ MeV b.} \quad (25)$$

We adopt the Bahcall and May (1969) value for  $S'_{11}(0)$

$$S'_{11}(0) = S_{11}(0)(11.2 \pm 0.1) \text{ MeV}^{-1}, \quad (26)$$

Bahcall and May (1969) also estimated dimensionally that  $S''_{11}(0)$  would enter at the level of  $\sim 1\%$ , for temperatures characteristic of the solar center. As this is now



comparable to the overall error in  $S_{11}$ , we recommend that a modern calculation of  $S''_{11}(0)$  be undertaken.

#### IV. THE $d(p,\gamma)^3\text{He}$ RADIATIVE CAPTURE REACTION

The radiative capture of protons on deuterium is the second reaction occurring in the pp chain. Because this reaction is so much faster than the pp weak rate discussed in the previous section, it effectively instantaneously converts deuterium to  $^3\text{He}$ , with no observable signature. Thus uncertainties in its rate have no consequences for solar energy generation. By comparing the pp and  $d(p,\gamma)^3\text{He}$  rates, one finds that the lifetime of a deuterium nucleus in the solar core is  $\sim 1$  s, and that the equilibrium abundance of deuterium relative to H is maintained at  $\sim 3 \times 10^{-18}$ .

However, the  $d(p,\gamma)^3\text{He}$  reaction plays a more prominent role in the evolution of protostars. As a cloud of interstellar gas collapses on itself, the gas temperature rises to the point of  $d(p,\gamma)^3\text{He}$  ignition,  $\sim 10^6$  K. The main effect of the onset of deuterium burning is to slow down the contraction and, in turn, the heating. As a consequence, the lifetime of the proto-star increases and its observational properties (surface luminosity and temperature) are frozen until the original deuterium is fully consumed (Stahler, 1988). Due to the slow evolutionary timescale, a large fraction of observed proto-stars are in the d-burning phase, while only a few are found in the earlier, cooler, rapidly evolving phase. A reliable knowledge of the rate of  $d(p,\gamma)^3\text{He}$  down to a few keV (the Gamow peak in a proto-star) is of fundamental importance for modeling proto-stellar evolution.

The pd reaction also plays an important role in Big Bang nucleosynthesis, which begins when the early universe has cooled to a temperature of  $\sim 100$  keV. The uncertainty in the pd reaction in the relevant energy window (25-120 keV) propagates into uncertainties in the deuterium,  $^3\text{He}$  and  $^7\text{Li}$  abundances, scaling roughly as

$$\frac{d}{\text{H}} \propto R_{\text{pd}}^{-0.32} \quad \frac{^3\text{He}}{\text{H}} \propto R_{\text{pd}}^{0.38} \quad \frac{^7\text{Li}}{\text{H}} \propto R_{\text{pd}}^{0.59}, \quad (27)$$

where  $R_{\text{pd}}$  is the value of  $S_{12}$  relative to the fiducial value in Cyburt (2004). Thus a 10% error in the pd capture rate propagates into roughly 3.2%, 3.8% and 5.9% uncertainties in the light element primordial abundances, d,  $^3\text{He}$  and  $^7\text{Li}$ , respectively.

##### A. Data sets

The extensive experimental data sets for pd radiative capture include total cross sections and spin polarization observables at center-of-mass energies  $E$  ranging from several tens of MeV to a few keV, covering all the relevant astrophysical energies. In the regime  $E \lesssim 2$  MeV (below the deuteron breakup threshold), the relevant experimental data include Bailey *et al.* (1970); Casella *et al.*

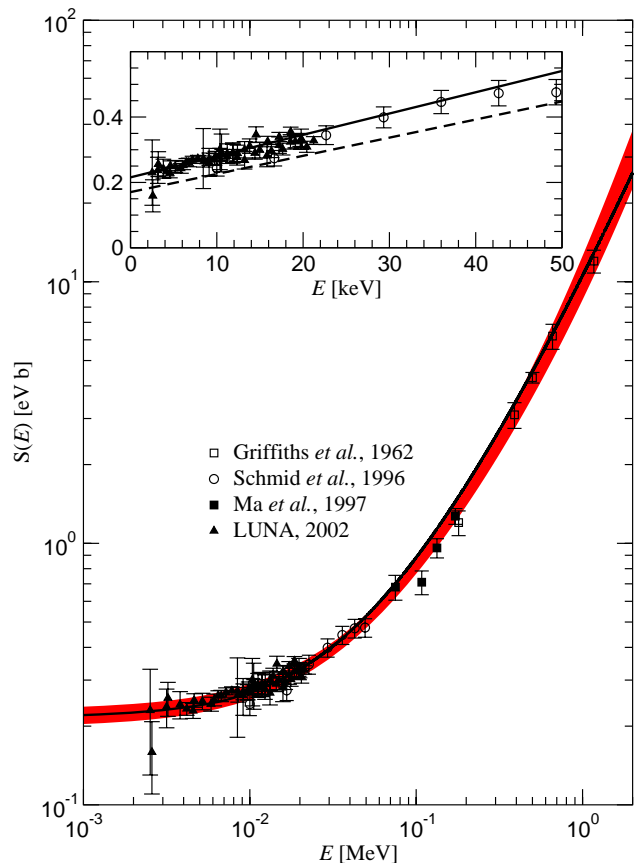


FIG. 3 (Color online) The astrophysical  $S_{12}$ -factor datasets (Casella *et al.*, 2002; Griffiths *et al.*, 1962; Ma *et al.*, 1997; Schmid *et al.*, 1996) are plotted together with theoretical predictions of Marcucci *et al.* (2005). The solid line represents the “full” theoretical calculation, while the red band represents the 68% lower and upper bounds of the adopted quadratic best fit to the four experimental datasets (see text and Eq. (29) for more explanation). In the insert, the  $S_{12}$ -factor of the  $^2\text{H}(p,\gamma)^3\text{He}$  reaction in the energy range 0-50 keV, obtained with the Argonne  $v_{18}$  two-nucleon and Urbana IX three-nucleon Hamiltonian model in the impulse approximation (dashed line) and with inclusion of interaction currents (solid line), is compared with the experimental results.

(2002); Griffiths *et al.* (1963, 1962); Ma *et al.* (1997); Schmid *et al.* (1995, 1996). The Griffiths *et al.* (1963) and Bailey *et al.* (1970) low energy data may be  $\sim 15\%$  too high because of the use of incorrect stopping powers (Ma *et al.*, 1997; Schmid *et al.*, 1995, 1996). Also, the Schmid *et al.* (1995, 1996) data sets may have not propagated their energy-dependent systematic uncertainties. In Fig. 3, the data for  $S_{12}$  used for the best fit in Sec. IV.C are plotted together with theoretical predictions of Marcucci *et al.* (2005). The observed linear dependence of  $S_{12}$  on  $E$  at low energies, as well as the angular distributions of the cross section and polarization observables, indicate that the  $d(p,\gamma)^3\text{He}$  reaction proceeds predominantly through s- and p-wave capture, induced, respectively, by magnetic

( $M1$ ) and electric ( $E1$ ) dipole transitions. The  $M1$  transitions (proceeding through  ${}^2S_{1/2}$  and  ${}^4S_{3/2}$  pd channels) are especially interesting, as the one-body  $M1$  operator cannot connect the main s-state components of the pd and  ${}^3\text{He}$  wave functions at low energies. Because of this “pseudo-orthogonality” only the small components of the wave functions contribute in the impulse approximation (IA). In contrast, as exchange-current operators are not similarly hindered, their matrix elements are exceptionally large relative to those obtained with the one-body  $M1$  operator. The suppression of matrix elements calculated in the IA and their consequent enhancement by exchange-current contributions are a feature common to other  $M1$ -induced processes in  $A=3$  and 4 systems, such as the nd and  $n{}^3\text{He}$  radiative captures at thermal neutron energies.

## B. Theoretical studies

The most extensive and recent theoretical studies of the  $d(p,\gamma){}^3\text{He}$  reaction at low energies have been carried out by Marcucci *et al.* (2005). The calculated  $S_{12}$ , shown in Fig. 3, is in excellent agreement with data. To describe the pd continuum and  ${}^3\text{He}$  bound states, these authors used variational wave functions built in a correlated-hyperspherical-harmonics (CHH) basis for a Hamiltonian consisting of the Argonne  $v_{18}$  two-nucleon (Wiringa *et al.*, 1995) and the Urbana IX (Pudliner *et al.*, 1995) three-nucleon potentials. This Hamiltonian is known to reproduce a variety of three-nucleon bound- and scattering-state properties, including binding energies, charge radii, elastic and inelastic cross sections, and low-energy polarization observables, while the accuracy of the CHH variational method is comparable to that of other quasi-exact methods (Nogga *et al.*, 2003).

The nuclear electromagnetic current consists of one-body terms (the IA currents), originating from the convection and spin-magnetization currents of individual protons and neutrons, and two- and three-body exchange currents, constructed from the corresponding potentials by a procedure that preserves current conservation (CC). The method by which this is achieved has been improved over the years (Riska, 1984; Schiavilla *et al.*, 1998), and its latest implementation is discussed at length by Marcucci *et al.* (2005). The currents are still model dependent, of course, as CC places no constraints on their transverse components.

The calculated value for  $S_{12}(0)$  including exchange-current contributions is 0.219 eV b, in excellent agreement with the value extrapolated from the LUNA measurements ( $0.216 \pm 0.010$  eV b), and evaluations by Cyburt (2004) ( $0.227 \pm 0.014$  eV b), Descouvemont *et al.* (2004) ( $0.223 \pm 0.007$  eV b) and Serpico *et al.* (2004) ( $0.214 \pm 0.007$  eV b). In Descouvemont *et al.* (2004) systematic and statistical errors are combined before following a standard fitting procedure. However, as this artificially reduces the impact of systematic errors, their cited

uncertainties have been underestimated. Serpico *et al.* (2004) properly separates systematic and statistical errors in their treatment, but do not cite 68% confidence limits, also yielding an error that is too small. The evaluation by Cyburt (2004) separates systematic and statistical uncertainties and cites errors consistent with 68% confidence limits, yielding realistic uncertainties.

## C. Summary

In this report, we evaluate the Casella *et al.* (2002), Griffiths *et al.* (1962), Schmid *et al.* (1996) and Ma *et al.* (1997) data, determining  $S_{12}(E)$  as a function of the center-of-mass energy by fitting the four data sets by a quadratic polynomial in  $E$ . We adopt this fitting procedure, despite our earlier arguments favoring fitting formulas that are motivated by theory, because the energy window of interest is fully covered by the experiments. This yields

$$S_{12}(0) = 0.214_{-0.016}^{+0.017} \text{ eV b}, \quad (28)$$

in agreement with previous evaluations. The error is larger here, because of the exclusion of the Bailey *et al.* (1970) data.

We also determined the 68% upper and lower bounds for the quadratic parameterizations, valid for  $E \lesssim 1$  MeV, the range spanned by the data we considered. The results are (see also Fig. 3)

$$\begin{aligned} S_{12}^{\text{lower}}(E) &= 0.1983 + 5.3636 \left( \frac{E}{\text{MeV}} \right) \\ &\quad + 2.9647 \left( \frac{E}{\text{MeV}} \right)^2 \text{ eV b} \\ S_{12}^{\text{best}}(E) &= 0.2145 + 5.5612 \left( \frac{E}{\text{MeV}} \right) \\ &\quad + 4.6581 \left( \frac{E}{\text{MeV}} \right)^2 \text{ eV b} \\ S_{12}^{\text{upper}}(E) &= 0.2316 + 5.7381 \left( \frac{E}{\text{MeV}} \right) \\ &\quad + 6.5846 \left( \frac{E}{\text{MeV}} \right)^2 \text{ eV b}. \end{aligned} \quad (29)$$

The results determine the S-factor and its uncertainty in the vicinity of the solar Gamow peak. In particular, for a temperature characteristic of the Sun’s center,  $1.55 \times 10^7$  K,

$$S_{12}(E_0 = 6.64 \text{ keV}) = 0.252 \pm 0.018 \text{ eV b}, \quad (30)$$

so that the estimate uncertainty is  $\sim 7.1\%$ .

## V. THE ${}^3\text{He}({}^3\text{He},2p){}^4\text{He}$ REACTION

The  ${}^3\text{He}({}^3\text{He},2p){}^4\text{He}$  reaction is the termination of the ppI cycle and thus, as Solar Fusion I describes in more

detail, uncertainties in this cross section played a prominent role in early speculations about a nuclear astrophysics solution to the solar neutrino problem. As an increase in  $S_{33}(E)$  would reduce the branchings to the ppII and ppIII cycles – thus also reducing the neutrino fluxes measured by Davis – the possibility of an undiscovered narrow resonance at energies beyond the reach of early experiments was raised by Fetisov and Kopysov (1972) and Fowler (1972). This motivated efforts to measure  $S_{33}(E)$  at lower energies, and particularly stimulated the efforts of the LUNA collaboration in the 1990s to map the cross section in the solar Gamow peak (Arpesella *et al.*, 1996; Bonetti *et al.*, 1999; Greife *et al.*, 1994; Junker *et al.*, 1998). The principal result since Solar Fusion I is the completion of this program by Bonetti *et al.* (1999), extending measurements to the lower edge of the Gamow peak at 16 keV, making  $S_{33}(E)$  the most directly constrained S-factor within the pp chain.

$S_{33}(E)$  remains of significant importance, as it controls the ppI/ppII+ppIII branching ratio and thus the ratio of the pp/pep to  ${}^7\text{Be}/{}^8\text{B}$  neutrino fluxes. This ratio is important to future strategies to better constrain neutrino oscillation parameters and matter effects, through comparison of high-energy (matter influenced) and low-energy (vacuum) fluxes. The ratio of  $S_{33}$  to  $S_{34}$  enters in computing the neutrino energy losses of the Sun, and thus influences the connection between the Sun’s photon luminosity and its total energy production.

### A. Data sets and fitting

We consider data available at the time of Solar Fusion I (Arpesella *et al.*, 1996; Bacher and Tombrello, 1965; Dwarakanath and Winkler, 1971; Greife *et al.*, 1994; Junker *et al.*, 1998; Krauss *et al.*, 1987) as well two new data sets: the extreme low energy data of LUNA (Bonetti *et al.*, 1999) and results from the OCEAN experiment (Kudomi *et al.*, 2004) at energies slightly above the solar Gamow region. In order to follow the recommended fitting prescription discussed in the Appendix, one needs a detailed discussion of systematic uncertainties, particularly common mode systematics. This requirement reduces the datasets considered to just four experiments. The earliest of these originates from the Muenster group (Krauss *et al.*, 1987), followed by the two LUNA publications Junker *et al.* (1998) (which supersedes Arpesella *et al.* (1996)) and Bonetti *et al.* (1999); and the OCEAN effort Kudomi *et al.* (2004). Krauss *et al.* (1987) and Kudomi *et al.* (2004) identified a common systematic error for their respective data sets while the LUNA group provided statistical and systematic errors at each experimental energy measured. In order to use a uniform treatment we calculated an average systematic error for the latter data sets. Larger systematic errors were noted only at the lowest energies (due to uncertainties in stopping power) where the total error is dominated by statistics.

Past efforts have fit data to an S-factor including screening corrections, with the bare S-factor a polynomial up to quadratic order,

$$S_{33}(E) = S_{33}^{\text{bare}}(E) \exp\left(\frac{\pi\eta(E)U_e}{E}\right) \quad (31)$$

$$S_{33}^{\text{bare}}(E) = S_{33}(0) + S'_{33}(0)E + \frac{1}{2}S''_{33}(0)E^2.$$

Although model calculations of  $S_{33}^{\text{bare}}(E)$  are available (see, e.g., Typel *et al.* (1991)), a phenomenological representation for the bare S-factor is appropriate because the data extend to the Gamow peak. There is no need for a theoretical model to guide an extrapolation, apart from the functional form of the screening potential.

The selected data for this review cover the range from the solar Gamow peak to 350 keV, providing a limited range with which to perform a four parameter fit to the S-factor including electron screening ( $S_{33}(0)$ ,  $S'_{33}(0)$ ,  $S''_{33}(0)$ ,  $U_e$ ). We test the robustness of the fit parameters, by varying the order of the polynomial for the bare S-factor. Our results are in Table II.

TABLE II Table of fit parameters and their total errors for constant, linear, and quadratic representations of the bare S-factor.

parameter	constant	linear	quadratic
$S_{33}(0)$ (MeV b)	$4.84 \pm 0.13$	$4.95 \pm 0.15$	$5.32 \pm 0.23$
$S'_{33}(0)$ (b)	N.A.	$-1.06 \pm 0.51$	$-6.44 \pm 1.29$
$S''_{33}(0)$ (MeV $^{-1}$ b)	N.A.	N.A.	$30.7 \pm 12.2$
$U_e$ (eV)	$395 \pm 50$	$360 \pm 55$	$280 \pm 70$
$\chi^2_{\text{tot}}$	35.4	34.1	31.8
$\chi^2_{\text{tot}}/\text{dof}$	0.40	0.39	0.37

Our quadratic fit agrees quite well with the fit derived by Krauss *et al.* (1987), adopted in the reaction rate compilation of Caughlan and Fowler (1988). However, there is a significant spread in fit parameter values for the different order polynomial fits, with slight decreases in the total  $\chi^2$ . One can also see this spread in fit results from other groups (Bonetti *et al.*, 1999; Junker *et al.*, 1998; Kudomi *et al.*, 2004). This suggests that the data do not have the resolving power to accurately determine all fit parameters: there are strong correlations for the choices of data and fitting functions made here. Adopting any *single* fit will underestimate the uncertainties due to the degeneracy between parameter values. From Bayes’s theorem, assuming that the S-factor in this region ( $E < 350$  keV) can be described without cubic terms, we can derive constraints on the parameters by weighting each fit in Table II by its total  $\chi^2$  value. This method takes into account the spread from fit-to-fit. We find

$$S_{33}(0) = 5.21 \pm 0.27 \text{ MeV b} \quad (32)$$

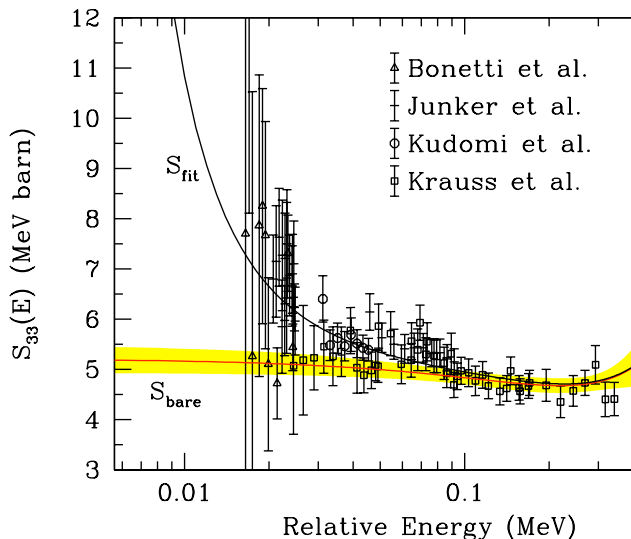


FIG. 4 (Color online) The data, the best quadratic+screening result for  $S_{33}(E)$ , and the deduced best quadratic fit (red line) and allowed range (yellow band) for  $S_{33}^{\text{bare}}$ . See text for references.

$$\begin{aligned} S'_{33}(0) &= -4.90 \pm 3.18 \text{ b} \\ S''_{33}(0) &= 22.4 \pm 17.1 \text{ MeV}^{-1} \text{ b} \\ U_e &= 305 \pm 90 \text{ eV}. \end{aligned}$$

The results reveal that existing data cannot strongly constrain all of the fitting parameters separately, and in particular do not sharply constrain  $U_e$ . To improve constraints on the screening potential one will need more precise data from near the Gamow peak, as well as new measurements up to the MeV range (with well documented systematics) to better determine the higher-order terms in the quadratic fit. New theory efforts in determining the shape of this S-factor would also be beneficial, as new low energy  ${}^3\text{He}$ - ${}^3\text{He}$  elastic scattering data could be used as an additional constraint.

However, our principal concern is the precision with which  $S_{33}^{\text{bare}}(E)$  can be determined in the vicinity of the Gamow peak, not the separate parameters. From the fit's correlation matrix we find

$$\begin{aligned} S_{33}^{\text{best}}(E) &= 5.21 - 4.90 \left( \frac{E}{\text{MeV}} \right) + 11.21 \left( \frac{E}{\text{MeV}} \right)^2 \text{ MeV b} \\ \delta S_{33}(E) &= \left[ 0.075 - 1.516 \left( \frac{E}{\text{MeV}} \right) + 14.037 \left( \frac{E}{\text{MeV}} \right)^2 \right. \\ &\quad \left. - 15.504 \left( \frac{E}{\text{MeV}} \right)^3 + 71.640 \left( \frac{E}{\text{MeV}} \right)^4 \right]^{1/2} \text{ MeV b} \end{aligned}$$

where

$$S_{33}^{\text{bare}}(E) \equiv S_{33}^{\text{best}}(E) \pm \delta S_{33}(E). \quad (33)$$

Because these results were obtained with a phenomenological fitting function, their reliability has been establish

only for the energy range covered by the data employed in the fit. Thus Eq. (33) should be used for energies  $E \lesssim 350$  keV. For a temperature  $1.55 \times 10^7$  K corresponding to the Sun's center, we find at the Gamow peak

$$S_{33}^{\text{bare}}(E_0 = 21.94 \text{ keV}) = 5.11 \pm 0.22 \text{ MeV b}, \quad (34)$$

so that the estimated uncertainty is 4.3%.

## VI. THE ${}^3\text{He}(\alpha, \gamma){}^7\text{Be}$ REACTION

When Solar Fusion I appeared, the most recent  ${}^3\text{He}({}^4\text{He}, \gamma){}^7\text{Be}$  measurement was 10 years old. The four new measurements that have been published since that time, in response to a challenge by John Bahcall, are the focus of this section.

For energies of interest,  $E \lesssim 1$  MeV,  ${}^3\text{He}({}^4\text{He}, \gamma){}^7\text{Be}$  is a nonresonant reaction, predominantly external direct capture (Christy and Duck, 1961) by electric dipole emission from s- and d-wave initial states to the two bound states of  ${}^7\text{Be}$ . Reaction measurements have been made by detecting the prompt  $\gamma$ -rays, the  ${}^7\text{Be}$  activity, and the  ${}^7\text{Be}$  recoils. Below we discuss the measurements, the theory needed to extrapolate the measurements to astrophysical energies, and our determination of  $S_{34}(0)$ .

### A. Experimental measurements

Groups at the Weizmann Institute (Singh *et al.*, 2004) and at the University of Washington-Seattle (Brown *et al.*, 2007) carried out cross section measurements in the center-of-mass energy range  $E = 0.42$  to  $0.95$  MeV and  $0.33$  to  $1.23$  MeV, respectively, using gas cells with Ni entrance windows. The LUNA collaboration (Bemmerer *et al.*, 2006a; Confortola *et al.*, 2007; Gyürky *et al.*, 2007) (see also Costantini *et al.* (2008)) carried out low-background measurements from  $E = 0.093$  to  $0.170$  MeV at the LUNA facility in the Gran Sasso underground laboratory, and a European collaboration (Di Leva *et al.*, 2009) (here called ERNA) made measurements from  $E = 0.65$  to  $2.51$  MeV, both with windowless gas cells.

An important concern in Solar Fusion I was whether  ${}^3\text{He}({}^4\text{He}, \gamma){}^7\text{Be}$  measurements made by detecting the  ${}^7\text{Be}$  activity might be affected by background  ${}^7\text{Be}$  produced by contaminant reactions. Possibilities include  ${}^6\text{Li}(d, n){}^7\text{Be}$  or  ${}^{10}\text{B}(p, \alpha){}^7\text{Be}$ , which could occur given proton or deuteron contamination in the  ${}^4\text{He}$  beam in combination with  ${}^6\text{Li}$  or  ${}^{10}\text{B}$  contamination in the gas cell, for example, in the foil or beam stop. Only one of the older experiments - that of Osborne - involved measurements of both prompt  $\gamma$ s and  ${}^7\text{Be}$  activity (see Solar Fusion I for older references). While the Osborne experiment found agreement between the  ${}^3\text{He}({}^4\text{He}, \gamma){}^7\text{Be}$  cross sections determined by the two methods, in general the cross section determined from activity-based experiments was somewhat larger than that determined from prompt- $\gamma$  experiments.

In the new experiments, all but the Weizmann group measured both prompt  $\gamma$ s and  ${}^7\text{Be}$  activity, while ERNA also measured  ${}^7\text{Be}$  recoils. In each of these experiments, the cross sections deduced by the different methods were consistent, leading to upper limits on nonradiative capture of 2-5% from  $E = 0.09$  to 2.5 MeV. This is consistent with theoretical calculations that indicate much smaller rates expected for  $E0$  capture and other electromagnetic processes that could produce  ${}^7\text{Be}$  without accompanying energetic prompt  $\gamma$ s (Snover and Hurd, 2003). All new experiments except that of the Weizmann group employed  ${}^4\text{He}$  beams and  ${}^3\text{He}$  targets, thus minimizing potential problems with background  ${}^7\text{Be}$  production. In the new experiments sensitive checks ruled out contaminant  ${}^7\text{Be}$  production at lower levels. Thus we see no reason to doubt the new activity measurements.

${}^7\text{Be}$  activity measurements provide a direct determination of the total cross section. In contrast, as prompt  $\gamma$ -ray yields are anisotropic, one must take into account detector geometry and the anisotropy to determine a total cross section. [The  $\sim 30\%$  capture branch to the 429-keV first excited state of  ${}^7\text{Be}$  has usually been determined from the isotropic 429 keV  $\rightarrow$  ground state yield.] Unfortunately, no angular distribution measurements exist at the needed level of precision. The theoretical angular distributions of Tombrello and Parker (1963a) (see also Kim *et al.* (1981)) were used to correct the prompt LUNA data, while the UW-Seattle data agree better with an assumed isotropic  $\gamma_0$  angular distribution than with theory. As the prompt anisotropy corrections can be comparable to the overall quoted cross section uncertainty, we decided to exclude the prompt data from our analysis. We do this in part because little additional precision would be gained by combining the highly correlated prompt and activation data. Hence we base our analysis on activation data, plus the ERNA recoil data.

The ERNA data and the older data of Parker and Kavanagh (1963) extend well above 1 MeV, where measurements may provide information useful for constraining theoretical models of  $S_{34}(E)$ . Of these two data sets, only ERNA shows evidence for a significant rise in  $S_{34}(E)$  above 1.5 MeV (see Fig. 1 of Di Leva *et al.* (2009)).

## B. Theory

Relative (but not absolute) S-factors at energies below 1 MeV vary by only a few percent among credible models, with small differences arising from non-external contributions and initial-state phase shifts. The two bound states of  ${}^7\text{Be}$  populated by  ${}^3\text{He}(\alpha, \gamma){}^7\text{Be}$  direct capture have large overlaps with  ${}^3\text{He} + {}^4\text{He}$  cluster configurations. The Pauli principle requires radial nodes in these overlaps, guaranteeing a small (but nonzero) short-range contribution because of cancellation in the matrix-element integral.

Considerable accuracy below 1 MeV can be achieved by a pure external-capture model, with hard-sphere scat-

tering at a radius chosen to reproduce measured phase shifts. In such a model  ${}^3\text{He}$  and  ${}^4\text{He}$  are treated as point particles, and final states are modeled only by their long-range asymptotic parts. This is the approach of the Tombrello and Parker (1963a) model, used to fit  $S_{34}$  in Solar Fusion I. A more realistic treatment of contributions from 2.8 to 7.0 fm is provided by potential models (Buck *et al.*, 1985; Buck and Merchant, 1988; Dubovichenko and Dzhazairov-Kakhramanov, 1995; Kim *et al.*, 1981; Mohr, 2009; Mohr *et al.*, 1993), which generate wave functions from a Woods-Saxon or similar potential, constrained by measured phase shifts.

Microscopic models take explicit account of nucleon short-range correlations. In the resonating-group method (RGM) a simplified nucleon-nucleon interaction is tuned to observables in the system being investigated (e.g., energies of the  ${}^7\text{Be}$  bound states), and the phase shifts are computed, not fitted. The RGM wave functions are sums of states consisting of simple cluster substructure; in most  ${}^7\text{Be}$  calculations, they are antisymmetrized products of Gaussians for  ${}^4\text{He}$  and  ${}^3\text{He}$ , multiplied by a function of the coordinate describing cluster separation.

The RGM calculations of Kajino (1986) and the potential-model of Langanke (1986) (which employed antisymmetrized many-body wave functions) predicted the energy dependence of the  ${}^3\text{H}(\alpha, \gamma){}^7\text{Li}$  reaction quite accurately, prior to the precise measurement of Brune *et al.* (1994). On the other hand, there is some variation of the computed  ${}^3\text{He}(\alpha, \gamma){}^7\text{Be}$  S-factors among RGM models using different interaction types and different Gaussian widths within the clusters. This variation has been shown to correlate with measures of the diffuseness of the  ${}^7\text{Be}$  ground state (Csóto and Langanke, 2000; Kajino, 1986). Substantial changes in the S-factor and phase shifts also occur when  ${}^6\text{Li} + \text{p}$  configurations are added to the RGM wave functions (Csóto and Langanke, 2000; Mertelmeier and Hofmann, 1986).

Calculations using highly accurate nucleon-nucleon potentials are now possible. In Nollett (2001), both bound states were computed using the variational Monte Carlo method, while the relative motion of the initial-state nuclei was modeled by one-body wave functions from the earlier potential-model studies. This approach should provide additional realism to the nuclear wave function at short range, and it features initial states that fit the measured phase shifts. It produced very nearly the same  $S_{34}(E)$  energy dependence as Kajino (1986), and an absolute  $S_{34}(0)$  that is lower by about 25%.

Through a numerical coincidence, the branching ratio for captures to the two final states is very nearly constant at low energy (Kajino, 1986). This circumstance and the external-capture nature of the reaction suggest that laboratory data can be extrapolated to low energy by fitting a single rescaling parameter that multiplies a model  $S_{34}(E)$  to match the data. Such a rescaling does not have a strong physical justification for microscopic models, as they do not have undetermined spectroscopic factors. However, rescaled microscopic models should be

at least as accurate as potential models and more accurate than the hard-sphere model.

A different approach was followed in Cyburt and Davids (2008), where a parameterized function fit was made to three of the four modern data sets over a wider energy interval than we used to determine our recommended  $S_{34}(0)$  (see below), with the result  $S_{34}(0) = 0.580 \pm 0.043$  keV b. Their fitting function is motivated by recent work emphasizing external capture and subthreshold poles in low-energy S-factors (Jennings *et al.*, 1998a,b; Mukhamedzhanov and Nunes, 2002), and it matches expressions for zero phase shift derived in Mukhamedzhanov and Nunes (2002). For  $S_{34}$ , the d-waves have small phase shifts, and the function describes d-wave capture quite well. In the more-important s-wave capture, the function does not match detailed models of  $S_{34}(E)$ , irrespective of fitted parameters; its closeness to the expressions of Mukhamedzhanov and Nunes (2002) suggests that some other functional form is needed to account for nonzero phase shifts.

### 1. Model selection for $S_{34}(0)$ determination

To determine  $S_{34}(0)$  from experimental capture data, we use the microscopic models of Kajino (1986) and Nollett (2001) (Kim A potential), rescaled to fit the data below  $E = 1$  MeV (see below). We selected these two models based on several factors.

- i) They both accurately reproduce the s-wave phase shifts (as given by the phase-shift analysis of Tombrello and Parker (1963b)) and the long-range asymptotics of the  ${}^7\text{Be}$  bound states. The Kajino model reproduces the phase shifts without having been fitted to them.
- ii) They contain more short-range physics than hard-sphere or potential models, which may extend the energy range over which they describe the reaction correctly.
- iii) They agree well with each other even though they were generated by very different computational approaches.
- iv) They reproduce the measured energy dependence of  $S_{34}(E)$  well, up to at least  $E = 1.5$  MeV (see Fig. 5, also Fig. 3 of Di Leva *et al.* (2009)).
- v) They calculate other electromagnetic observables in  ${}^7\text{Li}$  and  ${}^7\text{Be}$ , that are in reasonable agreement with experiment.

### 2. Region of $S_{34}(E)$ fitting

We restricted the energy range for fitting to  $E \leq 1$  MeV. The scatter among models (which differ mainly at short range) becomes much larger at energies above 1

MeV, suggesting that the calculations are most reliable at lower energies, where poorly-constrained short-range contributions to  $S_{34}(E)$  are minimized. In Nollett (2001), the contribution of  ${}^3\text{He}$ - ${}^4\text{He}$  separations less than 4 fm was about 4% of  $S_{34}(0)$  and about 8% of  $S_{34}(1 \text{ MeV})$ . Since a uniform 4% at all energies could be absorbed into the rescaling, the difference between short-range contributions at 0 and 1 MeV suggests 4% as a conservative estimate of the rescaling error.

### 3. Theoretical uncertainty in the $S_{34}(0)$ determination

We estimate a theoretical uncertainty in the  $S_{34}(0)$  determination by rescaling several models to the capture data in the same manner used to determine the recommended value of  $S_{34}(0)$ , and examining the resulting spread in  $S_{34}(0)$  values. We restrict our consideration to microscopic models that reproduce the s-wave phase shifts, choosing those of Walliser *et al.* (1984), Csótó and Langanke (2000) (only those with  ${}^3\text{He} + {}^4\text{He}$  clusterization), Nollett (2001), and new variants of the Nollett (2001) calculation possessing phase shifts perturbed from the empirical values.

The full spread among the chosen set of models is  $\pm 0.030$  keV b, relative to the Kajino (1986) and Nollett (2001) (Kim A potential) fits. We somewhat arbitrarily recommend two-thirds of this value; i.e.,  $\pm 0.02$  keV b, as an approximate  $1\text{-}\sigma$  theoretical error. The scatter among these models is not independent of the rescaling uncertainty estimated above; hence, we have not included an explicit rescaling contribution in this estimate.

### 4. S-factor derivatives

The data do not provide a useful constraint on low-energy derivatives of  $S_{34}(E)$ . Microscopic models that reproduce the phase shifts and simpler models that focus on wave-function asymptotics produce values of  $S'_{34}(0)/S_{34}(0)$  in the range  $-0.55$  to  $-0.79 \text{ MeV}^{-1}$ . These values depend on both the model and the method of estimation. Only Williams and Koonin (1981), Walliser *et al.* (1983), and Walliser *et al.* (1984) published enough information to allow one to extract an estimate for  $S''_{34}$ , yielding  $S''_{34}(0)/S_{34}(0) = 0.26$  to  $0.43 \text{ MeV}^{-2}$ . We base our recommendations on the Nollett (2001) (Kim A) model, which yields effectively  $S'_{34}(0)/S_{34}(0) = -0.64 \text{ MeV}^{-1}$  and  $S''_{34}(0)/S_{34}(0) = 0.27 \text{ MeV}^{-2}$  from a quadratic fit below 0.5 MeV.

### 5. Comment on phase shifts

As the bound-state  ${}^7\text{Be}$  wave functions have known asymptotic forms, differences of the low-energy  $S(E)$  among models arise from differing s-wave phase shifts and from short-range contributions. The short-range contributions, which are difficult to compute convincingly, are



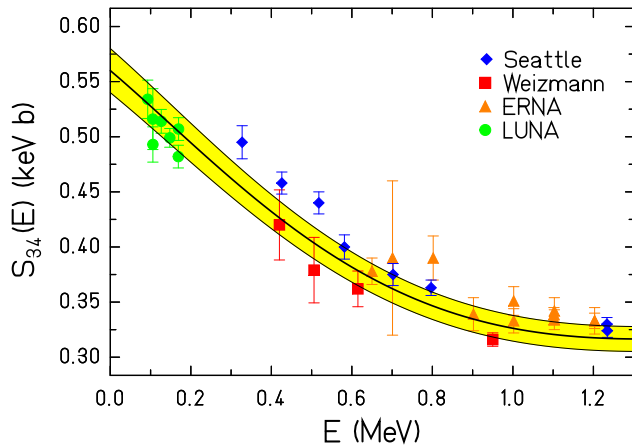


FIG. 5 (Color online)  $S_{34}(E)$  vs.  $E$ . Data points: LUNA - green circles; Weizmann - red squares; UW-Seattle - blue diamonds; ERNA - brown triangles. Solid curve - best fit scaled Nollelt theory to the data with  $E \leq 1.002$  MeV. The yellow band indicates the  $\pm 1\text{-}\sigma$  error band. Data are shown with statistical-plus-varying-systematic errors only; overall systematic errors are not included.

probed by capture experiments above 1 MeV. With the exception of Mohr *et al.* (1993) and Mohr (2009), phase-shift fitting for studies of the  ${}^3\text{He}(\alpha, \gamma){}^7\text{Be}$  reaction has been based almost entirely on the phase-shift analysis of Tombrello and Parker (1963b). While this phase-shift analysis provides a useful constraint, it depends mainly on a single experiment from the early 1960s, and it does not include an error estimation. The modern Mohr *et al.* (1993) experiment extended to lower energies, but it has no published error estimate or phase-shift analysis.

### C. $S_{34}(0)$ determination

Figure 5 shows the low energy data with  $E \leq 1.23$  MeV, and the fit obtained by scaling the Nollelt (Kim A potential) theory to best match the data with  $E \leq 1.002$  MeV. We used the analytic function

$$S_{34}(E) = S_{34}(0) e^{-0.580E} \times (1 - 0.4054E^2 + 0.577E^3 - 0.1353E^4), \quad (35)$$

where  $E$  is in units of MeV. Below one MeV this expression is valid to better than 0.3%, on average.

The best-fit curve in Fig. 5 was obtained by fitting each data set separately with the scaled theory, and then fitting the set of four  $S_{34}(0)$  values to determine the mean  $S_{34}(0)$  value and its error.

As can be seen from Table III, the fits to the individual data sets are good, indicating consistency with the theoretical energy dependence, within the limited energy ranges of each set. The fit to the combined set of four  $S(0)$  values is of marginal quality, indicating a lack of good agreement in the absolute normalizations of the different experiments. The combined fit has  $\chi^2/dof = 2.3$

TABLE III Experimental  $S_{34}(0)$  values and  $1\text{-}\sigma$  uncertainties determined from fits of the scaled Nollelt (Kim A potential) theory to published data with  $E \leq 1.002$  MeV. Total errors are quoted, including inflation factors, and systematic errors of LUNA:  $\pm 2.9\%$ ; Weizmann:  $\pm 2.2\%$ ; UW-Seattle:  $\pm 3.0\%$ ; ERNA:  $\pm 5.0\%$ .

Experiment	$S_{34}(0)$ (keV b)	Error (keV b)	Inflation Factor
LUNA	0.550	0.017	1.06
Weizmann	0.538	0.015	1.00
UW-Seattle	0.598	0.019	1.15
ERNA	0.582	0.029	1.03
Combined result	0.560	0.016	1.72

( $dof = 3$ ), corresponding to  $P(\chi^2, dof) = 0.07$ . All of the errors given in Table III include the inflation factors determined from the goodness of fit (see the Appendix, Sec. XIII.B). Fits to these data using the scaled theory of Kajino yield slightly smaller  $\chi^2$  values, and reproduce the low-energy UW-Seattle data somewhat better; however, the mean  $S_{34}(0)$ , 0.561 keV b, is essentially identical to the result obtained with Nollelt’s theory.

We have focused here on measurements published since Solar Fusion I. We do so because in general they are better documented than the older ones, and address issues such as contaminant  ${}^7\text{Be}$  production in a quantitative manner that lends greater confidence to the results. One may judge from the Kajino-fit analysis presented in Brown *et al.* (2007), that including older measurements would lower the mean  $S(0)$  by at most 0.01 keV b or so. Thus including the older measurements would not change our result significantly.

Given the marginal quality of the mean experimental  $S_{34}(0)$  fit, we round off the values given above, and quote a “best” result,

$$S_{34}(0) = 0.56 \pm 0.02(\text{expt}) \pm 0.02(\text{theor}) \text{ keV b}, \quad (36)$$

based on activation data and the ERNA recoil data, and taking the theoretical error from Sec. VI.B.3.

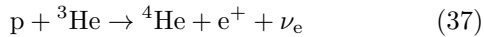
Our best  $S_{34}(0)$  estimate may be compared to the value  $S_{34}(0) = 0.53 \pm 0.05$  keV b given in Solar Fusion I.

New capture experiments below 1 MeV would be most valuable for reducing the experimental uncertainty in  $S_{34}(E)$ , particularly ones that maximize overlap with the existing modern data sets. New scattering and capture experiments above 1 MeV, as well as precise angular distribution measurements, could be useful for constraining future theoretical calculations.<sup>1</sup>

<sup>1</sup> Note added in proof: Recent fermionic molecular dynamics (FDM) calculations (Neff *et al.*, 2010) of  $S_{34}(E)$  are in excellent agreement, in both absolute magnitude and energy dependence, with the experimental data shown in Fig. 5 and with the high-

## VII. THE ${}^3\text{He}(p, e^+ \nu_e){}^4\text{He}$ REACTION

The hep reaction



is the source of the pp chain’s most energetic neutrinos, with an endpoint energy of 18.8 MeV. The Super-Kamiokande and SNO collaborations have placed interesting limits on the hep neutrino flux by searching for these neutrinos in the energy window above the  ${}^8\text{B}$  neutrino endpoint, even though the expected flux is very low (see Fig. 7). The hep rate is beyond the reach of current experiments: this process is induced by the weak interaction and further suppressed by a Coulomb barrier and by other aspects of the nuclear physics, as explained below. Thus theory provides our only estimate of  $S_{\text{hep}}$ .

The calculation of  $S_{\text{hep}}$  is a difficult challenge. The leading one-body (1B) Gamow-Teller (GT) transition operator cannot connect the main s-state components of the  $p+{}^3\text{He}$  and  ${}^4\text{He}$  initial- and final-state wave functions.<sup>2</sup> Hence, at the 1B level the reaction proceeds through the small components of the  ${}^3\text{He}$  and  ${}^4\text{He}$  wave functions, such as d-state components. Consequently, the relative importance of other transition operators, such as axial meson-exchange currents (MEC), is enhanced, as is the contribution from p-wave  $p+{}^3\text{He}$  capture, normally kinematically suppressed at solar temperatures. The situation is further complicated by the fact that the axial 1B and MEC “corrections” have opposite signs, making s-wave hep capture even more suppressed.

### A. hep calculations

Some of the features mentioned above are shared by the hen process ( $n+{}^3\text{He} \rightarrow {}^4\text{He}+\gamma$ ), in particular the strong suppression of 1B contributions. The possibility of deducing  $S_{\text{hep}}$  from the known hen cross section was explored in early studies: while these reactions are not isospin mirrors, there is a close relationship between the isovector spin contribution to hen and the GT contribution to hep. However the hep S-factors determined in these studies differed, in some cases, by orders of magnitude.

In an attempt to understand the origin of this large uncertainty, fully microscopic calculations of both the hep

and hen reactions were performed by Carlson *et al.* (1991) and Schiavilla *et al.* (1992), using a realistic Hamiltonian with two- and three-nucleon interactions. Among the approximations made in the Schiavilla *et al.* (1992) calculation were the description of the  $p+{}^3\text{He}$  initial state as s-wave and the omission of the dependence of the weak operators on the lepton pair momentum. Corrections to the 1B GT operator were evaluated, with the largest two-body (2B) contributions coming from the excitation of intermediate  $\Delta$ -isobars. The  $\Delta$ -isobar degrees of freedom were explicitly included in the nuclear wave functions, using a scaled-down approach to the full  $N + \Delta$  coupled-channel problem known as the transition-correlation operator method. Carlson *et al.* (1991) and Schiavilla *et al.* (1992) found that effects such as the different initial-state interactions for  $n+{}^3\text{He}$  and  $p+{}^3\text{He}$  were so substantial that the known hen cross section was not a useful constraint on hep. Two estimates were given for the hep S-factor at zero energy (Schiavilla *et al.*, 1992),

$$S_{\text{hep}}(0) = \left\{ \begin{array}{c} 1.4 \\ 3.1 \end{array} \right\} \times 10^{-20} \text{ keV b}, \quad (38)$$

depending on the method used to fix the weak  $N - \Delta$  coupling constant,  $g_{\beta N\Delta}$ : the larger of the results corresponds to the naïve quark model prediction for  $g_{\beta N\Delta}$ , while in the smaller,  $g_{\beta N\Delta}$  was determined empirically from tritium  $\beta$  decay. The Solar Fusion I best value for  $S_{\text{hep}}$  is the average of the values in Eq. (38).

This problem was revisited nearly a decade later, following improvements in the description of bound and continuum four-body wave functions. The wave functions of Marcucci *et al.* (2000) were obtained with the correlated-hyperspherical-harmonics (CHH) variational method (Viviani *et al.*, 1995, 1998), using the Argonne  $v_{18}$  (AV18) two-nucleon (Wiringa *et al.*, 1995) and Urbana IX (UIX) three-nucleon interactions (Pudliner *et al.*, 1995). The method produced binding energies of  ${}^3\text{He}$  and  ${}^4\text{He}$  and the singlet and triplet  $p+{}^3\text{He}$  scattering lengths in excellent agreement with experiment.

The Marcucci *et al.* (2000) calculation included all s- and p-wave capture channels in the  $p+{}^3\text{He}$  initial state and all multipole contributions in the expansion of the weak vector and axial-vector transition operators. The weak operators corresponding to the space component of the 1B weak vector current and the time component of the 1B axial current, both of order  $v/c$ , have significant exchange-current corrections of the same order from pion-exchange. These two-body operators were constructed to satisfy (approximately) the constraints of current conservation and PCAC (partial conservation of the axial-vector current). Corrections to the allowed GT operator include both  $(v/c)^2$  1B and exchange-current contributions. The treatment of the latter followed Carlson *et al.* (1991) and Schiavilla *et al.* (1992) in using the transition-correlation operator scheme and in fixing  $g_{\beta N\Delta}$  to the experimental GT strength in tritium  $\beta$  decay.

---

energy ERNA data up to 2.5 MeV. The FDM is a nearly *ab initio* microscopic method employing realistic effective interactions.

<sup>2</sup> While the radial wave functions of the four nucleons in  ${}^4\text{He}$  can all be 1s, with the various single-particle states distinguished by spin and isospin, this is not the case for the three protons in  $p+{}^3\text{He}$ : the Pauli principle requires that one must be radially excited. The GT transition operator does not alter radial quantum numbers, only spin and isospin. Thus the GT matrix element between  $p+{}^3\text{He}$  and  ${}^4\text{He}$  is suppressed due to the s-wave orthogonality.



TABLE IV  $S_{\text{hep}}$  in units of  $10^{-20}$  keV b, calculated with CHH wave functions generated from the AV18/UIX Hamiltonian (Marcucci *et al.*, 2000) for three  $p+{}^3\text{He}$  center-of-mass energies  $E$ . The ‘‘One-body’’ and ‘‘Full’’ labels denote calculations with the one-body and full (one- and two-body) nuclear weak transition operators. Contributions from the  ${}^3\text{S}_1$  channel and from all s- and p-wave channels are listed separately.

	$E = 0$ keV		$E = 5$ keV		$E = 10$ keV	
	${}^3\text{S}_1$	s+p	${}^3\text{S}_1$	s+p	${}^3\text{S}_1$	s+p
One-body	26.4	29.0	25.9	28.7	26.2	29.2
Full	6.38	9.64	6.20	9.70	6.36	10.1

Table IV gives the resulting  $S_{\text{hep}}$  at three center-of-mass energies. The energy dependence is rather weak. The p waves have a significant effect, accounting for about one-third of the total cross section at  $E=0$ . Despite the delicacy of the calculation, Marcucci *et al.* (2000) concluded that the degree of model dependence was moderate: the calculations were repeated for the older Argonne  $v_{14}$  (Wiringa *et al.*, 1984) two-nucleon and Urbana VIII (Wiringa, 1991) three-nucleon interactions, but the predictions for  $S_{\text{hep}}$  differed only by 6%. The best estimate of Marcucci *et al.* (2000),  $S_{\text{hep}} = (10.1 \pm 0.6) \times 10^{-20}$  keV b, is about four times the value given in Solar Fusion I.

A further development came with the use of heavy-baryon chiral perturbation theory (HBChPT) to derive the needed electroweak current operators systematically, with Park *et al.* (2003) carrying out the expansion to next-to-next-to-next-to leading order ( $\text{N}^3\text{LO}$ ), thereby generating all possible operators to this order. These operators represent the short-range physics that resides above the scale of the EFT, which Park *et al.* (2003) defined via a Gaussian regulator with a cutoff  $\Lambda$ , a parameter that was varied in the calculations between 500 and 800 MeV (see Sec. III).  $S_{\text{hep}}$  was obtained by calculating the matrix elements of these EFT current operators with phenomenological wave functions, obtained using the AV18/UIX Hamiltonian and the CHH method. (See Sec. III for a more extended discussion of such hybrid EFT\* approaches.)

To this order, the resulting currents are 1B and 2B: three-body operators arise at order  $\text{N}^4\text{LO}$ . The expansion reproduces the one-pion exchange-current corrections to the space component of the vector current and charge component of the axial current, as dictated by chiral symmetry, while the time component of the vector current has no MEC corrections. The MEC contributions to the axial GT operator include both a one-pion-exchange term and a (non-derivative) two-nucleon contact-term. The low-energy constant determining the strength of the contact term must be determined from an observable. Following the treatment of  $g_{\beta N\Delta}$  by Marcucci *et al.* (2000), this was done by fitting the GT transition strength extracted from tritium  $\beta$  decay.

Table V gives the values determined by Park *et al.*

TABLE V The hep GT matrix element  $\bar{L}_1(q; A)$  (in  $\text{fm}^{3/2}$ ) for the transition from the initial  ${}^3\text{S}_1$   $p+{}^3\text{He}$  state to the final  ${}^4\text{He}$  state, as a function of the cutoff  $\Lambda$  (Park *et al.*, 2003), at  $E=0$ .  $\bar{L}_1(q; A)$  is evaluated at  $q = 19.2$  MeV, the momentum carried out by the lepton pair.  $S_{\text{hep}}$  (in  $10^{-20}$  keV b) is also given.

$\Lambda$ (MeV)	500	600	800
$\bar{L}_1(q; A)$ : 1B	-0.081	-0.081	-0.081
$\bar{L}_1(q; A)$ : 2B (no contact term)	0.093	0.122	0.166
$\bar{L}_1(q; A)$ : 2B (with contact term)	-0.044	-0.070	-0.107
$\bar{L}_1(q; A)$ : 2B-total	0.049	0.052	0.059
$S_{\text{hep}}$	9.95	9.37	7.32

(2003) for  $S_{\text{hep}}(0)$  and for the GT matrix element between the  ${}^3\text{S}_1$   $p+{}^3\text{He}$  initial and the  ${}^4\text{He}$  final states, as a function of  $\Lambda$ . By fixing the strength of the contact term to an observable, one hopes in such hybrid EFT\* approaches to remove most of the calculation’s cutoff dependence. Heuristically, the contact term compensates for high-momentum components in the phenomenological wave functions that would not be there had both operators and wave functions been derived rigorously from EFT, with a common cutoff. However, the table shows that significant cutoff-dependence remains in the total amplitude because of cancellation between the 1B and 2B contributions: the variation in  $S_{\text{hep}}$  is  $\sim 15\%$ . This is taken as the uncertainty in the Park *et al.* (2003) estimate for  $S_{\text{hep}}$ ,  $S_{\text{hep}}(0) = (8.6 \pm 1.3) \times 10^{-20}$  keV b. The result is consistent with that of Marcucci *et al.* (2000).

The prediction of Park *et al.* (2003) was used by Bahcall *et al.* (2006) and by Peña-Garay and Serenelli (2008) in their latest determinations of the hep neutrino flux,  $\phi_\nu(\text{hep}) = (8.22 \pm 1.23) \times 10^3 \text{ cm}^{-2} \text{ s}^{-1}$ , where the error reflects again the 15% uncertainty quoted above. The value for  $\phi_\nu(\text{hep})$  is in agreement with the Super-Kamiokande (Fukuda *et al.*, 2001) and SNO (Aharmin *et al.*, 2006) upper limits at 90% confidence level,  $40 \times 10^3$  and  $23 \times 10^3 \text{ cm}^{-2} \text{ s}^{-1}$ , respectively.

## B. Summary

Given the two consistent calculations presented above, with the internal checks on the sensitivities to input wave functions and to cutoffs, and given the compatibility with the limits established by Super-Kamiokande and SNO, we recommend

$$S_{\text{hep}}(0) = (8.6 \pm 2.6) \times 10^{-20} \text{ keV b}, \quad (39)$$

where the uncertainty is obtained by doubling the cutoff-dependence found in the Park *et al.* (2003) calculation. One anticipates that the cutoff dependence would be reduced if the operator expansion were carried out beyond  $\text{N}^3\text{LO}$ . Thus such a program could increase confidence in Eq. (39) and narrow the uncertainty, even without a

fully consistent treatment of both operators and wave functions.

Other ancillary calculations that could strengthen confidence in this S-factor estimate include

- new studies of the hep reaction in which a broad spectrum of Hamiltonian models are explored, as was done by Schiavilla *et al.* (1998) for the pp reaction;
- study of related electroweak reactions where rates are known, such as muon capture, as was done by Marcucci *et al.* (2002) and Gazit (2008) for  $\mu^- + {}^3\text{He} \rightarrow {}^3\text{H} + \nu_\mu$ ; and
- further work to understand the relationship between the suppressed processes hep and hen.

### VIII. ELECTRON CAPTURE BY ${}^7\text{Be}$ , pp, AND CNO NUCLEI

Electron capture is the source of line features in the solar neutrino spectrum, and represents an important pathway for energy production in the pp chain. Solar electron-capture lifetimes differ substantially from laboratory values because light nuclei are highly ionized and because the continuum electron density is large.

The relative rates of  ${}^7\text{Be}$  electron capture and  ${}^7\text{Be}(p,\gamma){}^8\text{B}$  determine the ppII/ppIII branching ratio and thus the ratio of the  ${}^7\text{Be}$  and  ${}^8\text{B}$  neutrino fluxes. The electron capture proceeds by the mirror transition to the ground state of  ${}^7\text{Li}$  ( $3/2^-$ ) and by an allowed transition to the first excited state ( $1/2^-$ , 478 keV). By normalizing the solar rate to the known terrestrial decay rate, the nuclear physics dependence of the solar rate can be eliminated. The ratio of rates depends on the relative electron probability densities averaged over the nucleus. This requires a calculation of the atomic probability densities governing the K and L terrestrial electron capture rates, the continuum electron probability densities at the nucleus for the solar rate, and corrections to the solar rate resulting from incomplete ionization. The solar continuum calculation was done by Bahcall (1962), and estimates of the bound-electron contributions have been made by Iben, Jr. *et al.* (1967), Bahcall and Moeller (1969), and Bahcall (1994). The solar continuum calculations have typically been done by employing the Debye-Hückel approximation for plasma screening. Electrons within the local Debye sphere screen the nuclear potential, thus lowering the electron density at the nucleus and the electron capture rate, while protons penetrating that radius would enhance the rate.

Our recommended rate is based on the calculation of Bahcall and Moeller (1969), with updates including the currently adopted  ${}^7\text{Be}$  half-life of  $53.22 \pm 0.06$  days, a total-to-continuum capture ratio of  $1.217 \pm 0.002$  (Bahcall, 1994), and a terrestrial L/K capture ratio of  $0.040 \pm 0.006$  (Voytas *et al.*, 2001). We use the original estimate

of Bahcall (1962) for the terrestrial K-electron probability at the nucleus. The result,

$$R({}^7\text{Be} + e^-) = 5.60(1 \pm 0.02) \times 10^{-9}(\rho/\mu_e) \times T_6^{-1/2}[1 + 0.004(T_6 - 16)] \text{ s}^{-1}, \quad (40)$$

valid for  $10 < T_6 < 16$ , is identical to Eq. (26) of Solar Fusion I. Here  $\rho$  is the density in units of  $\text{g}/\text{cm}^3$ ,  $T_6$  is the temperature in units of  $10^6\text{K}$ , and  $\mu_e$  is the mean molecular weight per electron. The assigned uncertainty of 2% is dominated by possible corrections to the Debye-Hückel approximation for charge fluctuations (reflecting the small number of electrons within the Debye sphere), and by breakdowns in the adiabatic approximation, as evaluated by Johnson *et al.* (1992) in self-consistent thermal Hartree calculations. The small rate enhancement they found, 1.3%, is incorporated into and dominates the error in Eq. (40).

Despite the lack of changes since Solar Fusion I, there have been developments in two areas, each concerned with screening corrections. First, a series of precise measurements of the terrestrial electron capture rate have been carried out to assess the dependence of screening on target chemistry, which could alter the L/K ratio (because of L-capture sensitivity to changes in the valence electrons). Over the past decade such changes, first suggested by Segrè (1947), have been explored in a series of half-life measurements in which  ${}^7\text{Be}$  was implanted in metals and insulators, or encapsulated in fullerene (Das and Ray, 2005; Limata *et al.*, 2006; Nir-El *et al.*, 2007; Norman *et al.*, 2001; Ohtsuki *et al.*, 2004; Ray *et al.*, 1999, 2002, 2006; Wang *et al.*, 2006). The pattern of results is somewhat confused, with claims of variations up to 1.1%, but with other studies limiting effects to levels  $\lesssim (0.2\text{-}0.4)\%$  (Limata *et al.*, 2006; Nir-El *et al.*, 2007), despite use of host materials with substantially different electron affinities. Our tentative conclusion is that the uncertainty assigned in Eq. (40) is sufficient to allow for likely variations in terrestrial screening corrections.

Second, questions about the adequacy of solar plasma screening corrections, detailed in Solar Fusion I, have not died out. Quarati and Scarfone (2007, 2009) reconsidered the plasma fluctuation contributions to the electron-capture rate of  ${}^7\text{Be}$ , concluding that corrections of 7 - 10% are required. The *ansatz* of Quarati and Scarfone (2007) was previously considered and rejected by Bahcall *et al.* (2002), however. The influence of protons on the rate of  ${}^7\text{Be}$  electron capture in the Sun was claimed to be more significant by Belyaev *et al.* (2007) than was previously thought. Davids *et al.* (2008), however, reject their argument, pointing out that only the previously investigated electromagnetic contributions of protons play a role, and that the approximations under which a putative three-body electromagnetic contribution was calculated are invalid.

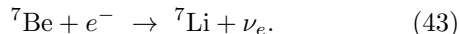
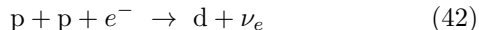
The electron captures on p+p and on CNO nuclei compete with the corresponding  $\beta$  decays, and thus these rates have been conventionally normalized to solar  $\beta$  decay rates. As electron capture and  $\beta$  decay depend on

the same allowed nuclear matrix element, the ratio is independent of the nuclear physics. The result from Solar Fusion I, from Bahcall and May (1969), is

$$R^{\text{Tree}}(\text{pep}) = 1.102(1 \pm 0.01) \times 10^{-4}(\rho/\mu_e) \times T_6^{-1/2}[1 + 0.02(T_6 - 16)]R^{\text{Tree}}(\text{pp}), \quad (41)$$

where the superscript ‘‘Tree’’ indicates that the relationship omits radiative corrections, which are discussed below. The range of validity is  $10 < T_6 < 16$ .

Radiative corrections were evaluated by Kurylov *et al.* (2003) for the two pp-chain reactions under discussion,



The radiative corrections were given as

$$\frac{\Gamma_{\text{Capt}}}{\Gamma_{\text{Capt}}^{\text{Tree}}} = \left[ 1 + \frac{\alpha}{\pi} g_{\text{Capt}}(E_e, Q) \right] \equiv C^{\text{rad}}(E_e, Q), \quad (44)$$

where  $\Gamma_{\text{Capt}}$  is the total decay width,  $\Gamma_{\text{Capt}}^{\text{Tree}}$  is the tree-level width without radiative corrections, and  $g_{\text{Capt}}(E_e, Q)$  is a calculated factor that depends on both the total energy  $E_e$  of the captured electron and the  $Q$ -value of the transition. Figure 6 shows the resulting correction factors.

Because Eq. (40) corresponds to a ratio of stellar and terrestrial electron capture rates, the radiative corrections should almost exactly cancel: although the initial atomic state in the solar plasma differs somewhat from that in a terrestrial experiment, the short-range effects that dominate the radiative corrections should be similar for the two cases. [Indeed, this is the reason the pp and  ${}^7\text{Be}$  electron corrections shown in Fig. 6 are nearly identical.] However the same argument cannot be made for the ratio of pep electron capture to pp  $\beta$  decay, as the electron kinematics for these processes differ. With corrections Eq. (41) becomes

$$R(\text{pep}) = \frac{\langle C^{\text{rad}}(\text{pep}) \rangle}{\langle C^{\text{rad}}(\text{pp}) \rangle} 1.102(1 \pm 0.01) \times 10^{-4}(\rho/\mu_e) \times T_6^{-1/2}[1 + 0.02(T_6 - 16)]R(\text{pp}), \quad (45)$$

where the radiative corrections have been averaged over reaction kinematics. Kurylov *et al.* (2003) found a 1.62% radiative correction for the  $\beta$  decay rate,  $\langle C^{\text{rad}}(\text{pp}) \rangle \sim 1.016$  (see discussion in Sec. III), while  $\langle C^{\text{rad}}(\text{pep}) \rangle \sim 1.042$ . Thus  $\langle C^{\text{rad}}(\text{pep}) \rangle / \langle C^{\text{rad}}(\text{pp}) \rangle \sim 1.026$ , so that our final result becomes

$$R(\text{pep}) = 1.130(1 \pm 0.01) \times 10^{-4}(\rho/\mu_e) \times T_6^{-1/2}[1 + 0.02(T_6 - 16)]R(\text{pp}). \quad (46)$$

While certain improvements could be envisioned in the Kurylov *et al.* (2003) calculation – for example, in the matching onto nuclear degrees of freedom at some characteristic scale  $\sim \text{GeV}$  – rather large changes would be

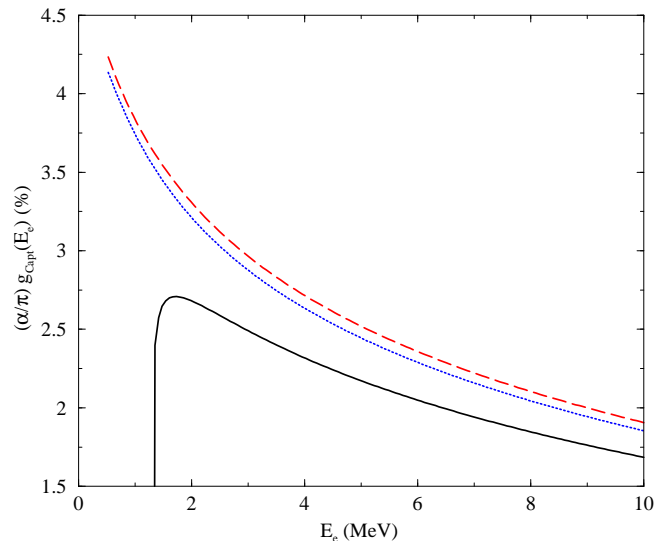


FIG. 6 (Color online) Calculated radiative corrections for  $p+p+e^- \rightarrow d+\nu_e$  (dashed line) and  ${}^7\text{Be}+e^- \rightarrow {}^7\text{Li}+\nu_e$  (dotted line). The solid line is for  $p+e^- \rightarrow n+\nu_e$ . Figure from Kurylov *et al.* (2003).

needed to impact the overall rate at the relevant 1% level. For this reason, and because we have no obvious basis for estimating the theory uncertainty, we have not included an additional theory uncertainty in Eq. (46). However, scrutiny of the presently unknown hadronic and nuclear effects in  $g_{\text{Capt}}(E_e, Q)$  would be worthwhile. As one of the possible strategies for more tightly constraining the neutrino mixing angle  $\theta_{12}$  is a measurement of the pep flux, one would like to reduce theory uncertainties as much as possible.

The electron capture decay branches for the CNO isotopes  ${}^{13}\text{N}$ ,  ${}^{15}\text{O}$ , and  ${}^{17}\text{F}$  were first estimated by Bahcall (1990). In his calculation, only capture from the continuum was considered. More recently, Stonehill *et al.* (2004) have re-evaluated these line spectra by including capture from bound states. Between 66% and 82% of the electron density at the nucleus is from bound states. Nevertheless, the electron-capture component is more than three orders of magnitude smaller than the  $\beta^+$  component for these CNO isotopes, and it has no effect on energy production. However, the capture lines are in a region of the neutrino spectrum otherwise unoccupied except for  ${}^8\text{B}$  neutrinos, and they have an intensity that is comparable to the  ${}^8\text{B}$  neutrino intensity per MeV (Fig. 7), which may provide a spectroscopically cleaner approach to measuring the CNO fluxes than the continuum neutrinos do.

The recommended values for the ratio of line neutrino flux to total neutrino flux are listed in Table VI.

The ratio depends weakly on temperature and density, and thus on radius in the Sun. The values given are for the SSM and do not depend significantly on the details of the model. The branching ratio for  ${}^7\text{Be}$  decay to the

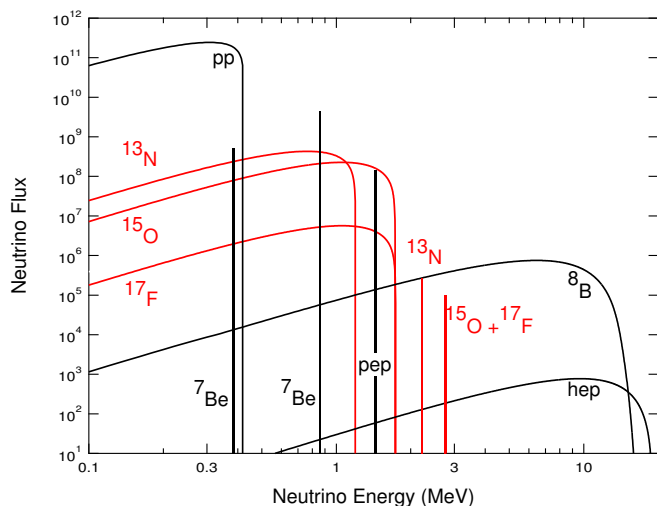


FIG. 7 (Color online) Solar neutrino fluxes based on the “OP” calculations of Bahcall *et al.* (2005), with the addition of the new line features from CNO reactions. Line fluxes are in  $\text{cm}^{-2} \text{s}^{-1}$  and spectral fluxes are in  $\text{cm}^{-2} \text{s}^{-1} \text{MeV}^{-1}$ . Figure adapted from Stonehill *et al.* (2004).

TABLE VI The ratios of neutrino line intensity to the total intensity, after integration over the solar model.

Source	$R_{\text{line}}/R_{\text{total}}$	Ref.
p+p	$2.35 \times 10^{-3}$ <sup>a</sup>	Bahcall (1990)
$^3\text{He}+\text{p}$	$4 \times 10^{-8}$ <sup>b</sup>	Bahcall (1990)
	$\leq 7 \times 10^{-7}$ <sup>c</sup>	Bahcall (1990)
$^7\text{Be}$	0.8951 <sup>d</sup>	see text
	0.1049 <sup>e</sup>	
$^8\text{B}$	$2 \times 10^{-7}$	Bahcall (1990)
$^{13}\text{N}$	$7.9 \times 10^{-4}$	Stonehill <i>et al.</i> (2004)
$^{15}\text{O}$	$4.0 \times 10^{-4}$	Stonehill <i>et al.</i> (2004)
$^{17}\text{F}$	$5.9 \times 10^{-4}$	Stonehill <i>et al.</i> (2004)

<sup>a</sup>includes a 2.6% radiative correction from Kurylov *et al.* (2003)

<sup>b</sup>to  $^4\text{He}$  ground state

<sup>c</sup>to  $^4\text{He}$  excited state

<sup>d</sup>to  $^7\text{Li}$  ground state

<sup>e</sup>to  $^7\text{Li}$  excited state

first excited state in the laboratory is a weighted average of the results from Balamuth *et al.* (1983), Donoghue *et al.* (1983), Mathews *et al.* (1983), Davids *et al.* (1983), Norman *et al.* (1983a,b), and an average of earlier results,  $10.37 \pm 0.12\%$  (see Balamuth *et al.* (1983)). The adopted average,  $10.45 \pm 0.09\%$  decay to the first excited state, is corrected by a factor 1.003 for the average electron energy in the solar plasma, 1.2 keV (Bahcall, 1994), to yield a recommended branching ratio of  $10.49 \pm 0.09\%$ .

## IX. THE $^7\text{Be}(p,\gamma)^8\text{B}$ REACTION

The  $^7\text{Be}(p,\gamma)^8\text{B}$  reaction at low energies is predominantly nonresonant  $E1$ ,  $s$ - and  $d$ -wave capture into the weakly-bound ground state of  $^8\text{B}$  (Robertson, 1973). At solar energies the reaction proceeds by external direct capture, with matrix-element contributions dominated by  $^7\text{Be}$ - $p$  separations on the order of tens of fermis. The energy dependence near the Gamow peak cannot be determined from simple extrapolations of higher energy data, but must be taken from models. The narrow  $1^+$  resonance at  $E_p = 720$  keV as well as resonances at higher energies are usually treated separately, and have little influence on solar rates.

In Solar Fusion I only one direct  $^7\text{Be}(p,\gamma)^8\text{B}$  measurement was found to be sufficiently well documented to allow an independent assessment of the systematic errors. Consequently the recommended  $S_{17}(0)$  was based on a single experiment, that of Filippone *et al.* (1983). Since Solar Fusion I new direct  $^7\text{Be}(p,\gamma)^8\text{B}$  measurements have been carried out at Bordeaux/Orsay (Hamache *et al.*, 1998, 2001), the Weizmann Institute (Baby *et al.*, 2003a,b) (see also Hass *et al.* (1999)), Bochum (Strieder *et al.*, 2001) and the University of Washington-Seattle/TRIUMF (Junghans *et al.*, 2010, 2002, 2003). These modern measurements form the basis for our Solar Fusion II  $S_{17}(0)$  recommendation.

Other new measurements include two performed with  $^7\text{Be}$  beams (Bardayan *et al.*, 2009; Gialanella *et al.*, 2000). Although inverse measurements of this sort are much more difficult, they offer the attraction of different systematic errors. However, these experiments did not reach a precision useful for our purposes and thus play no role in our current assessment.

In addition to direct measurements,  $S_{17}(0)$  has been determined indirectly from Coulomb dissociation, as summarized below in Sec. IX.C, and from peripheral heavy-ion transfer and breakup reactions. General aspects of such techniques are discussed in Sec. XII.

### A. The direct $^7\text{Be}(p,\gamma)^8\text{B}$ reaction

All modern  $^7\text{Be}(p,\gamma)^8\text{B}$  experiments have employed the same basic method of counting  $\beta$ -delayed  $\alpha$ s from the decay of  $^8\text{B}$  to determine the reaction yield. However, different experimental techniques were used, and different levels of precision were achieved in the procedures for converting measured yields into cross sections and  $S$ -factors. Below we discuss the most important issues.

#### 1. Beam-target overlap

In a conventional experiment with a beam area smaller than the target area, it can be difficult to determine accurately the overlap of the beam with the target, due to non-uniformities in the areal density of typical tar-

gets. This is frequently the case for radioactive target experiments, as target designs are often quite compact, with cross sections comparable to the beam area, in order to minimize unused target material. This potential problem has been avoided in the most recent  ${}^7\text{Be}(p,\gamma){}^8\text{B}$  experiments by using small-area targets irradiated by uniform beam fluxes. The reaction yield is then proportional to the product of the beam flux and the total number of  ${}^7\text{Be}$  atoms. The latter quantity can be determined accurately from the  ${}^7\text{Be}$  decay radioactivity. As the target density may have tails extending to large radii, and as the beam density may not be perfectly uniform, it is necessary to carry out ancillary measurements to demonstrate the accuracy of this technique. Measurements can include separate determinations of the radial dependence of the beam density and the target density, and/or the radial dependence of the product of the beam and target densities. While the Bochum, Weizmann, and UW-Seattle/TRIUMF experiments all used the small-area target/uniform-beam-flux method, only the latter two experiments provided sufficient information to permit an independent assessment of procedures.

## 2. ${}^8\text{B}$ backscattering

A systematic error in  ${}^7\text{Be}(p,\gamma){}^8\text{B}$  measurements that was identified after Solar Fusion I is the loss of  ${}^8\text{B}$  reaction products due to backscattering out of the target (Strieder *et al.*, 1998; Weissman *et al.*, 1998). This loss is particularly significant for high-Z target backings and low proton energy. The Filippone *et al.* (1983) and Bordeaux/Orsay experiments used Pt backings, for which the backscattering corrections are significant. In the Bordeaux/Orsay experiment, calculated backscattering corrections were applied to the data, while the Filippone *et al.* (1983) experiment was performed prior to the identification of  ${}^8\text{B}$  backscattering as a serious concern. Junghans *et al.* (2003) estimated that the backscattering correction for the Filippone *et al.* (1983) data would be between -2% and -4% (a factor of two smaller than the estimate given in Weissman *et al.* (1998)). Here we ignore this correction because it is well within the overall precision claimed in the Filippone *et al.* (1983) experiment and because it is incomplete, as effects due to target thickness nonuniformity (unknown) and surface composition have not been included.

For the other modern experiments,  ${}^8\text{B}$  backscattering losses are not an issue: the Bochum experiment used a low-Z backing, while the UW-Seattle/TRIUMF experiments used an intermediate-Z backing and demonstrated by direct measurement that backscattering losses were very small. The Weizmann experiment used implanted targets with an intermediate-Z substrate.

## 3. Proton energy loss corrections

Low-energy data must be corrected by energy-averaging to account for proton energy loss in the target. This requires knowledge of the energy loss profile of the target and the target composition, as well as the monitoring of possible carbon buildup during bombardment. The most detailed determination of these quantities was made in the UW-Seattle/TRIUMF experiments, where the target profile was determined from the narrow ( $\Gamma \ll 1$  keV)  ${}^7\text{Be}(\alpha,\gamma){}^{11}\text{C}$  resonance at  $E_\alpha = 1377$  keV. In Junghans *et al.* (2010) a more detailed resonance profile analysis of the previously published data was presented, allowing for possible depth-dependent target composition. The varying systematic errors on the low energy “BE3” thick-target data were increased over the original results in Junghans *et al.* (2003) due primarily to larger assumed  $dE/dx$  uncertainties.

In the Filippone *et al.* (1983) experiment, the energy loss profile of the target was deduced from the measured shape of the 12-keV wide  ${}^7\text{Li}(p,\gamma)$  resonance at  $E_p = 441$  keV, assuming the  ${}^7\text{Li}$  and  ${}^7\text{Be}$  distributions in the target were the same. In the Bordeaux/Orsay experiment, Rutherford backscattering and (d,p) measurements were used to determine the target composition and proton energy loss. In the Bochum and Weizmann experiments, the  $\Gamma = 36$  keV  ${}^7\text{Be}(p,\gamma)$  resonance at  $E_p = 720$  keV was used to determine the proton energy loss. The Weizmann experiment used implanted targets with known composition, verified by direct secondary ion mass spectrometry measurements. In the Filippone *et al.* (1983) and Bochum measurements, limits on the composition were inferred from the fabrication process.

Other important factors include determination and monitoring of the  ${}^7\text{Be}$  target activity, corrections for sputtering losses, and determination of the efficiency for  $\alpha$  detection. For the implanted target of the Weizmann experiment, target sputtering losses were shown to be negligible. The UW-Seattle/TRIUMF experiments have the most extensive error analysis of the modern experiments. Measurements were made with two targets of different thicknesses (labeled BE1 and BE3) and with two different methods for determining the detection efficiency for  $\alpha$ s. The resulting statistical and systematic errors are the smallest yet achieved.

## B. Theory

Among the many theoretical models that have been published, the simplest are those in which the interaction between the  ${}^7\text{Be}$  nucleus and proton are described by a Woods-Saxon or similar potential (Aurdal, 1970; Barker, 1980; Bertulani, 1996; Davids and Typel, 2003; Esbensen, 2004; Kim *et al.*, 1987; Krauss *et al.*, 1993; Nunes *et al.*, 1997a,b, 1998; Riisager and Jensen, 1993; Robertson, 1973; Tombrello, 1965; Typel *et al.*, 1997). The main constraints on such models are the ground-

state energy, the energies of low-lying resonances, and s-wave scattering lengths (Angulo *et al.*, 2003). Charge symmetry has been used to obtain potentials from  ${}^7\text{Li}+n$  scattering lengths and the  ${}^7\text{Li}(n,\gamma){}^8\text{Li}$  cross section, but persistent difficulties in simultaneously reproducing the absolute cross sections for  ${}^7\text{Be}(p,\gamma){}^8\text{B}$  and  ${}^7\text{Li}(n,\gamma){}^8\text{Li}$  may reflect the greater sensitivity of neutron capture to the inner part of the wave function (Barker, 1980; Esbensen, 2004). Among potential models, only those of Nunes *et al.* (1997a,b, 1998) include coupling to inelastic channels, open above the 430 keV threshold for excitation of  ${}^7\text{Be}$ . No significant effect was found, consistent with results of microscopic models.

Potential models yield a reasonably accurate description of the external part of the direct capture. The wave function at  $r < 5$  fm is not tightly constrained in potential models but contributes to the capture at all energies, particularly above 500 keV (Csóttó, 1997; Jennings *et al.*, 1998b). However, one requirement is the existence of a node in s-wave scattering states, as the scattered wave function must be orthogonal to those of the closed He core assumed in the description of  ${}^7\text{Be}$  (Aurdal, 1970). Model spectroscopic factors have been taken from shell-model studies, fixed to match transfer-reaction results (including the asymptotic normalization coefficients discussed in Sec. XII), or determined by rescaling computed S-factors to match capture data.

R-matrix models of direct capture (Barker, 1995; Barker and Mukhamedzhanov, 2000) resemble potential models in their lack of explicit  ${}^7\text{Be}$  substructure, their need for fitting constraints, their apparent fidelity at large  ${}^7\text{Be}$ -p separation, and their relative lack of short-range details. Similar data are fitted and similar results produced. The R-matrix as applied to direct capture differs from the discussion in Sec. II only in its need for radiative widths and attention to the long-range tails of bound states (Barker, 1995).

“Microscopic” models explicitly containing eight nucleons can include substructure within  ${}^7\text{Be}$  and configurations not reducible to  ${}^7\text{Be}+p$ , calculated from the (effective) nucleon-nucleon interaction. The antisymmetry between the last or scattering proton and those within  ${}^7\text{Be}$  is maintained. Fully microscopic calculations to date generally apply versions of the resonating group method (RGM) to significantly simplify the many-body problem (Csóttó, 1997; Csóttó *et al.*, 1995; Descouvemont, 2004; Descouvemont and Baye, 1988, 1994; Johnson *et al.*, 1992). For  $S_{17}$  the interaction is usually tuned to reproduce the proton separation energy of  ${}^8\text{B}$ , but may also be adjusted to reproduce the scattering length of  ${}^7\text{Be}+p$  in the  $S = 2$ ,  $L = 0$  channel that dominates capture at zero energy (Descouvemont, 2004). RGM models do roughly as well as potential models in the external ( $> 5$  fm) region while providing a more realistic description of structure in the internal region. Nonetheless, RGM results depend on the choice of nucleon-nucleon interaction and on the data used to fix parameters. RGM predictions of absolute cross sections tend to be high relative to measured val-

ues. Thus RGM results are frequently rescaled, so that theory is used only to predict the energy dependence of S-factors, in extrapolating higher energy data to the region of the Gamow peak.

Other microscopic approaches have used effective interactions in combination with the shell model, adapted to treat weakly-bound and unbound states of  $p$ -shell nuclei (Bennaceur *et al.*, 1999; Halderson, 2006). These studies focused on spectroscopic properties of  $A = 8$  nuclei rather than the radiative capture. While this approach is not as well developed as the RGM method, it has produced low-energy S-factors similar to those of the RGM and other models. The absolute S-factor of Bennaceur *et al.* (1999) is in good agreement with the data, while that of Halderson (2006) is  $\sim 40\%$  larger than experiment.

Ideally microscopic calculations would be carried out with realistic nucleon-nucleon interactions, but this is challenging due to the complexity of the interaction and the need for very large spaces. The only published example is that of Navrátil *et al.* (2006a,b), in which the overlap integrals between  ${}^8\text{B}$  and  ${}^7\text{Be}+p$  were computed from seven- and eight-body wave functions obtained with the *ab initio* no-core shell model (NCSM). Due to the finite range of the harmonic oscillator basis, the long tails of the  ${}^7\text{Be}+p$  overlaps were corrected by matching their logarithmic derivatives to Whittaker functions at intermediate distances. These overlaps were then used as final states, with initial scattering states drawn from previous potential-model studies. The resulting  $S_{17}(0)$ , 22.1 eV b, is close to the experimental value. The calculated  $S_{17}(E)$  is relatively insensitive to the choice of initial state for  $E < 100$  keV, but more so at higher energies (e.g., with variations of 20% at 1.6 MeV).

The envelope of predicted energy dependences of theoretical models has about a 30% spread over the energy range fitted below. While efforts have been made to fit  $S_{17}(E)$  with as little theoretical input as possible, some degree of model input appears necessary (Cyburt *et al.*, 2004).

We adopt the RGM calculation of Descouvemont (2004) as the standard to extrapolate the experimental data to energies of astrophysical interest. Among available RGM calculations, this one is the most complete numerically. Of the two  $NN$  interactions used in Descouvemont (2004), the Minnesota interaction was judged to describe light nuclei more accurately. The predicted  $S_{17}(0) = 24.69$  eV b is 19% larger than our recommended value, while the calculated shape of  $S_{17}(E)$  provides a marginally better fit to the data, compared to other models we considered. Other  ${}^8\text{B}$  and  ${}^8\text{Li}$  properties computed in this model also match experiment reasonably well. Nevertheless, the substantial theoretical error bar assigned to our end result of Sec. IX.D – to remove much of the dependence on choice of model – dominates the overall uncertainty in our value for  $S_{17}(0)$ .

Low-order polynomial representations of  $S_{17}(E)$  that span both the solar Gamow peak and energies where data are available have poor convergence due to a pole in the

S-factor at  $-138$  keV (Jennings *et al.*, 1998a,b; Williams and Koonin, 1981). Thus instead we fit the models over a more limited energy range important to stellar fusion, 0 to 50 keV. A quadratic expansion then provides a good representation. This procedure yields  $S'_{17}(0)/S_{17}(0)$  between  $-1.4/\text{MeV}$  and  $-1.83/\text{MeV}$  for the models used in our fitting. We recommend as a best value and probable range

$$\frac{S'_{17}(0)}{S_{17}(0)} = (-1.5 \pm 0.1)/\text{MeV}. \quad (47)$$

The corresponding values for  $S''_{17}(0)/S_{17}(0)$  vary from  $7.2/\text{MeV}^2$  to  $20.4/\text{MeV}^2$ ; we recommend

$$\frac{S''_{17}(0)}{S_{17}(0)} = (11 \pm 4)/\text{MeV}^2. \quad (48)$$

The ranges are consistent with other published values where derivatives were defined by similar procedures (Barker, 1983; Bennaceur *et al.*, 1999; Descouvemont and Baye, 1988; Kolbe *et al.*, 1988). Published values outside our recommended ranges (Adelberger *et al.*, 1998; Baye, 2000; Baye and Brainis, 2000; Baye and Descouvemont, 1985; Baye *et al.*, 1998; Jennings *et al.*, 1998b; Johnson *et al.*, 1992; Williams and Koonin, 1981) are either mathematical derivatives at  $E = 0$  or fits over a wider energy interval. For the adopted Descouvemont (2004) model with MN potential, the corresponding numbers are  $S'_{17}(0)/S_{17}(0) = -1.51/\text{MeV}$  and  $S''_{17}(0)/S_{17}(0) = 13.5/\text{MeV}^2$ .

### C. $^8\text{B}$ Coulomb dissociation measurements

Estimates of direct  $(p,\gamma)$  capture cross sections can be derived from Coulomb Dissociation (CD) measurements (see Sec. XII). Because of the complexity of the associated analysis and the absence of convincing benchmarks for the CD method, the Solar Fusion I authors concluded that it would be premature to use information from the CD of  $^8\text{B}$  in deriving a recommended value for  $S_{17}(0)$ . However, the CD of  $^8\text{B}$  was identified as a prime test case for this method, because this reaction can be studied both directly and indirectly, is characterized by a low proton binding energy, and is dominated by  $E1$  transitions. Three groups have performed CD experiments with radioactive  $^8\text{B}$  beams of incident energies between 44 and 254 A MeV. A comparison of their results to those from radiative proton capture allows one to assess the precision that might be possible with the CD method.

Exclusive CD measurements were performed at 47 A MeV (Iwasa *et al.*, 1996; Motobayashi *et al.*, 1994) and 52 A MeV (Kikuchi *et al.*, 1997, 1998) at RIKEN, at 83 A MeV at MSU (Davids *et al.*, 2001a,b), and at 254 A MeV at GSI (Iwasa *et al.*, 1999; Schümann *et al.*, 2003, 2006). For the RIKEN and GSI experiments, the most recent publications supersede the previously published ones. The RIKEN experiment measured the CD of  $^8\text{B}$

in complete kinematics including  $\gamma$ -rays, but had to cope with a large background induced by reactions in the He bag between the target and the fragment detectors. The MSU experiment suffered from a low detection efficiency, particularly at high  $p$ - $^7\text{Be}$  relative energies. The GSI experiment eliminated background by reconstruction of the break-up vertex and utilized a focusing spectrometer with large momentum acceptance that provided high geometric detection efficiency. These considerations suggest that the GSI measurement of Schümann *et al.* (2006) represents the most complete experimental study of  $^8\text{B}$  CD to date.

The extraction of  $S_{17}(E)$  from the differential CD cross section  $d\sigma/dE$ , which varies rapidly with energy, is not trivial. The poor energy resolution in CD experiments, together with the influence of experimental cuts, require careful simulations of this distribution using a theoretical model. In addition to the dominant single  $E1$  photon exchange, other potentially important factors are  $E2$  transitions, nuclear break-up, and higher-order corrections. All of these effects are expected to be smaller at the higher energy of the GSI experiment than at the lower energies of the RIKEN and MSU experiments. However, a proper analysis of the GSI experiment requires relativistic modeling, a step so far taken only in perturbation theory (Bertulani, 2005; Ogata and Bertulani, 2009).

For the RIKEN case, Kikuchi *et al.* (1997) presented differential cross sections  $d\sigma/d\theta_8$ , where  $\theta_8$  is the scattering angle of the excited  $^8\text{B}^*$  system reconstructed from the  $^7\text{Be}$  and  $p$  momentum vectors, relative to that of the incoming  $^8\text{B}$ . The measured distribution was compared to first-order perturbative calculations that included  $E1$  and both nuclear and Coulomb  $\ell = 2$  transition amplitudes. At low relative energies, the authors found good agreement of their measured distributions with those from a model that assumes only a dipole contribution. Later investigations of the same data employed more sophisticated reaction models, stressing the importance of all the effects mentioned above (Alt *et al.*, 2003, 2005; Esbensen *et al.*, 2005; Goldstein *et al.*, 2007; Ogata *et al.*, 2006; Summers and Nunes, 2005). For example, the value of  $S_{17}(0)$  obtained from the continuum-discretized coupled-channels (CDCC) analysis of Ogata *et al.* (2006) is 13% larger than that determined in the first-order calculation of Kikuchi *et al.* (1998).

At MSU, inclusive measurements were performed to test the prediction that interference between  $E1$  and  $E2$  transitions in the CD of  $^8\text{B}$  would produce asymmetries in the longitudinal momentum distributions of the emitted fragments (Esbensen and Bertsch, 1996). Longitudinal momentum distributions of the  $^7\text{Be}$  fragments from the break-up of  $^8\text{B}$  on Pb and Ag targets at beam energies of 44 and 81 A MeV were measured (Davids *et al.*, 1998, 2001b). Asymmetries in these distributions were incontrovertibly observed and were interpreted with both first-order perturbative and CDCC calculations. The  $E2$  strengths deduced from first order perturbation theory were found to be somewhat smaller than or consistent



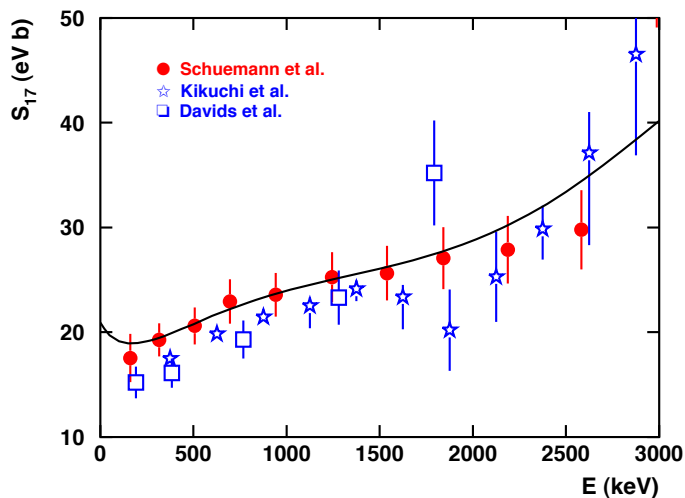


FIG. 8 (Color online)  $S_{17}$  values from CD experiments. Full red circles: latest analysis of the GSI CD experiment (Schümann *et al.*, 2006); open blue stars: Kikuchi *et al.* (1998) analyzed in first-order perturbation theory; open blue squares: Davids and Typel (2003). The error bars include statistical and estimated systematic errors. The curve is taken from the cluster-model theory of Descouvemont *et al.* (2004), normalized to  $S_{17}(0) = 20.8$  eV b.

with all published models of  ${}^8\text{B}$  structure. Later, the longitudinal momentum distributions of the emitted protons were studied in the exclusive MSU measurement at 83 A MeV (Davids *et al.*, 2001a,b) and found to be consistent with the  ${}^7\text{Be}$  distributions observed in the inclusive measurement. The  $S_{17}(E)$  distribution was extracted from  $d\sigma/dE$  (Davids and Typel, 2003) with a requirement that  $\theta_8 < 1.8^\circ$ , corresponding classically to an impact parameter of 30 fm; a small  $E2$  contribution derived from the inclusive measurements was taken into account.

Schümann *et al.* (2006) published the most extensive set of differential cross sections for the GSI experiment. All distributions were gated by  $\theta_8 < 1^\circ$ , corresponding to an impact parameter of 18.5 fm. The measured distributions were compared to theoretical ones filtered by the experimental efficiency and resolution using a GEANT-3 simulation. The event generator employed a simple first-order perturbation-theory description of Coulomb breakup with only  $E1$  transitions included. The authors chose this simple model for its ease in numerical calculations and for its fidelity in reproducing, e.g., the inclusive  $\theta_8$  distribution (Fig.11 of Schümann *et al.* (2006)) and the surprisingly symmetric  $\theta_{cm}^p$  distributions of the protons in the  ${}^8\text{B}^*$  reference system (Fig. 13 in Schümann *et al.* (2006)). Consequently,  $S_{17}(E)$  was deduced from this model under the assumption that, contrary to theoretical expectations,  $E2$  transitions could be ignored. The data points resulting from all three CD experiments are shown in Fig. 8. (Note that the RIKEN data points were taken from the first-order perturbation-theory analysis by Kikuchi *et al.* (1998).)

The different assumptions made in analyzing the ex-

periments as well as the number and precision of the CD  $S_{17}(E)$  data points prevent a precise determination of the shape, which therefore has to be taken from the radiative-capture measurements. In Fig. 8 we display the best-fit curve for the direct  $(p, \gamma)$  data, including the dominant  $E1$  multipole but not the  $M1$  contribution (see Sec. IX.D).

It is difficult to quantitatively assess the impact of the different theories and energy ranges used in analyzing the three CD experiments on the derived  $S_{17}(0)$  values. The resulting values are  $21.4 \pm 2.0$  eV b for the RIKEN experiment, as reanalyzed by Ogata *et al.* (2006);  $20.6 \pm 1.4$  eV b for the GSI experiment; and  $17.8^{+1.4}_{-1.2}$  eV b for the MSU experiment. Empirically these values are consistent with the range Solar Fusion I defined for direct measurements,  $S_{17}(0) = 19^{+4}_{-2}$  eV b. Moreover, the good agreement between the shapes of the GSI CD and the radiative capture data eliminates the concern about systematically different slopes of  $S_{17}(E)$  derived from the respective methods. However, we believe it would be premature to include the CD results in our determination of a recommended value for  $S_{17}(0)$ , as a better understanding of the role of  $E2$  transitions and higher order effects in  ${}^8\text{B}$  breakup at various energies is needed. Further discussions can be found in Sec. XII.

#### D. Direct ${}^7\text{Be}(p, \gamma){}^8\text{B}$ analysis and $S_{17}(0)$ determination

Figure 9 shows the modern  ${}^7\text{Be}(p, \gamma){}^8\text{B}$  data with center-of-mass energy  $E \leq 1250$  keV. We analyzed the Filippone *et al.* (1983) data using the  ${}^7\text{Li}(d, p)$  cross section given in Solar Fusion I. Total errors, including systematic errors, are shown on each data point, to facilitate a meaningful comparison of different data sets. All data sets exhibit a similar  $S_{17}(E)$  energy dependence, indicating that they differ mainly in absolute normalization.

Following the discussion in Sec. IX.B, we determine our best estimate of  $S_{17}(0)$  by extrapolating the data using the scaled theory of Descouvemont (2004) (MN calculation). We performed two sets of fits, one to data below the resonance, with  $E \leq 475$  keV, where we felt the resonance contribution could be neglected. In this region, all the individual  $S_{17}(0)$  error bars overlap, except for the Bochum result, which lies low.

We also made a fit to data with  $E \leq 1250$  keV, where the  $1^+$  resonance tail contributions had to be subtracted. We did this using the resonance parameters of Junghans *et al.* (2003) ( $E_p=720$  keV,  $\Gamma_p=35.7$  keV and  $\Gamma_\gamma = 25.3$  meV), adding in quadrature to data errors an error of 20% of the resonance subtraction. In order to minimize the error induced by variations in energy-averaging between experiments, we excluded data close to the resonance, from 490 to 805 keV, where the S-factor is strongly varying and the induced error is larger than 1.0 eV b. Above the resonance, the data have smaller errors. Only the Filippone *et al.* (1983) and Weizmann group error bars overlap the UW-Seattle/TRIUMF error bars.



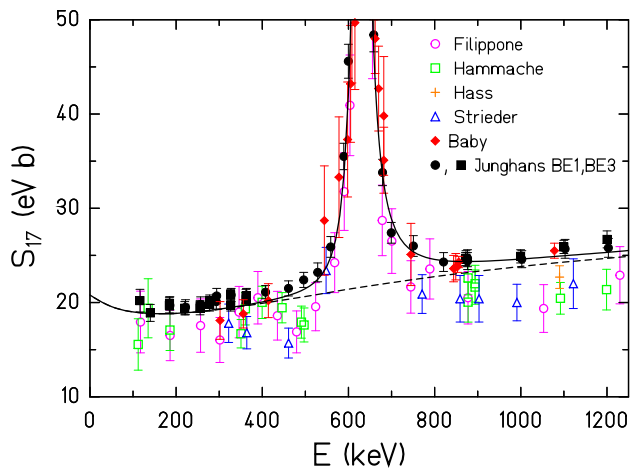


FIG. 9 (Color online)  $S_{17}(E)$  vs. center-of-mass energy  $E$ , for  $E \leq 1250$  keV. Data points are shown with total errors, including systematic errors. Dashed line: scaled Descouvemont (2004) curve with  $S_{17}(0) = 20.8$  eV b; solid line: including a fitted  $1^+$  resonance shape.

Figure 9 shows the best-fit Descouvemont (2004) (MN interaction) curve from the  $E \leq 475$  keV fit (together with the  $1^+$  resonance shape determined in Junghans *et al.* (2003), shown here for display purposes). Our fit results are shown in Table VII. The errors quoted include the inflation factors, calculated as described in the Errors Appendix. The main effect of including the inflation factors is to increase the error on the combined result by the factor 1.7 for  $E \leq 475$  keV, and by 2.0 for  $E \leq 1250$  keV. Both the  $S_{17}(0)$  central values and uncertainties from the combined fits for these two energy ranges agree well, the latter because the added statistical precision in the  $E \leq 1250$  keV fit is mostly offset by the larger inflation factor.

We also did fits in which the low energy cutoff was varied from 375 to 475 keV and the high energy exclusion region was varied from 425-530 to 805-850 keV. The central value of  $S_{17}(0)$  changed by at most 0.1 eV b. On this basis we assigned an additional systematic error of  $\pm 0.1$  eV b to the results for each fit region.

To estimate the theoretical uncertainty arising from our choice of the nuclear model, we also performed fits using the shapes from other plausible models: Descouvemont (2004) plus and minus the theoretical uncertainty shown in Fig. 8 of that paper; Descouvemont and Baye (1994); the CD-Bonn 2000 calculation shown in Fig. 15 of Navrátil *et al.* (2006b); and four potential model calculations fixed alternately to reproduce the  ${}^7\text{Li} + n$  scattering lengths, the best-fit  ${}^7\text{Be} + p$  scattering lengths, and their upper and lower limits (Davids and Typel, 2003). The combined-fit results for all these curves, including Descouvemont (2004), are shown in Table VIII.

We estimate the theoretical uncertainty on  $S_{17}(0)$  from the spread of results in Table VIII:  $\pm 1.4$  eV b for the  $E \leq 475$  keV fits, and  ${}^{+1.5}_{-0.6}$  eV b from the  $E \leq 1250$  keV fits (the smaller error estimate in the latter case reflects

TABLE VII Experimental  $S_{17}(0)$  values and (inflated) uncertainties in eV b, and  $\chi^2/dof$  determined by fitting the Descouvemont (2004) MN calculation to data with  $E \leq 475$  keV and with  $E \leq 1250$  keV, omitting data near the resonance in the latter case.

Fit Range	$E \leq 475$ keV			$E \leq 1250$ keV		
Experiment	$S_{17}(0)$	$\sigma$	$\chi^2/dof$	$S_{17}(0)$	$\sigma$	$\chi^2/dof$
Baby	20.2	1.4 <sup>a</sup>	0.5/2	20.6	0.5 <sup>a</sup>	5.2/7
Filippone	19.4	2.4	4.7/6	18.0	2.2	15.8/10
Hammache	19.3	1.1	4.8/6	18.2	1.0	12.5/12
Hass				18.9	1.0	0/0
Junghans BE3	21.6	0.5	7.4/12	21.5	0.5	12.3/17
Strieder	17.2	1.7	3.5/2	17.1	1.5	5.1/6
Mean	20.8	0.7	9.1/4	20.3	0.7	18.1/5

<sup>a</sup>We include an additional 5% target damage error on the lowest 3 points, consistent with the total error given in the text of Baby *et al.* (2003a) (M. Hass, private communication, 2009).

TABLE VIII Experimental  $S_{17}(0)$  values and (inflated) uncertainties in eV b, and  $\chi^2$  determined by fitting nine calculations to the data sets of Table VII. The  $E \leq 475$  keV fits have  $dof = 4$  and the  $E \leq 1250$  keV fits have  $dof=5$ . D04 is Descouvemont (2004), DB94 is Descouvemont and Baye (1994), and NBC06 is Navrátil *et al.* (2006b).

Fit Range	$E \leq 475$ keV			$E \leq 1250$ keV		
Model	$S_{17}(0)$	$\sigma$	$\chi^2$	$S_{17}(0)$	$\sigma$	$\chi^2$
D04 (central)	20.8	0.7	9.1	20.3	0.7	18.1
D04 (upper)	20.1	0.7	10.0	19.7	0.7	18.5
D04 (lower)	21.5	0.7	8.1	21.0	0.7	17.3
DB94	21.4	0.7	8.4	21.5	0.7	16.7
NBC06	22.1	0.7	7.4	21.8	0.8	18.5
${}^7\text{Be}+p$ (central)	21.2	0.7	8.7	20.2	0.7	19.7
${}^7\text{Be}+p$ (upper)	19.4	0.8	11.7	17.3	0.7	21.6
${}^7\text{Be}+p$ (lower)	21.7	0.7	8.2	21.0	0.7	19.4
${}^7\text{Li}+n$	20.5	0.7	9.7	19.1	0.7	20.9

the exclusion of the poorer potential-model fits). We note that the estimated uncertainties are substantially larger than those given in Junghans *et al.* (2003) and in Descouvemont (2004).

We expect the model dependence<sup>3</sup> of the fit to be greater above the resonance because of the demonstrated dependence of the S-factor in this range on

<sup>3</sup> Recently Yamaguchi *et al.* (2009) discussed a contribution of a possible higher energy (3.2 MeV)  $2^-$  resonance to  ${}^7\text{Be}(p,\gamma)$ . They estimate its contribution by taking the transition strength to be a Weisskopf unit. As low-lying E1 transitions are typically strongly inhibited, this estimate is unlikely to be realistic. Our S-factor estimate is based on a fit to low-energy data that would be free from any significant influence of this distant resonance, regardless of such assumptions.

the less-constrained short-range part of the wave functions (Cs6t6, 1997; Descouvemont, 2004; Jennings *et al.*, 1998b). We base our  $S_{17}(0)$  recommendation on the  $E \leq 475$  keV fit,

$$S_{17}(0) = 20.8 \pm 0.7(\text{expt}) \pm 1.4(\text{theor}) \text{ eV b.} \quad (49)$$

This value is in agreement with, but substantially more precise than, the Solar Fusion I recommendation,  $S_{17}(0) = 19_{-2}^{+4}$  eV b.

## X. THE SPECTRUM OF ${}^8\text{B}$ NEUTRINOS

The  ${}^8\text{B}$  neutrino spectrum differs from an allowed shape primarily because the principal state populated in the decay is a broad resonance. A precise determination of the neutrino spectrum is important to the analyses of the  ${}^8\text{B}$  neutrino data obtained by the Super-Kamiokande and SNO collaborations. Uncertainties in the spectrum are a source of systematic error in these experiments, potentially affecting conclusions about the hep flux, MSW spectral distortions, etc. The neutrino spectrum can be determined from laboratory measurements of  ${}^8\text{B}$   $\beta^+$  decay in which the decays of final-state  ${}^8\text{Be}$  resonances are observed.

The  ${}^8\text{B}$   $\beta^+$  decay from the  $J^\pi = 2^+$  ground state is followed by the emission of two  $\alpha$  particles from excited  $2^+$  states of  ${}^8\text{Be}$  (see Fig. 10). Although the region of interest is dominated by a single state in  ${}^8\text{Be}$  with  $E_x \sim 3$  MeV, the width of this resonance is quite large,  $\Gamma \sim 1.5$  MeV. Consequently the  $\alpha$  spectrum yields a continuum, so that other  $2^+$  states need to be considered. The  $\alpha$  spectrum was first measured by Farmer and Class (1960), and later by Wilkinson and Alburger (1971). R-matrix analyses were presented by Barker (1989) and Warburton (1986) (but see the caveat of Bhattacharya and Adelberger (2002)). Bahcall *et al.* (1996) used the existing data to produce a recommended neutrino spectrum that was widely used in subsequent analyses of neutrino experiments.

Ortiz *et al.* (2000) claimed a discrepancy with previous determinations of the  $\alpha$  spectrum. Subsequently Winter *et al.* (2003) and Bhattacharya *et al.* (2006) studied the spectrum via experiments with very different systematic uncertainties, finding excellent agreement with each other but disagreement with the claim of Ortiz *et al.* (2000). It was reported (A. Garc6a, private communication, 2009) that Ortiz *et al.* (2000) now recognize that they underestimated uncertainties related to the energy loss generated by carbon buildup in their targets, so that a claim of a disagreement with earlier measurements no longer should be made. We recommend using the  $\alpha$  spectrum of Winter *et al.* (2006) and the consistent and higher precision spectrum of Bhattacharya *et al.* (2006). These experiments do not suffer from the energy calibration problems that affected earlier experiments, as discussed by Bahcall *et al.* (1996). Finally we recommend the neu-

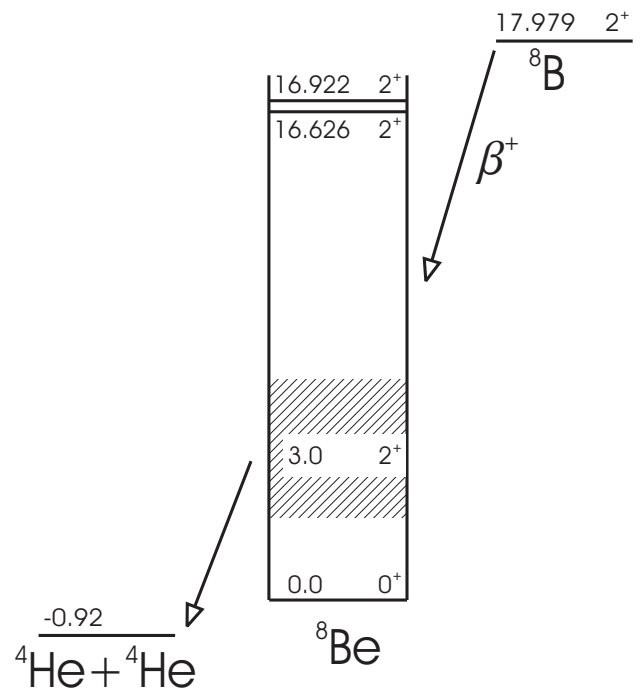


FIG. 10 Energy levels from the  ${}^8\text{B}(\beta^+){}^8\text{Be}(2\alpha)$  decay chain.

trino spectrum tabulated in Winter *et al.* (2006)<sup>4</sup>. [The neutrino spectrum was not calculated by Bhattacharya *et al.* (2006).]

The positron spectrum can be deduced from the  $\alpha$  spectrum in a similar fashion, and is useful as a test of data consistency. The measurements of Napolitano *et al.* (1987) have been shown by Winter *et al.* (2006) to be in good agreement with the results from the  $\alpha$  spectrum.

Forbidden corrections are at the level of a few percent. Many measurements have been performed to determine needed matrix elements (Bowles and Garvey, 1978; De Braeckeleer *et al.*, 1995; McKeown *et al.*, 1980; Nathan *et al.*, 1975; Paul *et al.*, 1977; Tribble and Garvey, 1974, 1975). Radiative corrections are smaller at a fraction of one percent and have been calculated by Sirin (1967) and by Batkin and Sundaresan (1995). Both sets of corrections are described by Winter *et al.* (2006), and incorporated into the spectrum given there. Bahcall (1991) showed that red-shift distortions associated with the Sun's gravitational potential are insignificant, affecting the spectrum at the fractional level of  $\sim 10^{-5}$ . Bacrania *et al.* (2007) have placed a 90% confidence-level bound on the branching ratio for  ${}^8\text{B}$   $\beta$  decay to the  $0^+$  ground state of  ${}^8\text{Be}$  (a second-forbidden transition) of  $7.3 \times 10^{-5}$  (see Fig. 10), limiting uncertainties in the high energy portion of the  ${}^8\text{B}$  neutrino spectrum.

<sup>4</sup> The strength function and the neutrino and positron spectra are in electronic repositories available online through Phys. Rev. C.

## XI. THE CNO CYCLES

The need for two mechanisms to account for the stellar burning of hydrogen to helium was recognized in the pioneering work of Bethe and collaborators. The pp chain, which dominates energy production in low-mass main-sequence stars, can operate in metal-free stars, synthesizing  ${}^4\text{He}$  from H, while creating equilibrium abundances of deuterium,  ${}^3\text{He}$ , and  ${}^7\text{Be}/{}^7\text{Li}$ , the elements participating in intermediate steps of Fig. 2.

Heavier main-sequence stars produce their energy dominantly through the CNO cycles, where reactions are characterized by larger Coulomb barriers. Hence, the energy production rises more steeply with increasing temperature ( $\epsilon_{\text{CNO}} \propto T^{18}$  compared to  $\epsilon_{\text{pp}} \propto T^4$  at solar core temperature, as illustrated in Fig. 1). The CNO cycle was proposed by Bethe and Weizsäcker to account for the evolutionary tracks of massive stars. Unlike the pp-chain, the CNO bi-cycle of Fig. 2 requires pre-existing metals to process H into  ${}^4\text{He}$ . Thus the contribution to energy generation is directly proportional to the solar-core number abundance of the primordial metals. The CN-cycle, denoted by I in Fig. 2, is an important SSM neutrino source. It also accounts for about 1% of solar energy generation. The cycle conserves the number abundance, but alters the distribution of solar metals as it burns into equilibrium, eventually achieving equilibrium abundances proportional to the inverse of the respective rates. In the Sun this leads to the conversion of almost all of the core's primordial  ${}^{12}\text{C}$  into  ${}^{14}\text{N}$ . This change in the chemical composition alters the core's opacity and, at the 3% level, the heavy element mass fraction  $Z$ , SSM effects first explored by Bahcall and Ulrich (1988).

The  ${}^{14}\text{N}(p,\gamma)$  reaction – the slowest reaction in the CN cycle at low temperatures and thus the rate-controlling step – determines whether equilibrium has been achieved. The  ${}^{14}\text{N}$  lifetime is shorter than the age of the Sun for temperatures  $\gtrsim 1.33 \times 10^7$  K. Therefore equilibrium for the CN cycle has been reached only for  $R \lesssim 0.1R_{\odot}$ , corresponding to the central 7% of the Sun by mass. Consequently, over a significant portion of the outer core,  ${}^{12}\text{C}$  has been converted to  ${}^{14}\text{N}$ , but further reactions are inhibited by the  ${}^{14}\text{N}(p,\gamma)$  bottleneck.

### A. The reaction ${}^{14}\text{N}(p,\gamma){}^{15}\text{O}$

#### 1. Current status and results

Figure 11 shows the level structure of  ${}^{15}\text{O}$ , relative to the threshold energy for  ${}^{14}\text{N}(p,\gamma)$ .

Solar Fusion I gave  $3.5_{-1.6}^{+0.4}$  keV b as the recommended total S-factor for the  ${}^{14}\text{N}(p,\gamma){}^{15}\text{O}$  reaction. This was based on the energy dependence determined by Schröder *et al.* (1987). In the Schröder *et al.* (1987) analysis the ground state transition accounted for half of the total S-factor at zero energy, primarily because of the contribution of a subthreshold resonance at  $E = -504$  keV

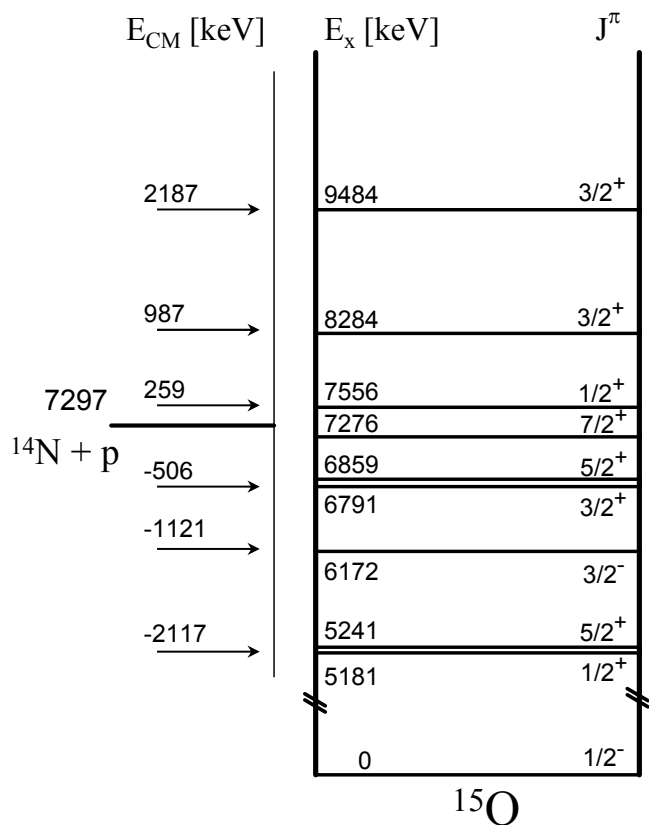


FIG. 11 The energy levels of  ${}^{15}\text{O}$  and their relationship to the threshold energy for  ${}^{14}\text{N}(p,\gamma)$ .

(corresponding to the 6.79 MeV state in  ${}^{15}\text{O}$ ). However, a reanalysis based on an R-matrix calculation by Angulo and Descouvemont (2001) indicated that the strength of the ground state transition in Schröder *et al.* (1987),  $S_{14}^{\text{gs}}(0) = 1.55$  keV b, had been significantly overestimated, and should be reduced to 0.08 keV b.

This finding prompted a series of new experiments using direct (Bemmerer *et al.*, 2006b; Formicola *et al.*, 2004; Imbriani *et al.*, 2005; Lemut *et al.*, 2006; Marta *et al.*, 2008; Runkle *et al.*, 2005) and indirect approaches (Bertone *et al.*, 2001, 2002; Mukhamedzhanov *et al.*, 2003; Nelson *et al.*, 2003; Schürmann *et al.*, 2008; Yamada *et al.*, 2004). The prompt-capture  $\gamma$ -radiation was measured in experiments by the TUNL group (Runkle *et al.*, 2005) in a surface laboratory and by the LUNA group (Formicola *et al.*, 2004; Imbriani *et al.*, 2005; Marta *et al.*, 2008) in Gran Sasso. From these experiments – carried out with Ge detectors – the contributions of each transition could be extracted. In an additional measurement by the LUNA Collaboration (Bemmerer *et al.*, 2006b; Lemut *et al.*, 2006) the total cross section was determined. These recent experiments cover an energy range from 70 to 480 keV, still far from the solar Gamow window at  $E_0 = 27$  keV. Additional information is provided by experiments that probe the width of the subthreshold state at  $E = -506$  keV by the Doppler shift attenuation method

(Bertone *et al.*, 2001; Schürmann *et al.*, 2008) and by Coulomb excitation (Yamada *et al.*, 2004). Asymptotic normalization coefficients (ANC) for the ground state and selected excited states were determined from transfer reaction measurements for  $^{14}\text{N}(^3\text{He,d})^{15}\text{O}$  by Bertone *et al.* (2002) and Mukhamedzhanov *et al.* (2003). All experiments and subsequent analyses confirmed that the value for the ground-state contribution determined in the extrapolations of Schröder *et al.* (1987) had been too high. Current estimates of  $S_{14}^{\text{gs}}(0)$  range from 0.08 keV b (Angulo and Descouvemont, 2001) to 0.45 keV b (Runkle *et al.*, 2005). Hence, the S-factor for  $^{14}\text{N}(p,\gamma)^{15}\text{O}$  is now determined largely by the transition to the 6.79 MeV state. Minor contributions arise from transitions to the 5.18, 5.24, 6.17, 6.86 and 7.28 MeV states in  $^{15}\text{O}$ .

## 2. R-matrix analysis and normalization

We have performed an R-matrix fit to the three strongest transitions using the data of Imbriani *et al.* (2005), Marta *et al.* (2008), Runkle *et al.* (2005), and Schröder *et al.* (1987) and the code of Descouvemont (Descouvemont and Baye, 2010). In this way we obtain the most robust weighted mean. The recent direct experiments (Bemmerer *et al.*, 2006b; Formicola *et al.*, 2004; Imbriani *et al.*, 2005; Lemut *et al.*, 2006; Marta *et al.*, 2008; Runkle *et al.*, 2005) cover only a relatively narrow energy window. Thus, as no new information is available for the higher lying resonances, a reliable extrapolation to zero energy requires the high-energy data of Schröder *et al.* (1987). However, systematic differences are apparent in the data sets of Imbriani *et al.* (2005), Runkle *et al.* (2005), and Schröder *et al.* (1987). In order to minimize systematic uncertainties, all data sets were renormalized to the weighted mean of the strength of the 259 keV resonance in  $^{14}\text{N}(p,\gamma)^{15}\text{O}$ . Table IX summarizes the available absolute determinations of the resonance strength with a weighted mean of  $\omega\gamma_{259} = 13.1 \pm 0.6$  meV. The uncertainty was obtained by calculating the error on the weighted mean, excluding the common systematic uncertainty on the stopping power of protons in nitrogen (Ziegler *et al.*, 2008). The latter was summed in quadrature with the weighted mean error to obtain the final uncertainty.

In Schröder *et al.* (1987) the data were normalized to an absolute cross section determination at  $E = 760$  keV,  $\sigma(E = 760 \text{ keV}) = 620 \pm 80$  nb. This value is an adopted mean based on several experimental methods, while the measurement relative to  $\omega\gamma_{259}$  gives  $\sigma(E = 760 \text{ keV}) = 609$  nb (Schröder *et al.*, 1987). Thus, based on the difference between the value for  $\omega\gamma_{259}$  used by Schröder *et al.* (1987), 14 meV (Becker *et al.*, 1982), and the new determination,  $13.1 \pm 0.6$  meV, a precise renormalization of  $\sigma(E = 760 \text{ keV})$  can be made, relative to this resonance. One finds  $\sigma(E = 760 \text{ keV}) = 570$  nb. Moreover, we note that the energy dependence of Schröder *et al.* (1987) was corrected for summing contributions, as dis-

TABLE IX Summary of the published values for  $\omega\gamma_{259}$ , along with their estimated statistical, systematic, and total uncertainties. All quantities are in units of meV. The last row gives the recommended value.

	$\omega\gamma_{259}$	stat.	syst.	total
Becker <i>et al.</i> (1982) <sup>a</sup>	14			1.0
Runkle <i>et al.</i> (2005)	13.5		1.2	1.2
Imbriani <i>et al.</i> (2005)	12.9	0.4	0.8	0.9
Bemmerer <i>et al.</i> (2006b)	12.8	0.3	0.5	0.6
recommended value	13.1			0.6

<sup>a</sup>used in Schröder *et al.* (1987)

cussed by Imbriani *et al.* (2005). The renormalizations for Runkle *et al.* (2005) and Imbriani *et al.* (2005) are 3% and 2%, respectively.

The ANCs for the ground, 6.79 MeV, and 6.17 MeV states as well as  $\Gamma_\gamma$  of the 6.79 MeV state are important parameters in the R-matrix analysis determining  $S(0)$ . Parameter values determined in the analysis will reflect the quality of the input data. Thus the R-matrix results can be validated by comparing these values with those determined independently by transfer reactions and other indirect measurements (see Table X).

## 3. Transition to the ground state and 6.79 MeV in $^{15}\text{O}$

The transitions to the ground and 6.79 MeV states in  $^{15}\text{O}$  are connected through the reduced proton width of the  $-0.506$  MeV subthreshold state. This width can also be expressed in terms of the subthreshold state ANC via the Whittaker function at the R-matrix radius  $a$  that appears in Eq. (3.60) of Descouvemont and Baye (2010) (see references therein). Both transitions are discussed together here.

*Transition to the 6.79 MeV state:* The reaction mechanism for the transition to the 6.79 MeV state appears rather simple, primarily an external capture process whose magnitude is determined by the value of the ANC. Hence  $S_{14}^{6.79}(0)$  is dominated by the external capture process. In the present analysis the data of Runkle *et al.* (2005), Imbriani *et al.* (2005), and Schröder *et al.* (1987) are included after renormalization, as described above. As the recent low-energy data do not strongly constrain the R-matrix radius, high-energy data are needed. The resulting  $S_{14}^{6.79}(E)$  fails to reproduce the high-energy data for radii  $5.5 \text{ fm} < a < 6.5 \text{ fm}$ , as in Fig. 4 of Angulo and Descouvemont (2001). A better fit can be obtained by choosing smaller radii. However, this choice also impacts fits for the ground state transition, which favor larger radii. Consequently, we have not used the transition to the 6.79 MeV state to determine the R-matrix radius in this way. Instead, R-matrix fits were done

- i) taking all renormalized data (Imbriani *et al.*, 2005; Runkle *et al.*, 2005; Schröder *et al.*, 1987) into ac-

TABLE X Published ANC values and  $\Gamma_\gamma$  for the 6.79 MeV transition. All ANC values are given in the coupling scheme of Angulo and Descouvemont (2001). The recommended values in the last row were obtained as a weighted mean considering as weights the experimental errors only. Finally, the recommended uncertainty was obtained by summing in quadrature the weighted mean error and an average theoretical uncertainty. The latter is according to information provided by the authors. As existing measurements of  $\Gamma_\gamma(6.79 \text{ MeV})$  are discrepant, no recommended value is given.

	$C_{\text{gs}^{3/2}} \text{ (fm}^{-1/2}\text{)}^a$	$C_{6.79} \text{ (fm}^{-1/2}\text{)}$	$C_{6.17^{1/2}} \text{ (fm}^{-1/2}\text{)}^b$	$C_{6.17^{3/2}} \text{ (fm}^{-1/2}\text{)}^a$	$\Gamma_\gamma(6.79) \text{ (eV)}$
Mukhamedzhanov <i>et al.</i> (2003)	$7.4 \pm 0.4$	$4.9 \pm 0.5$	$0.47 \pm 0.03$	$0.53 \pm 0.03$	
Bertone <i>et al.</i> (2002)	$7.9 \pm 0.9$	$4.6 \pm 0.5$	$0.45 \pm 0.05$	$0.51 \pm 0.06$	
Bertone <i>et al.</i> (2001)					$0.41^{+0.34}_-0.13^c$
Yamada <i>et al.</i> (2004)					$0.95^{+0.6}_-0.95$
Schürmann <i>et al.</i> (2008)					$> 0.85$
recommended value	$7.4 \pm 0.5$	$4.8 \pm 0.5$	$0.47 \pm 0.03$	$0.53 \pm 0.04$	

<sup>a</sup>channel spin  $I = 3/2$

<sup>b</sup>channel spin  $I = 1/2$

<sup>c</sup>the quoted uncertainty represents a 90% confidence limit

count;

ii) limiting the data sets to  $E < 1.2 \text{ MeV}$ ; and

iii) same as i), but introducing an unidentified  $J^\pi = 5/2^-$  pole at  $E = 6 \text{ MeV}$ .

In each case the ANC values and the radii were determined. The results for the three cases are

- i)  $C_{6.79} = 4.61 \pm 0.02 \text{ fm}^{-1/2}$  for  $a = 4.14 \text{ fm}$  and  $S_{114}^{6.79}(0) = 1.11 \text{ keV b}$ . This solution has the lowest  $\chi^2$  but was rejected for the reasons given above.
- ii)  $C_{6.79} = 4.65 \pm 0.02 \text{ fm}^{1/2}$  for  $a = 4.6 \text{ fm}$  and  $S_{114}^{6.79}(0) = 1.15 \text{ keV b}$ .
- iii)  $C_{6.79} = 4.69 \pm 0.02 \text{ fm}^{1/2}$  for  $a = 5.4 \text{ fm}$  and  $S_{114}^{6.79}(0) = 1.18 \text{ keV b}$ .

The latter two fits are in very good agreement with Runkle *et al.* (2005) and about 5% lower than Imbriani *et al.* (2005). All three fits are shown in Fig. 12.

In summary, the dominant systematic uncertainty for  $S_{114}^{6.79}(0)$  arises from the interpretation of the high-energy data. This uncertainty is estimated from cases i) to iii) to be about 4%. One could speculate that the deviation of the higher energy data from the R-matrix fit is due to broad unidentified structures in this transition (Fig. 12). We recommend  $S_{114}^{6.79}(0) = 1.18 \pm 0.05 \text{ keV b}$ . The error includes both systematic and statistical uncertainties, though the former are much larger.

The weighted mean of the ANC for the 6.79 MeV state from indirect measurements,  $C_{6.79} = 4.8 \pm 0.5 \text{ fm}^{-1/2}$  (Table X), is in excellent agreement with the results of the R-matrix analysis.

*Ground state transition:* Three data sets (Imbriani *et al.*, 2005; Runkle *et al.*, 2005; Schröder *et al.*, 1987), normalized to  $\omega\gamma_{259}$  as discussed above, were used in the ground-state analysis. The results from Marta *et al.* (2008) – three data points with high precision above the 259 keV resonance and essentially free from summing effects – are relative to the yield of the transition to the 6.79

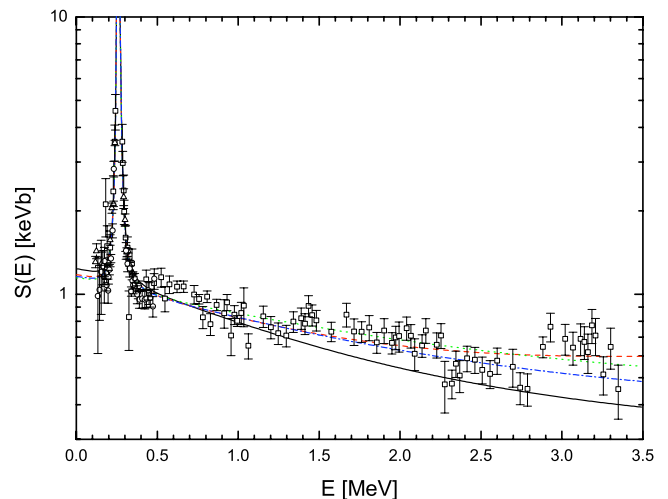


FIG. 12 (Color online) R-matrix fits to the  $^{14}\text{N}(p,\gamma)^{15}\text{O}$  6.79 MeV transition together with the data of Schröder *et al.* (1987) (open squares), Imbriani *et al.* (2005) (open triangles), and Runkle *et al.* (2005) (open circles). The cases i, ii, and iii (see text) are represented by the dotted green, dash-dotted blue, and dashed red lines, respectively. The black line is a calculation similar to iii), but without the unidentified  $J^\pi = 5/2^-$  pole at  $E=6 \text{ MeV}$ , comparable to fits in past work.

MeV state. These data were normalized to the weighted mean of the renormalized S-factor (see Sec. XI.A.2) from Schröder *et al.* (1987), Runkle *et al.* (2005), and Imbriani *et al.* (2005) in the energy region  $311 \text{ keV} < E < 360 \text{ keV}$ .

The R-matrix fit was based on the same poles as in Angulo and Descouvemont (2001) with starting parameters as given in Ajzenberg-Selove (1991). The sensitivity to radius was tested for a broad range of ANC values,  $6 \text{ fm}^{-1/2} < C_{\text{gs}^{3/2}} < 9 \text{ fm}^{-1/2}$ . The minimum  $\chi^2$  was obtained for  $a = 5.6 \pm 0.1 \text{ fm}$ . Thus, we selected  $a = 5.5 \text{ fm}$  as an appropriate average for the ground and 6.79

MeV states, employing this value for all subsequent R-matrix fits. This value was used previously in Runkle *et al.* (2005), Imbriani *et al.* (2005), Marta *et al.* (2008), and Mukhamedzhanov *et al.* (2003). The reduced width for the subthreshold state was fixed through  $C_{6.79}$  (see above) to  $\gamma^2=0.37$  MeV. The narrow resonances at 0.987 MeV ( $\Gamma_p = 3.6$  keV, see Fig. 13) and 2.191 MeV ( $J^\pi = 5/2^-, \Gamma_p = 10$  keV) are not relevant for  $S_{114}^{\text{gs}}(0)$  and thus were excluded from the fit. In order to optimize the fit off-resonance, contributions to  $\chi^2$  from points near the 2.191 MeV and 0.259 MeV ( $\Gamma_p \sim 1$  keV) resonances were omitted. As slopes are steep and counting rates peak near the resonances, the inclusion of near-resonance data forces the fit in arbitrary ways. The region excluded depends on resonance width and on target thickness, which can spread the effects of a resonance over a larger energy interval. We omitted data in the interval between  $E_R - 20\Gamma$  and  $E_R + 1.5\Delta$ , where  $\Delta$  is the target thickness. Target thickness effects are especially prominent in the data of Schröder *et al.* (1987), representing the integral over the target thickness of  $\sim 30$  keV.

In the fit the  $\chi^2$  decreases with increasing ANC, reaching a minimum at  $C_{\text{gs}^{3/2}} \sim 11 \text{ fm}^{-1/2}$ , a value outside the ranges determined by Mukhamedzhanov *et al.* (2003) and Bertone *et al.* (2002). At the  $9 \text{ fm}^{-1/2}$  upper bound for  $C_{\text{gs}^{3/2}}$ , we obtain  $S_{114}^{\text{gs}}(0) = 0.29$  keV b, while at the  $6 \text{ fm}^{-1/2}$  lower bound,  $S_{114}^{\text{gs}}(0) = 0.24$  keV b. These fits do not include the possibility of a small contribution from  $C_{\text{gs}^{1/2}}$ , interfering with the 259 keV resonance. We expand the uncertainty to account for such a possibility, recommending  $S_{114}^{\text{gs}}(0) = 0.27 \pm 0.05$  keV b with  $\Gamma_\gamma(\text{int}) = 1.1$  eV. The latter value is the internal part of the  $-0.504$  MeV subthreshold state radiative width (at  $E = 0$ ), a fit parameter in the R-matrix calculation. The total radiative width, which can be compared to experimental values obtained from, e.g., lifetime measurements, is derived following the approach of Holt *et al.* (1978) and Barker and Kajino (1991), giving  $\Gamma_\gamma(6.79) = |\Gamma_\gamma(\text{int})^{1/2} \pm \Gamma_\gamma(\text{ch})^{1/2}|^2$ , where the relative sign of the two amplitudes is unknown. The channel (external) radiative width  $\Gamma_\gamma(\text{ch}) = 0.57$  eV can be directly calculated from the adopted value of  $C_{\text{gs}^{3/2}}$ . If the minus sign is chosen in the relationship for  $\Gamma_\gamma(6.79)$ , one obtains a lifetime in excess of 4 fs, in disagreement with Bertone *et al.* (2001) and Schürmann *et al.* (2008). If the plus sign is chosen, a lifetime shorter than 0.2 fs is obtained. Such a lifetime is presently beyond the reach of Doppler shift lifetime measurements, but still in agreement with Schürmann *et al.* (2008). However, the Coulomb excitation work of Yamada *et al.* (2004) gives a lower limit of 0.4 fs, apparently ruling out such a short lifetime. We conclude that the current experimental situation is unsatisfactory and calls for further work. Lifetimes larger than 0.4 fs require  $C_{\text{gs}^{3/2}} < 6 \text{ fm}^{-1/2}$ , again in disagreement with Bertone *et al.* (2002) and Mukhamedzhanov *et al.* (2003). The somewhat larger range in  $C_{\text{gs}^{3/2}}$  used in the present analysis, compared to the uncertainty recommended in Table X, takes account of this dilemma.

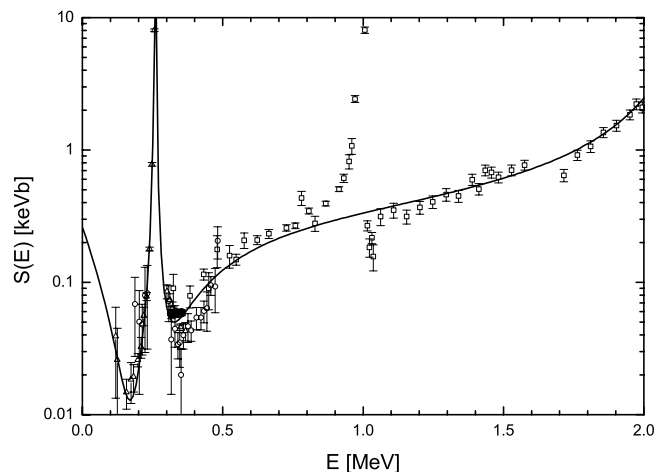


FIG. 13 R-matrix fit to the  $^{14}\text{N}(p,\gamma)^{15}\text{O}$  ground state transition. The filled circles are from Marta *et al.* (2008). All other data are labeled as in Fig. 12.

Most recent treatments of  $^{14}\text{N}(p,\gamma)^{15}\text{O}$  direct measurements have failed to address issues connected with the total radiative width.

#### 4. Transition to the 6.17 MeV state

This transition was analyzed with the poles given by Angulo and Descouvemont (2001) except that we also allowed for an external capture contribution (channel spin  $I = 3/2$ ), improving the fit substantially. The primary uncertainty in predicting  $S_{114}^{6.17}(0)$  arises from the choice of the poles, i.e., more poles at higher energies and their interference pattern, respectively, could be included in the fit. However, a full study of all possible minor contributions is far beyond the scope of the present work and would be hampered by the lack of precise data. The best fit yields  $S_{114}^{6.17}(0) = 0.13$  keV b with  $C_{6.17^{1/2}} = 0.43 \pm 0.02 \text{ fm}^{-1/2}$  and  $C_{6.17^{3/2}} = 0.49 \pm 0.02 \text{ fm}^{-1/2}$ . These ANCs are in good agreement with those deduced by Mukhamedzhanov *et al.* (2003) and Bertone *et al.* (2002) (see Table X). Previous results without the contribution from channel spin 3/2 external capture led to  $S_{114}^{6.17}(0) = 0.08$  keV b (Imbriani *et al.*, 2005) and 0.04 keV b (Runkle *et al.*, 2005). Thus, we have adopted  $S_{114}^{6.17}(0) = 0.13 \pm 0.06$  keV b where the error reflects the uncertainty in the R-matrix input as well as the spread of this value in the literature (Angulo and Descouvemont, 2001; Imbriani *et al.*, 2005; Nelson *et al.*, 2003; Runkle *et al.*, 2005). In Nelson *et al.* (2003) a  $M1$  contribution was inferred from an analyzing power experiment. The fit only extends to  $E \sim 327$  keV and trends above the data for higher energies. Runkle *et al.* (2005) showed that there is no significant difference in  $S_{114}^{6.17}(0)$  results from including the  $M1$  contribution specified by Nelson *et al.* (2003).



TABLE XI  $S_{114}(0)$  and the fractional uncertainty  $\Delta S_{114}(0)$  for the different transitions. Note that  $\text{tr}(5.24) \rightarrow 0$  includes contributions from the transition  $\text{tr} \rightarrow 6.86 \rightarrow 5.24$  and  $\text{tr} \rightarrow 7.28 \rightarrow 5.24$  with  $S_{114}(0) = 0.037 \pm 0.011$  and  $0.019 \pm 0.006$  keV b, respectively (from Schröder *et al.* (1987) with a 30% uncertainty). The contribution of  $\text{tr}(7.28) \rightarrow 0$  observed by Schröder *et al.* (1987) is negligible.

transition	$S_{114}(0)$ (keV b)	$\Delta S_{114}(0)$	reference
$\text{tr} \rightarrow 0$	$0.27 \pm 0.05$	19%	present
$\text{tr} \rightarrow 6.79$	$1.18 \pm 0.05$	4%	present
$\text{tr} \rightarrow 6.17$	$0.13 \pm 0.06$	38%	present
$\text{tr} \rightarrow 5.18$	$0.010 \pm 0.003$	30%	Imbriani <i>et al.</i> (2005)
$\text{tr}(5.24) \rightarrow 0^a$	$0.070 \pm 0.021$	30%	Imbriani <i>et al.</i> (2005)
R-Matrix sum	$1.66 \pm 0.08^b$	5%	
additional systematic uncertainty <sup>c</sup>		5%	
total	$1.66 \pm 0.12$	7%	

<sup>a</sup>value from the analysis of the secondary transition

<sup>b</sup>uncertainty from the R-matrix analysis only

<sup>c</sup>from normalization to  $\omega\gamma_{259}$

## 5. Total $S_{114}(0)$ and conclusions

We have obtained  $S_{114}^{\text{tot}}(0)$  from the data sets of Imbriani *et al.* (2005), Marta *et al.* (2008), and Schröder *et al.* (1987), normalized to the 259 keV resonance, and supported by an R-matrix analysis that defines the extrapolation to astrophysical energies. The R-matrix analysis focused on the systematic uncertainties associated with fitting and extrapolating the data, and made use of indirect measurements (Bertone *et al.*, 2001, 2002; Mukhamedzhanov *et al.*, 2003; Schürmann *et al.*, 2008; Yamada *et al.*, 2004) to constrain parameters in the fitting. Systematic uncertainties in this analysis dominate the errors: statistical uncertainties have minor consequences for the resulting  $S_{114}^{\text{tot}}(0)$ . The R-matrix radius  $a$  is a key parameter, fixed in the present analysis to the best-choice value of 5.5 fm (Sec. XI.A.3). The extrapolation for the strongest transition to the 6.79 MeV state is robust within 4%, while the extrapolations for transitions to the ground and 6.17 MeV states are less constrained. The transitions to the 5.18, 5.24, 6.86, and 7.28 MeV states combine to contribute 0.08 keV b to  $S_{114}^{\text{tot}}(0)$ ,  $\sim 5\%$  of the total. These contributions were obtained from literature (Imbriani *et al.*, 2005; Schröder *et al.*, 1987), scaled to the weighted mean of  $\omega\gamma_{259}$ . The errors on the individual transitions were enlarged to a more realistic uncertainty of 30%. Note that some of the weak transitions often have been neglected in past work. Finally, an additional systematic error of 5% due to the normalization of  $\omega\gamma_{259}$  (see Table IX) is included. Table XI summarizes the various contributions.

We find, after summing all contributions,  $S_{114}^{\text{tot}}(0) = 1.66 \pm 0.12$  keV b. The S-factor fits derived in the present study are shown in Figs. 12, 13, and 14 together with the renormalized data of Imbriani *et al.* (2005), Marta *et al.* (2008), Runkle *et al.* (2005), and Schröder *et al.* (1987). Figure 15 compares our results for the total  $S_{114}^{\text{tot}}(E)$  with the data from Lemut *et al.* (2006) and Bemmerer *et al.*

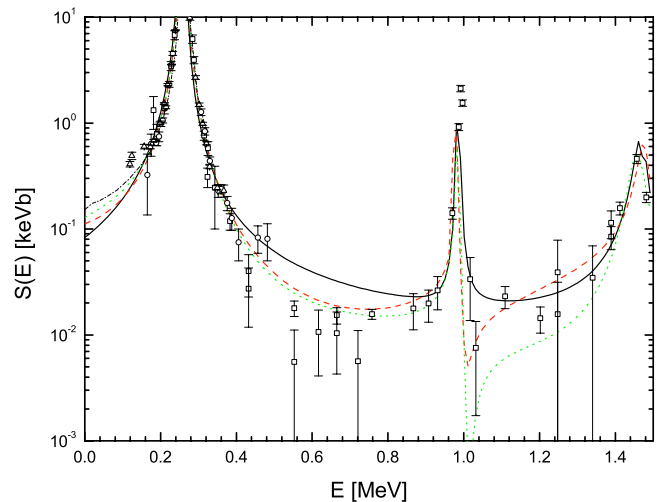


FIG. 14 (Color online) R-matrix fit to the  $^{14}\text{N}(p,\gamma)^{15}\text{O}$  6.17 MeV transition. The symbols are the same as in Fig. 12. The dotted green line corresponds to the present analysis. The solid black, dashed red, and dash-dotted black lines are the R-matrix fits of Imbriani *et al.* (2005), Runkle *et al.* (2005), and Nelson *et al.* (2003), respectively.

(2006b). Below  $E = 108$  keV the gas-target results and the R-matrix fit are not inconsistent, given uncertainties; at higher energies,  $E \sim 200$  keV, the average deviation is  $\sim 8\%$ . These data are an absolute determination of the S-factor and thus do not depend on the normalization of  $\omega\gamma_{259}$ .

$S_{114}^{\text{tot}}(E)$  below  $E \sim 130$  keV can be approximated to better than 1% by a second order polynomial

$$\begin{aligned}
 S_{114}^{\text{tot}}(0) &= 1.66 \text{ keV b} \\
 S_{114}^{\text{tot}'}(0) &= -0.0033 \text{ b} \\
 S_{114}^{\text{tot}''}(0) &= 4.4 \times 10^{-5} \text{ b/keV}. \quad (50)
 \end{aligned}$$

The absolute scale of this energy dependence has an un-

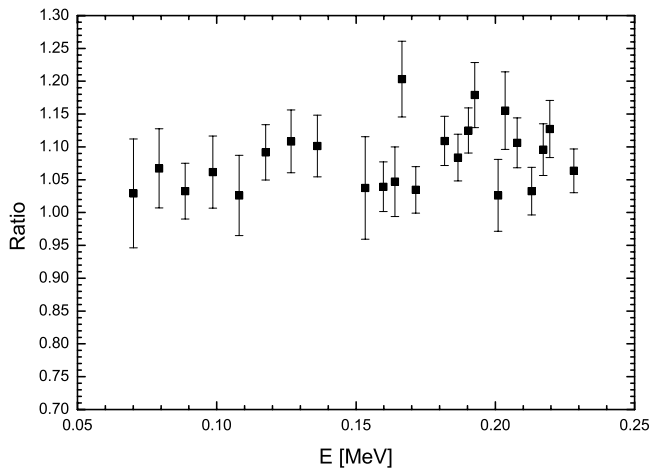


FIG. 15 Comparison of the  $S_{14}^{\text{tot}}$  obtained from the present R-matrix fit and gas target data. Note that the gas target data are corrected for electron screening (see Table 2 in Bemmerer *et al.* (2006b)) according to calculations of Assenbaum *et al.* (1987).

certainty of  $\pm 7\%$ . Recently, a coupled channel analysis of the data for  $^{14}\text{N}(p,\gamma)^{15}\text{O}$  has been reported (Grinevičute *et al.*, 2008) which gives  $S_{14}^{\text{tot}}(0) = 1.68$  keV b, in excellent agreement with the results presented here.

Further work on  $^{14}\text{N}(p,\gamma)^{15}\text{O}$  is needed. A better understanding of the reaction mechanism governing the transition to the 6.79 MeV state at high energies would help reduce systematic uncertainties. Moreover, additional experimental and theoretical work on the transition to the 6.17 MeV state is needed, as the existing database is lacking. A new determination of  $\Gamma_\gamma$  for the 6.79 MeV state with an alternative method would be desirable to constrain the R-matrix fit and to resolve slight discrepancies in existing data. Elastic scattering experiments could give an additional constraint. Finally, a high-precision measurement of  $\omega\gamma_{259}$  with significant improvements in the accuracy of stopping power data would reduce the systematic uncertainty in the normalization.<sup>5</sup>

<sup>5</sup> Note added in proof: A new R-matrix analysis of  $^{14}\text{N}(p,\gamma)^{15}\text{O}$  reaction appeared (Azuma *et al.*, 2010) after submission of the present work. This analysis, which served as a validity test for the AZURE code, yielded  $S_{14}^{\text{tot}}(0) = 1.81$  keV b, 9% larger than the central value recommended here. No uncertainty was provided. The differences between Azuma *et al.* (2010) and Solar Fusion II are connected with the 6.79 MeV transition. In the present work (i) a normalization procedure is employed to address needed corrections in the high-energy data and (ii) a background pole is introduced to achieve a better representation of that data. Without such adjustments, the procedure of Azuma *et al.* (2010) produces a fit that underestimates the high-energy data and consequently yields a larger  $S_{14}^{6.79}(0)$ . Nevertheless, the present and Azuma *et al.* (2010) results are consistent if one assigns a reasonable uncertainty to the latter.

## B. Other CNO-cycle reactions

While the  $^{14}\text{N}(p,\gamma)^{15}\text{O}$  reaction controls the cycling rate and the energy production by CN reactions at solar temperatures, other reactions in the cycle determine the extent to which the reaction flow moves out of the CN cycle toward heavier metals, oxygen in particular. These trends in turn affect the opacity evolution and temperature profiles as a function of solar age. There has been significant recent progress in determining the rates of many of these other reactions. The reader is referred to Solar Fusion I for summaries of other reactions for which there has not been new work reported since 1998. More recent reviews have been given by Angulo *et al.* (1999) (the “NACRE” compilation) and by Wiescher *et al.* (2010).

### 1. $^{12}\text{C}(p,\gamma)^{13}\text{N}$

In the starting phase of the CN cycle, before it has reached its equilibrium, this reaction controls the buildup of  $^{14}\text{N}$  (Haxton and Serenelli, 2008). A recent study using the ANC method by Burtebaev *et al.* (2008) yields a reaction rate consistent with that of Angulo *et al.* (1999), the rate recommended here.

### 2. $^{15}\text{N}(p,\alpha)^{12}\text{C}$

As the  $^{15}\text{N}(p,\alpha)^{12}\text{C}$  reaction competes with  $^{15}\text{N}(p,\gamma)^{16}\text{O}$ , a parallel study of the two is highly desirable. In Solar Fusion I, a weighted average of  $S_{15}^\alpha(0) = 67.5 \pm 4.0$  MeV b was recommended using the results of Redder *et al.* (1982) and Zyskind and Parker (1979). Recently the  $^{15}\text{N}(p,\alpha)^{12}\text{C}$  reaction has been measured by La Cognata *et al.* (2007), using the indirect Trojan Horse Method (TH method) (see Sec. XII). The new data have been analyzed along with  $^{15}\text{N}(p,\gamma)^{16}\text{O}$ , using a common R-matrix approach. The TH method allows one to extend the explored energy range down to about 20 keV, without the complication of electron screening enhancements that enter for direct measurements. Thus the TH measurements provide complementary information that can be helpful in checking the overall consistency of S-factor fits. La Cognata *et al.* (2007) determined  $S_{15}^\alpha(0) = 68 \pm 11$  MeV b from TH measurements. New R-matrix fits to direct data of Redder *et al.* (1982) by La Cognata *et al.* (2009) yielded  $S_{15}^\alpha(0) = 73 \pm 5$  and  $74 \pm 9$  MeV b, depending on the respective energy ranges fit (see La Cognata *et al.* (2009) for details), and  $S_{15}^\alpha(0) = 70 \pm 13$  MeV b for the indirect TH method data of La Cognata *et al.* (2007). An R-matrix fit by Barker (2008a), which did not include the TH method results, gave  $S_{15}^\alpha(0) = 80$  MeV b. We recommend the value  $S_{15}^\alpha(0) = 73 \pm 5$  MeV b obtained by La Cognata *et al.* (2009) by fitting direct data as the new best value for the  $^{15}\text{N}(p,\alpha)^{12}\text{C}$



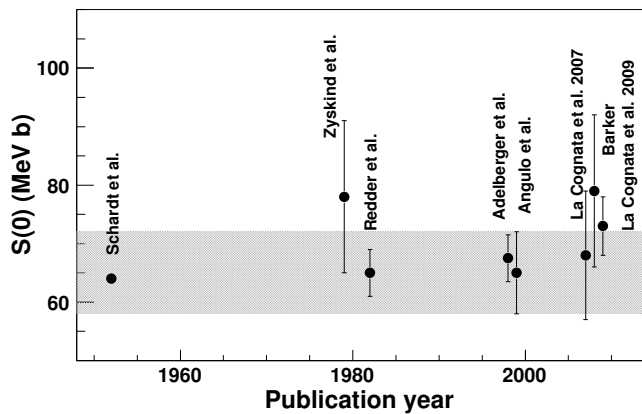


FIG. 16 Summary of the available measurements of  $S_{15}^{\alpha}(0)$ , showing values as originally reported on the dates indicated. The shaded band corresponds to the NACRE compilation (Angulo *et al.*, 1999). From La Cognata *et al.* (2009), by permission.

reaction (see Table XII). It is consistent with the two direct measurements, the indirect TH method data, and the R-matrix fit by Barker. A summary given by La Cognata *et al.* (2009) of  $S_{15}^{\alpha}(0)$  determinations is shown in Fig. 16. In Table XII the derivatives shown are those reported by Zyskind and Parker (1979), and may therefore not be completely consistent with the R-matrix energy dependence calculated by La Cognata *et al.* (2009).

### 3. $^{15}\text{N}(p,\gamma)^{16}\text{O}$

The  $^{15}\text{N}(p,\gamma)^{16}\text{O}$  reaction provides the path to form  $^{16}\text{O}$  in stellar hydrogen burning<sup>6</sup>, thus transforming the CN cycle into the CNO bi-cycle and CNO tri-cycle. In stellar environments, the reaction proceeds at very low energies, where it is dominated by resonant capture to the ground state through the first two interfering  $J^{\pi} = 1^{-}$  s-wave resonances at  $E_R = 312$  and 964 keV. In addition there is some direct capture to the ground state. Direct measurements have been reported by Hebbard (1960) for proton energies down to 220 keV and by Rolfs and Rodney (1974) down to proton energies of 155 keV. These measurements disagree significantly below 300 keV. In order to fit their low-energy data, Rolfs and Rodney (1974) included the interference of the two  $1^{-}$  resonant capture amplitudes with the nonresonant (direct) component to the ground state of  $^{16}\text{O}$  calculated in the hard-sphere approximation. The absolute normalization of the direct term is entirely determined by the ANC of the

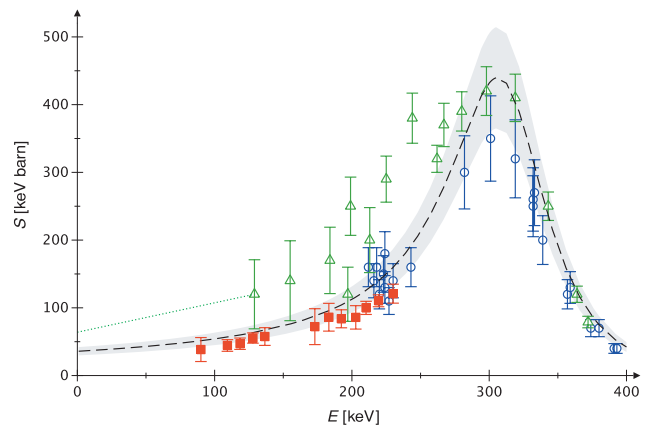


FIG. 17 (Color online)  $S(0)$  for the  $^{15}\text{N}(p,\gamma)^{16}\text{O}$  reaction. Data from Hebbard (1960) (blue circles, limited to  $E \geq 210$  keV), Rolfs and Rodney (1974) (green triangles), and Bemmerer *et al.* (2009) (red squares). Error bars reflect statistical and systematic uncertainties summed in quadrature. Dashed line, previous R-matrix fit and shaded area, its quoted 17% uncertainty, from Mukhamedzhanov *et al.* (2008). Dotted line: previous extrapolation by Angulo *et al.* (1999). Figure from Bemmerer *et al.* (2009), by permission.

bound state for  $^{15}\text{N} + p \rightarrow ^{16}\text{O}$ . The spectroscopic factor adopted by Rolfs and Rodney (1974) corresponds to an ANC almost an order of magnitude larger than the one determined from  $^{15}\text{N}(^3\text{He},d)^{16}\text{O}$  by Mukhamedzhanov *et al.* (2008).

A new analysis of the direct data using the two-level, two-channel R-matrix was presented by Mukhamedzhanov *et al.* (2008). The contribution from the  $\alpha - ^{12}\text{C}$  channel was also taken into account. The determined astrophysical factor  $S_{15}^{\gamma}(0) = 36 \pm 6$  keV b is about a factor of two lower than the previously accepted value  $S_{15}^{\gamma}(0) = 64 \pm 6$  keV b from Rolfs and Rodney (1974). Hebbard (1960) reported  $S_{15}^{\gamma} = 32 \pm 6$  keV b at 23.44 keV, which was converted by Mukhamedzhanov *et al.* (2008) to  $S_{15}^{\gamma}(0) = 29.8 \pm 5.4$  keV b using the polynomial extrapolation given by Hebbard. Mukhamedzhanov *et al.* (2008) conclude that for every  $2200 \pm 300$  cycles of the main CN cycle, one CN catalyst is lost due to this reaction, rather than 880 cycles recommended by Rolfs and Rodney (1974) and 1000 cycles recommended by the NACRE compilations (Angulo *et al.*, 1999). Their result coincides with the R-matrix analysis by Barker (2008b), which yielded a leak rate of  $1/2300$ . Barker's analysis was completed before the ANC data were available and shows a larger spread of  $S$  values.

New measurements of this reaction at LUNA by Bemmerer *et al.* (2009) yielded cross sections with improved precision for energies between 90 to 230 keV (Fig. 17). The extent of the agreement between the new LUNA data and the Hebbard data point to a possible unidentified systematic error affecting the low-energy data of Rolfs and Rodney (1974). The value  $S_{15}^{\gamma}(0) = 36 \pm 6$  keV b obtained by Mukhamedzhanov *et al.* (2008) may be

<sup>6</sup> Most of the  $^{16}\text{O}$  found in the Sun originates not from hydrogen burning in the Sun itself, but instead from the ashes of helium burning in earlier stars.

regarded as an interim recommendation pending an updated analysis taking full account of new data (e.g., completion of the analyses for recent LUNA and Notre Dame experiments). Further measurements at higher energies are also desirable in order to constrain the R-matrix fits.

#### 4. $^{16}\text{O}(\text{p},\gamma)^{17}\text{F}$

The cross section is dominated by direct capture to the ground and first excited states of  $^{17}\text{F}$ . Because the latter is weakly bound, its S-factor rises rapidly at low energies and the ground-state transition plays a minor role. Calculations of the direct capture process by Rolfs (1973), Morlock *et al.* (1997), Baye *et al.* (1998), and Baye and Brainis (2000) give a quantitative account of the energy dependence of both transitions. Baye *et al.* (1998) calculate  $S_{116}^{\gamma}(0)$  with two choices for the nuclear force, obtaining  $S_{116}^{\gamma}(0) = 10.2$  and  $11.0$  keV b when normalized to the data of Rolfs (1973) and Morlock *et al.* (1997). The value adopted here is  $S_{116}^{\gamma}(0) = 10.6 \pm 0.8$  keV b and the derivative is  $S_{116}^{\gamma \prime}(0) = -0.054$  b. A recent reevaluation by Iliadis *et al.* (2008) using both R-matrix theory and a potential model yielded reaction rates at temperatures  $\geq 10^7\text{K}$  that are consistent with these values (Angulo *et al.*, 1999), but with a lower assigned uncertainty.

#### 5. $^{17}\text{O}(\text{p},\alpha)^{14}\text{N}$

The  $^{17}\text{O}(\text{p},\alpha)^{14}\text{N}$  reaction closes branch II of the CNO bi-cycle. The reaction rate at solar energies is dominated by a subthreshold resonance at  $E_R = -3.1$  keV and a resonance at  $E_R = 65.1$  keV. Several recent experiments have clarified the strength and location of a  $2^-$  resonance at 183.3 keV that plays a significant role at the higher temperatures characteristic of novae and asymptotic giant branch stars (Chafa *et al.*, 2005, 2007; Moazen *et al.*, 2007). Chafa *et al.* (2007) find a low-energy cross section about a factor of three smaller than that given by Angulo *et al.* (1999), reflecting a re-evaluation of the proton width of the subthreshold resonance. No calculated value for  $S_{117}^{\alpha}(0)$  has been published.

#### 6. $^{17}\text{O}(\text{p},\gamma)^{18}\text{F}$

The cross section shows a number of resonances in the range relevant to the hot CNO cycle in novae. Effort has been recently devoted by Chafa *et al.* (2005, 2007) and Fox *et al.* (2004) to measuring the resonance parameters in both  $^{17}\text{O}(\text{p},\gamma)^{18}\text{F}$  and  $^{17}\text{O}(\text{p},\alpha)^{14}\text{N}$ . While the higher-lying resonances are not directly relevant to solar CNO processing, they do have a significant influence in modern interpretations of the work of Rolfs (1973), who measured the direct capture cross section that dominates at solar energies. Fox *et al.* (2005) and Chafa *et al.* (2007) both concluded that significant corrections are required. The recommended  $S_{117}^{\gamma}(0)$  in Table XII is taken from Chafa

*et al.* (2007). The large uncertainty ( $\sim 50\%$ ) makes a new round of measurements of the direct capture cross section desirable.<sup>7</sup>

#### 7. $^{18}\text{O}(\text{p},\alpha)^{15}\text{N}$

The  $^{18}\text{O}+\text{p}$  interaction represents a branching point in the CNO cycle: the  $^{18}\text{O}(\text{p},\alpha)^{15}\text{N}$  reaction leads to a recycling of CN catalytic material, while  $^{18}\text{O}(\text{p},\gamma)^{19}\text{F}$  may lead to a loss of this material, depending on the fate of the produced  $^{19}\text{F}$ . Nine resonances below 1 MeV influence the astrophysical rate for  $^{18}\text{O}(\text{p},\alpha)^{15}\text{N}$ , with those at 20, 144, and 656 keV dominating (Angulo *et al.*, 1999). The presence of strong resonances in the astrophysical regime makes extraction of a value for  $S_{118}^{\alpha}(0)$  inappropriate.

The strength of the 20-keV resonance had been known only from spectroscopic measurements performed by Champagne and Pitt (1986) through the transfer reaction  $^{18}\text{O}(^3\text{He},\text{d})^{19}\text{F}$  and through the direct capture reaction  $^{18}\text{O}(\text{p},\gamma)^{19}\text{F}$  measured by Wiescher *et al.* (1980). The cross section at 20 keV is a factor  $\sim 10^{11}$  smaller than the one at 70 keV owing to the Coulomb barrier penetration factor. This makes a direct measurement of the cross section impossible with present-day nuclear physics facilities. Furthermore the spin and parity of the 8.084 MeV level in  $^{19}\text{F}$  (corresponding to a 90 keV resonance in the  $^{18}\text{O}(\text{p},\alpha)^{15}\text{N}$  cross section) was not known. In order to reduce the nuclear uncertainties affecting the reaction rate, which La Cognata *et al.* (2008) estimated at about an order of magnitude, a new round of measurements has been made with the TH method by La Cognata *et al.* (2008, 2009, 2010). The deduced strength of the 20 keV resonance  $\omega\gamma = 8.3_{-2.6}^{+3.8} \times 10^{-19}$  eV eliminates much of the broad range given by NACRE (Angulo *et al.*, 1999),  $\omega\gamma = 6_{-5}^{+17} \times 10^{-19}$  eV, and decreases the uncertainty of the reaction rate by about a factor 8.5 (La Cognata *et al.*, 2008, 2009, 2010). In addition, the spin ( $3/2^-$ ) and strength of the 90-keV resonance, which was seen in the work of Lorentz-Wirzba *et al.* (1979), were determined. The La Cognata *et al.* (2008, 2009, 2010) and Lorentz-Wirzba *et al.* (1979) strengths agree.

## XII. INDIRECT METHODS AND THEIR VALIDATION

Three classes of experiments contribute to our understanding of solar fusion reactions, direct cross section measurements, indirect methods, and ancillary nuclear structure techniques for determining the properties of resonances (energies,  $\gamma$  and particle widths, and spins and parities). Indirect methods involve the use of nuclear reactions related to, but not identical to, the solar

<sup>7</sup> Note in proof: The direct capture cross section was recently extracted from new measurements between lab energies of 193 and 519 keV (Newton *et al.*, 2010).

TABLE XII Summary of updates to S-values and derivatives for CNO reactions.

Reaction	Cycle	S(0) keV b	S'(0) b	S''(0) keV <sup>-1</sup> b	References
$^{12}\text{C}(p, \gamma)^{13}\text{N}$	I	$1.34 \pm 0.21$	$2.6 \times 10^{-3}$	$8.3 \times 10^{-5}$	Recommended: Solar Fusion I
$^{13}\text{C}(p, \gamma)^{14}\text{N}$	I	$7.6 \pm 1.0$ $7.0 \pm 1.5$	$-7.83 \times 10^{-3}$	$7.29 \times 10^{-4}$	Recommended: Solar Fusion I NACRE: Angulo <i>et al.</i> (1999)
$^{14}\text{N}(p, \gamma)^{15}\text{O}$	I	$1.66 \pm 0.12$	$-3.3 \times 10^{-3}$	$4.4 \times 10^{-5}$	Recommended: this paper
$^{15}\text{N}(p, \alpha_0)^{12}\text{C}$	I	$(7.3 \pm 0.5) \times 10^4$	351	11	Recommended: this paper
$^{15}\text{N}(p, \gamma)^{16}\text{O}$	II	$36 \pm 6$ $64 \pm 6$ $29.8 \pm 5.4$			Mukhamedzhanov <i>et al.</i> (2008) Rofls and Rodney (1974) Hebbard (1960)
$^{16}\text{O}(p, \gamma)^{17}\text{F}$	II	$10.6 \pm 0.8$	-0.054		Recommended: this paper
$^{17}\text{O}(p, \alpha)^{14}\text{N}$	II		Resonances		Chafa <i>et al.</i> (2007)
$^{17}\text{O}(p, \gamma)^{18}\text{F}$	III	$6.2 \pm 3.1$	$1.6 \times 10^{-3}$	$-3.4 \times 10^{-7}$	Chafa <i>et al.</i> (2007)
$^{18}\text{O}(p, \alpha)^{15}\text{N}$	III		Resonances		See text
$^{18}\text{O}(p, \gamma)^{19}\text{F}$	IV	$15.7 \pm 2.1$	$3.4 \times 10^{-4}$	$-2.4 \times 10^{-6}$	Recommended: Solar Fusion I

reactions under study, as tools to probe properties of the solar reactions. References have been made in this review to three indirect methods, asymptotic normalization coefficients, Coulomb dissociation, and the Trojan horse method. As the connection between the indirect observable and the solar reaction of interest must be established through reaction theory, such methods entail a greater degree of model dependence, impacting systematic uncertainties. But indirect methods also have many virtues: they can be applied when direct measurements are difficult or impossible, have systematic uncertainties that are different from those of direct measurements, and provide supplementary information that can constrain R-matrix and other models used in the extrapolation of data from direct measurements. The role of indirect measurements in validating and constraining models is apparent from the discussions, for example, of Sec. XI.A.

### A. The asymptotic normalization coefficient method

The asymptotic normalization coefficient method constrains  $S(0)$  by exploiting the peripheral nature of many radiative capture reactions in nuclear astrophysics. Because of Coulomb and/or centrifugal barriers, most  $(p, \gamma)$  and  $(\alpha, \gamma)$  reactions are peripheral at solar energies. The cross section for a nonresonant radiative capture reaction  $A(p, \gamma)B$  at zero relative energy depends only on the long-distance behavior of the  $p+A$  wave function (and on the overlap of that extended wave function with  $B$ ). The detailed short-range behavior of the scattering state  $p+A$  or bound state  $B$ , governed by the strong interaction and nuclear length scales, are not relevant to the reaction mechanism. The bound-state wave function at long distances will contain a component corresponding to two separated clusters,  $p$  and  $A$ , with the cluster relative radial motion given by a Whittaker function. The

asymptotic normalization coefficient (ANC) is defined as the amplitude of this component (apart from an overall phase) (Mukhamedzhanov and Timofeyuk, 1990; Xu *et al.*, 1994). A distinct ANC will govern the nonresonant capture into each final state, i.e., the ground or bound excited states of  $B$ . Therefore, if one can identify another nuclear reaction that includes the vertex  $A + p \leftrightarrow B$  and is sensitive only to the tail of the radial overlap function, the needed ANC can be determined from that reaction. This measurement in a different system then determines the radiative capture cross section at zero relative energy (Mukhamedzhanov *et al.*, 2001), up to small corrections determined by the scattering wave function and the potential in the continuum (Capel and Nunes, 2006; Typel and Baur, 2005). While the method is limited to  $S(0)$ , providing a data point below the Gamow peak, this often complements the data from direct measurements, which are frequently limited to energies above the Gamow peak.

In most applications, the ANC is deduced from transfer reactions. The extraction relies on the distorted wave Born approximation (DWBA) and the direct proportionality between the transfer cross section and the square of the ANC. Provided that the transfer reaction is completely peripheral and the measured angular distributions are well described within the single-step DWBA, the ANC can be extracted. The main source of uncertainty comes from the optical model description, typically  $\gtrsim 10\%$  for reactions above the Coulomb barrier. For this reason, it is often important to also measure the elastic channel of the corresponding transfer reaction over a wide angular range, to help constrain optical model parameters. Investigations of effects beyond the single-step DWBA arising from target excitation suggest that deformed targets with strong couplings to low-lying excited states are not good candidates for the ANC method (Azhari *et al.*, 2001). Some of the applications of the

method involve loosely bound nuclei, opening up the possibility of multi-step processes through continuum states as viable alternatives to the direct reaction mechanism. So far there has only been one reaction for which the magnitude of this effect has been evaluated; in this case it was found to be negligible (Moro *et al.*, 2003), but a more systematic study should be done.

In Solar Fusion I the  $^{16}\text{O}(p,\gamma)^{17}\text{F}$  reaction was identified as a good test for the method. As a consequence, the  $^{16}\text{O}(^3\text{He},d)^{17}\text{F}$  reaction was measured at 30 MeV. The angular distributions of the ground state and the first excited state were well described within the DWBA and the inferred S factors agreed with the radiative capture data to better than 9% (Gagliardi *et al.*, 1999).

There have been many subsequent applications of this method, mostly involving peripheral transfer reactions on intermediate mass targets. Here we focus on those relevant to validating the method for solar fusion reactions. Two transfer reactions,  $^{10}\text{B}(^7\text{Be},^8\text{B})^9\text{Be}$  and  $^{14}\text{N}(^7\text{Be},^8\text{B})^{13}\text{C}$ , were used to extract the ANC for  $S_{17}(0)$  (Azhari *et al.*, 1999a,b). For both targets, the peripheral nature of the transfer reactions were checked carefully by evaluating the sensitivity of the extracted ANC to the single particle parameters of the binding potential in the DWBA analysis. Similar analyses have been done by invoking a radial cutoff in the distorted wave calculation (Fernandez *et al.*, 2000; Mukhamedzhanov *et al.*, 1997). In Tabacaru *et al.* (2006) a joint analysis was performed, yielding  $S_{17}(0)=18.0 \pm 1.9$  eV b, which can be compared to the best value from direct measurements,  $20.8 \pm 0.7 \pm 1.4$  eV b. In addition, the low-energy reaction  $^7\text{Be}(d,n)^8\text{B}$  at  $E_{\text{lab}}=7.5$  MeV (Liu *et al.*, 1996; Ogata *et al.*, 2003) was studied, but difficulties were encountered in the analysis. The (d,n) reaction model depends on the poorly constrained exit-channel neutron optical potential. In addition, the use of low energies, necessary to satisfy the peripherality condition given the low Z of the deuteron, leads to significant compound nuclear contributions, introducing additional uncertainties.

This review includes several illustrations of the use of ANC determinations to validate R-matrix descriptions of direct reaction data. In Sec. XI.A the example of the subthreshold-state (6.79 MeV) contribution to  $^{14}\text{N}(p,\gamma)^{15}\text{O}$  is described in some detail: the ANC determined from the R-matrix fit is in good agreement with that extracted by Bertone *et al.* (2002) and Mukhamedzhanov *et al.* (2003) from  $^{14}\text{N}(^3\text{He},d)^{15}\text{O}$ . Analogous work using  $^{15}\text{N}(^3\text{He},d)^{16}\text{O}$  to study  $^{15}\text{N}(p,\gamma)^{16}\text{O}$  is discussed in Sec. XI.B.

As ANCs can be related to spectroscopic factors, the latter can also be used to parameterize cross sections. However, spectroscopic factors have an additional dependence on the single-particle bound state orbitals assumed in their extraction. Consequently radiative capture reactions parameterized through ANCs and spectroscopic factors have somewhat different uncertainties. Further discussion can be found in Mukhamedzhanov *et al.* (2001) and Bertone *et al.* (2002).

Finally, it should be mentioned that breakup reactions  $B + T \rightarrow A + p + T$  can also be used to extract ANCs when they meet the peripherality condition (Trache *et al.*, 2004). However a detailed study of the uncertainties involved in the reaction theory has not yet been completed.

## B. The Coulomb dissociation method

Coulomb dissociation (CD), originally proposed as a method for extracting information on astrophysical fusion cross sections by Rebel, was developed theoretically shortly thereafter (Baur *et al.*, 1986). The process occurs when a beam of fast projectiles interacts with a heavy target such as Pb. An energetic virtual photon from the target can then dissociate the projectile, liberating a nucleon or  $\alpha$  particle. To the extent that the experimentalist can exploit the kinematics of this process to enhance the contributions from the long-distance exchange of single photons, this process can then be related by detailed balance to the corresponding radiative capture reaction. But several effects complicate this simple picture. Whereas nonresonant radiative captures generally proceed almost exclusively by  $E1$  transitions, the strong  $E2$  field in CD can be important. Moreover, the simple radiative capture/CD correspondence is complicated by multiple photon exchange and by the strong interaction, which can lead to nuclear diffraction dissociation and Coulomb-nuclear interference. Strong interaction effects can be reduced by restricting measurements to small angles, where long-range electromagnetic transitions dominate nuclear interactions. Multiple photon exchange (also known as post-acceleration) can be reduced by increasing the beam energy, shortening the time the projectile spends in the target's field.

In Solar Fusion I a proposal was made to test the validity of the CD method quantitatively through comparison with a corresponding radiative capture measurement. The radiative capture reaction was to have suitable properties, including a low Q value, a nonresonant  $E1$  reaction mechanism, reactants with similar mass/charge ratios, and a final nuclear state with relatively simple structure. Although no perfect reaction was identified,  $^7\text{Be}(p,\gamma)^8\text{B}$  appears to be a good choice. Several new measurements were made, and a great deal of theoretical effort was invested in their interpretation and in extracting the S factor. This work is summarized in Sec. IX.C and will not be discussed further here, except to repeat the conclusion that, while in several cases agreement between the CD method and direct measurements has been demonstrated at the 10-20% level, remaining uncertainties in the magnitude of  $S(0)$ , in independently determining the shape of  $S(E)$ , and in the theory argue that the inclusion of CD data in the current  $S_{17}$  evaluation would be premature.

Efforts also have been made to validate the CD method for the  $^{14}\text{C}(n,\gamma)^{15}\text{C}$  reaction. Although this reaction is

not directly relevant to solar fusion, the radiative capture rate is now known to a precision of  $\sim 10\%$  (Reifarth *et al.*, 2008). The corresponding CD of  $^{15}\text{C}$  on  $^{208}\text{Pb}$  has recently been remeasured at RIKEN (Nakamura *et al.*, 2009). Reaction models predict that the  $^{15}\text{C}$  breakup has an insignificant nuclear contribution and is dominated by  $E1$  transitions, provided the analysis is limited to events in which the  $^{15}\text{C}$  center-of-mass scattering angle and the relative energy of the breakup fragments are small. Independent analyses of these data (Esbensen, 2009; Summers and Nunes, 2008) find that the neutron capture cross section extracted from CD agrees very well with the direct measurement and has comparable precision. This appears to be a favorable case for the theoretical treatment due to the dominant nonresonant  $E1$  reaction mechanism, small  $E2$  and nuclear contributions, and relative simplicity of  $^{15}\text{C}$ , which can be described reasonably in a single-particle  $^{14}\text{C}+n$  potential model. While the agreement in this case is promising, some caution is warranted because the radiative capture measurement has not been confirmed by an independent measurement.

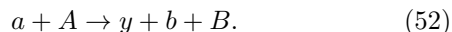
The ANC and CD methods are both well suited to measurements with low intensity radioactive beams because the transfer reaction and CD cross sections are much larger than the corresponding radiative capture reactions. Moreover, they are both applicable to radiative capture reactions.

### C. The Trojan Horse method

The Trojan Horse (TH) method (Baur, 1986; Spitaleri *et al.*, 2004) is an indirect technique to determine the astrophysical S factor for rearrangement reactions. It allows inference of the cross section of the binary process



at astrophysical energies through measurement of the TH reaction



The measurement is done with quasi-free kinematics, in which a TH  $a$  having a strong  $x + y$  cluster structure is accelerated to energies above the Coulomb barrier. After penetrating the Coulomb barrier, the nucleus  $a$  breaks up, leaving  $x$  to interact with the target  $A$  while the projectile fragment  $y$  flies away. From the measured cross section of reaction (52), the energy dependence of the binary subprocess (51) is determined. While the reaction (52) can occur in a variety of ways, the TH reaction mechanism should dominate in a restricted region of three-body phase space in which the momentum transfer to the spectator nucleus  $y$  is small, i.e., quasi-elastic scattering conditions apply. Since the transferred particle  $x$  in the TH reaction (52) is virtual, its energy and momentum are not related by the on-shell equation  $E_x = p_x^2/(2m_x)$ .

The main advantage of the TH method is that the low-energy cross sections can be deduced from a reaction

that is not strongly suppressed by Coulomb barriers or strongly altered by electron screening (Assenbaum *et al.*, 1987; Spitaleri *et al.*, 2001). The TH cross section can be used to determine the energy dependence of the bare nuclear S factor for the binary process (51) down to zero relative kinetic energy of  $x$  and  $A$ . The absolute value of  $S(E)$ , however, must be determined by normalizing to direct measurements at higher energies. To ensure quasi-free kinematics one should measure the momentum distribution of the spectator fragment  $y$  and the angular distributions of the fragments of the binary sub-reaction to check for contributions from non-TH mechanisms. As a check on distortions due to final state interactions, the momentum distribution of the spectator can be measured and compared with that of the spectator in the free TH nucleus (Pizzone *et al.*, 2009). Final state distortions can be treated in DWBA calculations (La Cognata *et al.*, 2010).

The uncertainty of the  $S(E)$  extracted from the TH method includes contributions from statistics, uncertainties due to the need to normalize the TH data, finite experimental energy resolution, and backgrounds due to other reaction mechanisms. The first successful test of the TH method was conducted for the  $^7\text{Li}(p,\alpha)^4\text{He}$  reaction (Lattuada *et al.*, 2001). The extracted  $S(0) = 55 \pm 6$  keV b includes an uncertainty of 10% from the normalization of the TH data to the direct data (Engstler *et al.*, 1992) and 5.5% from other sources, mainly statistics. In addition, in Sec. XI.B.2 we compare results for TH and direct determinations of the cross section for  $^{15}\text{N}(p,\alpha)^{12}\text{C}$ . Although promising, the TH method requires further validation by experiment, and its significant dependence on reaction theory calls for more investigation of the approximations by which TH reactions are related to their astrophysical analogs.

The TH method also provides an important test of electron screening potentials, which can be obtained from comparisons of direct and TH cross sections.

### D. Summary

The three indirect techniques discussed here provide alternatives to direct measurements of astrophysically important reaction rates. In some cases they provide the only practical means for determining stellar reaction rates. While their connection to solar reactions requires an additional level of reaction theory, experimental tests of their validity have often yielded agreement with direct measurements within 10-20%. Significant progress has been made since Solar Fusion I in benchmarking indirect techniques. Indirect methods are best applied to cases where there is a supporting body of experimental data that can be used to constrain the needed nuclear model input, such as optical potentials and effective interactions.

In actual practice, the distinction between direct and indirect methods is not sharp, but rather a matter of de-

gree. While a measurement may probe a stellar reaction directly, it often does so at a different energy or in a different screening environment. Thus direct methods also depend on reaction theory, to extrapolate data to stellar energies or, in cases like  $S_{33}$  where data in the Gamow peak have been obtained, to correct for the effects of screening in terrestrial targets. Still, the connection to stellar physics is typically much closer. Models play a less important role, and increasingly the needed modeling can be done microscopically, as direct measurements involve light nuclei.

For this reason we maintain a distinction between direct and indirect methods in this review, basing our recommendations on results from the former. However, indirect methods have had a significant impact on our analysis: they have been used in this review to constrain R-matrix fits to direct data and to check the consistency of conclusions based on analyses and modeling of direct data.

We recommend extending the benchmarking of indirect methods against direct methods over a wider range of reactions, as more data would be useful in quantifying the uncertainties in such techniques.

### XIII. FUTURE FACILITIES AND CURRENT CAPABILITIES

We noted in the introduction to this review the crucial role nuclear astrophysics experiments have played in the development of a quantitative SSM and in motivating solar neutrino experiments. We outlined the important goals that remain in this field – tests of weak interactions and of solar properties that make use of high precision solar neutrino measurements, helioseismology mappings of  $c(r)$ , and detailed solar modeling. There are also a host of related problems – Big Bang nucleosynthesis, red-giant evolution, the evolution of supernova progenitors, and a variety of transient explosive phenomena in astrophysics – where a quantitative understanding of the nuclear physics is essential. This chapter deals with the experimental facilities that have allowed progress in this field, and discusses the instrumental developments that will be important if we are to continue a similar rate of progress over the next decade.

The measurements that support the development of a quantitative theory of main-sequence stellar evolution primarily involve low energy proton- and  $\alpha$ -capture reactions that traditionally have been studied with small accelerators. The machines must be able to provide proton or  $\alpha$  beams of sufficient intensity to allow cross section measurements near the very low energies of the Gamow peak.

Because low energy charged-particle reaction cross sections are small, experiments must be designed for signal rates much smaller than background rates associated with cosmic rays, the natural radioactivity of the laboratory environment, and the induced activity arising

from beam interactions with target impurities. The ambient background can be roughly divided into muons and neutrons associated with cosmic rays, and  $\gamma$  rays and neutrons from natural radioactivity (uranium, thorium, potassium, and radon from surrounding geology). Today most charged-particle reaction measurements for nuclear astrophysics are being performed at above ground facilities, with various techniques then employed to mitigate backgrounds. The common technique is passive shielding around the detection region. Typically a layered combination of lead, copper, and polyethylene is used to reduce  $\gamma$  and neutron backgrounds within detectors with relatively small volumes. But additional strategies are available to further reduce backgrounds and thus allow measurements at energies nearer those relevant for astrophysics, including

1. use of more sophisticated detector setups with both passive and active shielding and with triggers to aid in event identification;
2. measurements in inverse kinematics using recoil separators in facilities above ground; and
3. measurements with direct kinematics using accelerators that are sufficiently deep underground to suppress penetrating cosmic-ray muons and the neutrons and other secondary activities they induce.

Passive shielding, active shielding, and coincidence gating techniques can enhance event identification and significantly reduce backgrounds in above-ground laboratory environments. As most resonance levels of astrophysical interest decay via  $\gamma$ -cascades (Rowland *et al.*, 2002)  $\gamma\gamma$ -coincidence techniques can be used to significantly reduce the single- $\gamma$  background. Q-value gating techniques, where only events in coincidence with the summing peak of the radiative capture reaction are accepted (Couture *et al.*, 2008), can allow one to extend measurements to lower energies, but at the cost of a decreased overall counting efficiency due to the coincidence requirement.

Alternative techniques have been developed to reduce backgrounds without such losses in detection efficiency. Two ideas that have demonstrated their promise are measurements in inverse kinematics – one detects the reaction recoil particles rather than the light particles or  $\gamma$ s of the reaction – and measurements in underground environments. Below we describe past and current experience with these two techniques as well as the future facilities, in progress or planned, that would allow these techniques to be further advanced.

#### A. Inverse kinematics measurements using recoil separators

In an inverse-kinematics experiment a heavy ion induces (p, $\gamma$ ) or ( $\alpha$ , $\gamma$ ) reactions when it interacts in a hydrogen or helium gas target. The projectiles and reaction products move within a narrow cone in the forward

direction. A recoil separator is used to reject the primary beam while focusing the reaction products for detection. The charged recoils can be detected with higher efficiency than the  $\gamma$ s produced in conventional proton- or  $\alpha$ -beam experiments. By detecting the  $\gamma$ s in coincidence with the reaction products, dramatic reductions in backgrounds can be achieved. Existing recoil separator facilities for nuclear astrophysics experiments include DRAGON at ISAC in TRIUMF (Hutcheon *et al.*, 2003), the Daresbury separator at HRIBF in Oak Ridge (Fitzgerald *et al.*, 2005), ERNA at the DTL in Bochum (Rogalla *et al.*, 2003), and the RMS at KUTL in Kyushu, Japan (Sagara *et al.*, 2005).

Recoil separators are not useful for  $(\alpha, n)$  reactions because separator acceptance angles are too small, given the momentum transfer in this process.

Recoil separators present several experimental challenges (Rogalla *et al.*, 2003), particularly for the low energies important in solar fusion cross section measurements. At such energies, the energy spread and the angular aperture are, for most solar fusion reactions, larger than the acceptance of any of the recoil separators cited above.

The following conditions must be fulfilled in experiments on absolute cross sections:

- the transmission of the recoils must be exactly known and should ideally be 100%;
- the charge-state distribution of the recoil products must be known or the reaction must be studied for all charge states produced (Di Leva *et al.*, 2008); and
- the interaction region must be well defined.

Therefore, experiments coming on-line in the near future are all planning to use compact high-density gas-jet targets instead of extended windowless gas targets.

Recoils of solar fusion reactions typically have relatively large emission angles and large energy spreads, both of which increase with decreasing reaction energies  $E$ , when  $E < Q$ . The angular distribution of recoils following emission of capture  $\gamma$ -rays of energy  $E_\gamma$  is characterized by an emission cone half-angle of

$$\theta = \arctan \frac{E_\gamma}{p} \quad (53)$$

where  $p$  is the momentum of the beam ( $c \equiv 1$ ). The total energy spread  $\Delta E$  of the recoil accompanying  $\gamma$  emission is

$$\frac{\Delta E}{E} = \frac{4E_\gamma}{p}. \quad (54)$$

Furthermore a large spatial separation between the reaction products and the beam is required, as the primary beam intensity is typically many orders of magnitude larger than that of the recoiling reaction products.

A clean separation is difficult for recoils with large energy spreads, making low-energy solar fusion reactions particularly challenging. Recoil separators are therefore more typically used for higher energies characteristic of helium- or explosive hydrogen-burning reactions. For example, the recoil-separator measurements of  $S_{34}$  at the ERNA facility in Bochum were limited to data above a center-of-mass energy of 700 keV (Di Leva *et al.*, 2009). Below this energy the angular divergence of the recoils exceeds the angular acceptance of the separator,  $\pm 25$  mrad (Di Leva *et al.*, 2008).

Two dedicated next-generation separators for low-energy nuclear astrophysics studies with stable ion beams will soon come on line, the St. George facility at Notre Dame's Nuclear Science Laboratory (Couder *et al.*, 2008) and the ERNA separator at the CIRCE facility in Caserta, Italy. The latter is based on a redesign of the Bochum ERNA separator (Rogalla *et al.*, 2003). Both separators feature large acceptances in angle and energy and will be equipped with high density gas-jet targets to ensure well defined interaction regions. Figure 18 shows the layout of the St. George recoil separator. The design is optimized for low-energy radiative  $\alpha$ -capture reactions important to stellar helium burning. It has a large angular acceptance of  $\pm 40$  mrad, an energy acceptance of  $\pm 7.5\%$ , and a mass resolving power  $M/\Delta M \sim 100$  (Couder *et al.*, 2008).

## B. Underground facilities

In all direct-kinematics capture-reaction measurements using  $\gamma$  or neutron spectroscopy, whether performed above ground or underground, sources of environmental radioactivity must be controlled. Background sources include radioactivity from intrusions and impurities in the rock and from construction materials, as well as sources intrinsic to targets and detectors. External sources can be reduced by careful shielding of the target and the detector environment. In addition, beam-induced backgrounds (e.g., backgrounds from activation of impurities in the target) must be controlled through careful ion beam optics and choice of vacuum component materials. Active shielding techniques and complex event identification can also help.

In surface facilities, however, the most difficult backgrounds are frequently those associated with cosmic rays. This background can be removed by exploiting the natural shielding provided by the rock overburden in underground sites. The improvements possible with this strategy have been demonstrated by the 50 keV LUNA I and 400 keV LUNA II programs at Gran Sasso. The laboratory's depth,  $\sim 3.0$  km.w.e. (kilometers of water equivalent, flat-site equivalent (Mei and Hime, 2006)), reduces the fluxes of muons and secondary neutrons, relative to surface values, by factors of  $10^6$  and  $10^3$ , respectively. Consequently, the LUNA I collaboration (Bonetti *et al.*, 1999) was able to map  $S_{33}$  throughout the Gamow peak:



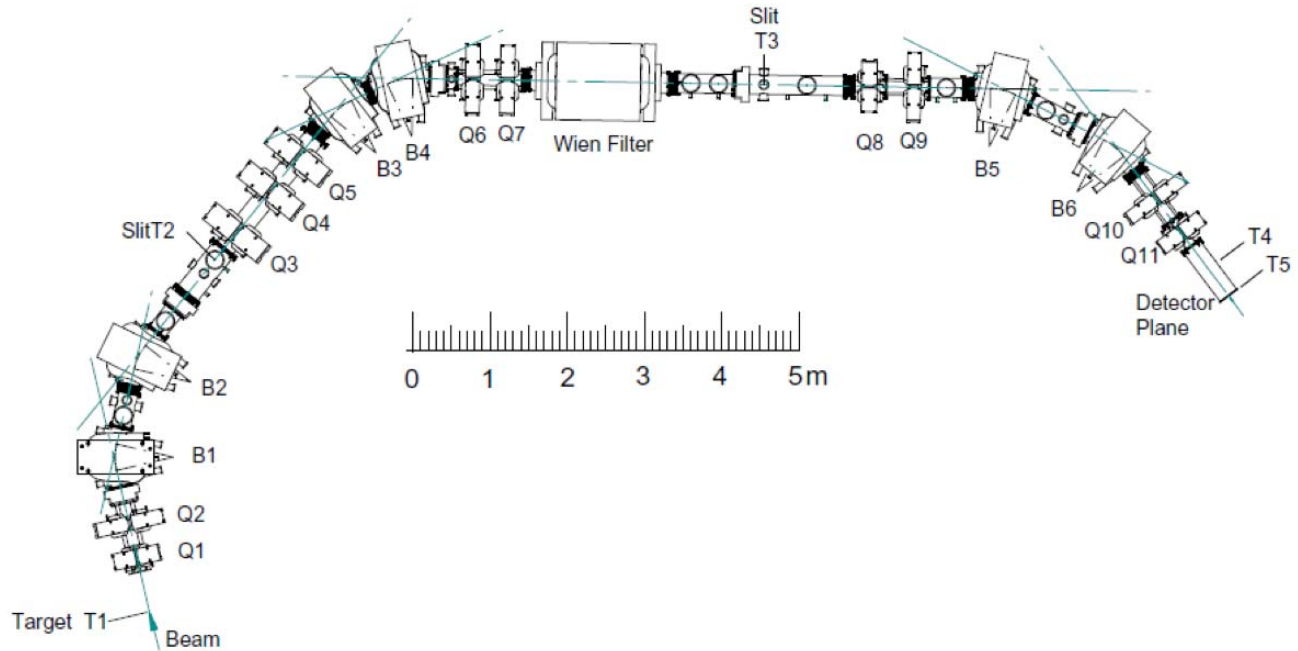


FIG. 18 Layout of the St. George recoil separator.

a counting rate of one event per month was achieved at the lowest energy,  $E = 16$  keV, with an uncertainty of 20 fb or  $2 \times 10^{-38}$  cm<sup>2</sup>. Other critical pp chain and CNO cycle cross sections were made at energies far lower than previously possible (Formicola *et al.*, 2003; Greife *et al.*, 1994; Imbriani *et al.*, 2005; Junker *et al.*, 1998).

The successes of LUNA have inspired plans for the new underground facilities we discuss in this section. Figure 19 shows a schematic of the present LUNA II set-up in Gran Sasso, which consists of a commercial 400 kV accelerator, a windowless gas target, and a solid target line.

Nuclear astrophysics has rather modest depth requirements. The hadronic cosmic-ray component is quickly attenuated, leaving penetrating high-energy muons as the dominant source of background at depth. These muons interact in the rock to produce neutrons and a continuous spectrum of high energy  $\gamma$ s. Thus the main requirement is an overburden sufficient to reduce muon-associated activities to a level well below natural background levels associated with activities in the laboratory's rock and concrete walls. The neutron fluxes in Gran Sasso,  $\sim 4 \times 10^{-6}$ /cm<sup>2</sup>/s (Bemmerer *et al.*, 2005; Laubenstein *et al.*, 2004), and in Spain's underground laboratory Canfranc,  $(3.80 \pm 0.44) \times 10^{-6}$ /cm<sup>2</sup>/s (Carmona *et al.*, 2004), are almost entirely due to local radioactivity. Taking these deep-laboratory values as typical of the environmental background component, one can determine the depth necessary to reduce the cosmic-ray-associated neutron contribution to 1% of the total. The simulations of Mei and Hime (2006) yield  $\sim 1.5$  km.w.e. (flat site equivalent).

lent).

Similar results are found for the  $\gamma$ -ray flux. The LUNA  $^{14}\text{N}(p,\gamma)$  counting goal was  $10^{-4}$  counts/keV/hr. The cosmic-ray muon-induced rate at 1.5 km.w.e. would be approximately an order of magnitude lower (Haxton *et al.*, 2007). As almost all deep physics laboratories now operating are at depths in excess of 1.5 km.w.e, one concludes that many locations are suitable for nuclear astrophysics – at least until order-of-magnitude reductions in the laboratory environmental neutron and  $\gamma$ -ray background are made.

Based on the success of the LUNA collaboration, several underground accelerator facilities are now being proposed. Table XIII shows the parameters of these facilities. The plans reflect design improvements from fifteen years of experience with LUNA.

The present LUNA facility is small and limited to the measurement of proton- and  $\alpha$ -capture reactions below 400 keV, with typical beam currents between 100 and 200  $\mu\text{A}$ . The available beam current has limited the statistical accuracy of data taken at the lowest energies. In addition, many reactions have complex resonance structures that must be adequately mapped, to provide the information needed to extrapolate cross sections to Gamow energies. This requires measurements over a broader energy range than is currently available at LUNA. Therefore, the LUNA collaboration has submitted a letter of intent for the installation of a higher energy accelerator that would allow the LUNA program to grow beyond solar fusion physics. This upgrade proposal is currently



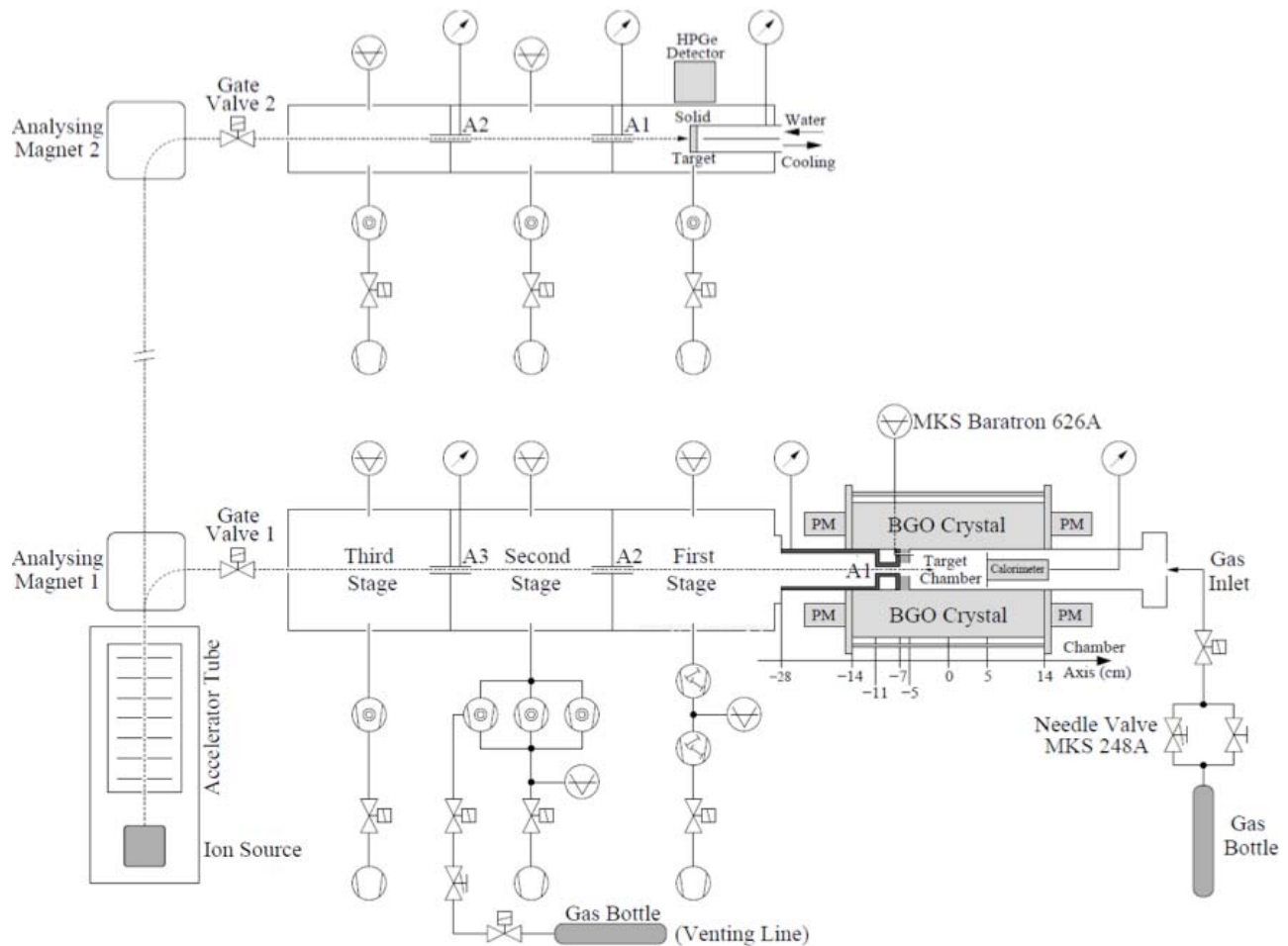


FIG. 19 A schematic of the present LUNA 400 keV set-up.

under review (Prati *et al.*, 2008) .

Three initiatives for new underground accelerator facilities are also under discussion:

- ELENA is a proposed facility for the Boulby salt mine in the UK, a site that has environmental neutron backgrounds less than half those of Gran Sasso  $[(1.72 \pm 0.61 \text{ (stat.)} \pm 0.38 \text{ (syst.)}) \times 10^{-6} / \text{cm}^2/\text{s}$  above 0.5 MeV (Carmona *et al.*, 2004)] and  $\gamma$ -ray backgrounds that are 5-30 times lower than Gran Sasso values, for  $E_\gamma \lesssim 3$  MeV (Aliotta, 2009). This reflects the low U and Th concentrations in salt. As the site is approximately at the same depth as Gran Sasso (2.8 vs. 3.1 km.w.e., taking proper account of the topography (Mei and Hime, 2006)), full advantage can be taken of the reduced environmental background.
- CUNA is a 3 MeV accelerator facility that has been proposed for Spain's Canfranc Laboratory, located in an abandoned train tunnel in the Pyrenees mountains (Bettini, 2009).

- DIANA, Dakota Ion Accelerators for Nuclear Astrophysics, would be the nuclear astrophysics facility for DUSEL (Deep Underground Science and Engineering Laboratory), a laboratory being planned in the abandoned Homestake gold mine, South Dakota (DIANA Collaboration, 2009).

As in the case of the proposed LUNA upgrade, these facilities would be capable of mapping cross sections over broad energy ranges with fixed configurations for target and detector.

We discuss DIANA in more detail, as an example of the improvements that would be possible in next generation nuclear astrophysics facilities. DIANA's proposed site is the 4850-foot level of Homestake, the same level where Davis operated his chlorine detector. The design combines a low-energy 400 kV high-intensity accelerator, a high-energy accelerator with a maximum voltage of 3 MV, and flexibly configured target stations and detector systems. Both accelerators will be coupled to a shared target station, in order to reduce uncertainties that would

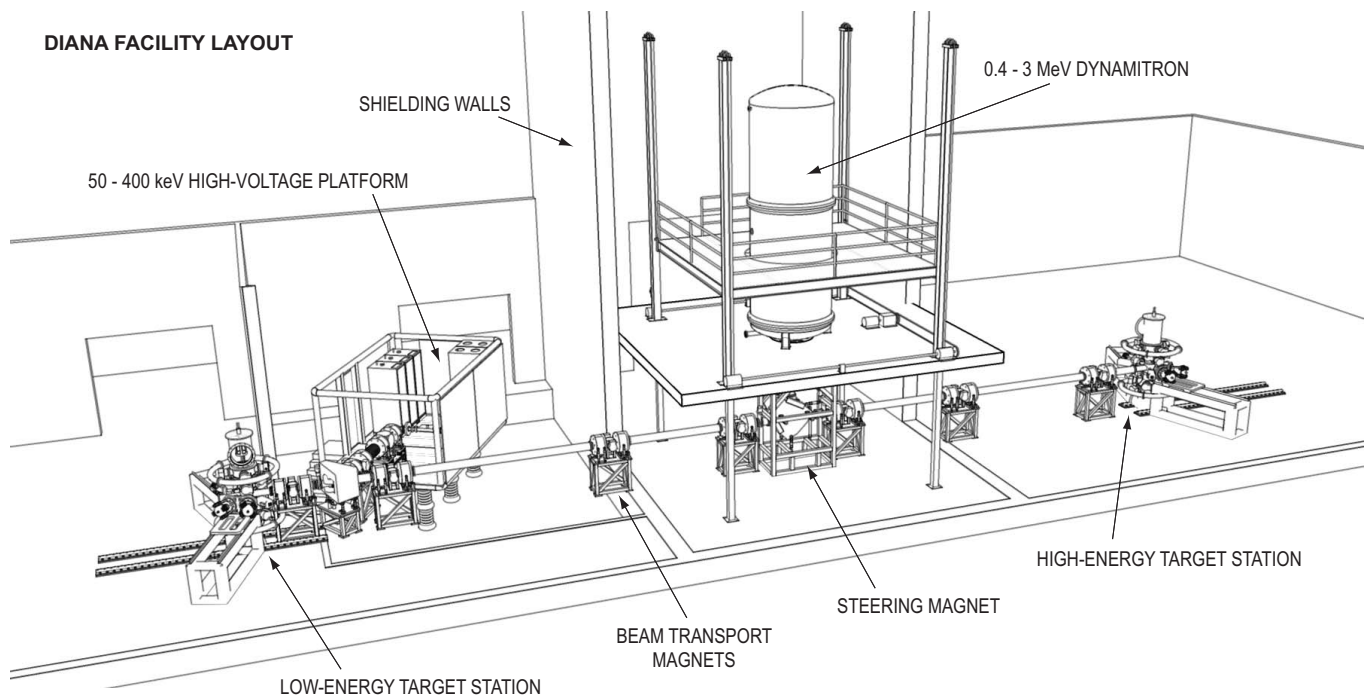


FIG. 20 Proposed layout of the DIANA facility.

arise when cross sections are measured at different facilities, with different targets and detector configurations. The accelerators will have a substantial overlap in their energy ranges due to the design of the ion source on the high-voltage platform of the low energy accelerator. This will reduce uncertainties in combining data sets. The pro-

posed beam current of several mA is at least one order of magnitude higher than any presently available. This enhances counting rates, but also requires increased attention to beam-induced backgrounds as well as targets capable of handling the power. Figure 20 shows DIANA’s conceptual design.

## Acknowledgments and Dedication

We would like to thank the Institute for Nuclear Theory for hosting and supporting the Solar Fusion II workshop and for providing technical assistance during the writing of this review. We thank A. Champagne, P. Descouvemont, A. Di Leva, and J. Toebbe for their generous help, including many discussions and advice or assistance with fitting. The research described in this review was supported by various agencies including the U.S. Department of Energy, the U.S. National Science Foundation, the Deutschen Forschungsgemeinschaft (cluster of excellence “Origin and Structure of the Universe” and grant SFB 634) and the Alliance Program EMMI of the Helmholtz Association.

We dedicate Solar Fusion II to John Bahcall, who proposed and led the effort on Solar Fusion I. John’s advocacy for laboratory astrophysics and his appreciation of its importance to solar neutrinos paved the way for many advances in our field.

## Appendix: Treating Uncertainties

### A. Introduction

This section describes our method for dealing with discrepant data sets that may occur, for example, when deriving recommended  $S(0)$  values from experimental measurements of nuclear reaction cross sections.

While the conventional  $\chi^2$  minimization method is adequate for analysing data sets that are in good agreement, there is no rigorous method for dealing with discrepant data sets and their underlying unidentified systematics. But reasonable procedures exist. In Solar Fusion II we adopt the Scale Factor method, here called the inflation factor method (IFM), that is used by the PDG (Amsler *et al.*, 2008). In this method, the fit errors from a conventional  $\chi^2$  minimization are inflated by a factor that depends on  $\sqrt{\chi^2/\nu}$ , where  $\nu$  is the number of degrees of freedom. This method is well known, widely used, and straightforward to apply.

TABLE XIII Attributes of proposed second-generation underground facilities for nuclear astrophysics.

FACILITY	LUNA Laboratory Underground for Nuclear Astrophysics	DIANA Dakota Ion Accelerators for Nuclear Astrophysics	ELENA Experimental Low-Energy Nuclear Astrophysics	CUNA Canfranc Nuclear Astrophysics Facility
Location	Gran Sasso, Italy	Homestake Mine, USA	Boulby Mine, UK	Canfranc, Spain
Rock type	hard limestone	metamorphic rock	salt	hard limestone
Depth (km.w.e, flat site)	3.1	4.3	2.8	~ 2.0
Low energy accelerator	50-400 keV 0.5-1.0 mA RF ion source (p,He <sup>+</sup> )	50-400 kV HV platform ≥ 10mA ECR ion sources, single, multiply charged	none	none
High energy accelerator	0.4-3.5 MeV electrostatic up to 0.3 mA ECR ion source	0.35-3.0 MeV electrostatic up to 10 mA ECR ion sources single, multiply charged	3.0 MeV accelerator electrostatic 0.5 mA ECR ion source	up to 5.0 MeV electrostatic

While the IFM is the only one discussed in the PDG Introduction, alternatives exist. We discuss some examples at the end of this Appendix.

## B. The inflation factor method

The IFM addresses systematic uncertainties when combining results from different and possibly discrepant data sets. The method inflates errors in proportion to the quoted errors originally given by the experimenters.

Discrepant data may be defined by the  $P$ -value of the fit, where  $P \equiv P(\chi^2, \nu)$  is the probability of obtaining a  $\chi^2$  value at least as large as the observed value. The inflation factor is conventionally chosen to be  $\sqrt{\chi^2/\nu}$  and is commonly applied in cases where  $\chi^2/\nu > 1$ . We use an alternative inflation factor  $\sqrt{\chi^2/\chi^2(P=0.5)}$  to account for the fact that, for small  $\nu$  and non-discrepant data, the expected value of  $\chi^2$  is smaller than unity. For large  $\nu$ , the two scaling factors are equivalent.

The IFM scales all experimental errors by the same fractional amount, resulting in equal internal and external errors on the mean. Because one generally cannot identify a specific mechanism accounting for discrepant data, this procedure (like all other procedures) has no rigorous mathematical justification. However qualitative arguments support its reasonableness. As the method maintains the relative precision of discrepant data sets, it apportions a larger absolute fraction of the identified systematic error to the less precise data sets. This is consistent with naive expectations that a large, unidentified systematic error is more likely to “hide” within a low-precision data set than within a high-precision one, given the advantages a high-precision data set offers an

experimentalist who does “due-diligence” cross checks to identify systematic errors. The IFM is generally considered the most appropriate procedure in the absence of information that would support alternatives, such as omitting certain data, or increasing errors on some data but not others.

We employ error inflation whenever  $\chi^2 > \chi^2(P=0.5)$ , and no error scaling otherwise. With this general rule, errors are inflated a bit even when  $\chi^2$  is only slightly in excess of  $\chi^2(P=0.5)$ , despite the lack of compelling evidence of discrepancy in such a case. This procedure yields a continuous formula and avoids the introduction of an arbitrary threshold for inflation.

In extreme cases one may obtain errors that are deemed too small. For example, when analyzing data containing a few results with small errors and a larger number of results with large errors, the large-error data will reduce the error on the mean by increasing  $\nu$ , even though they may have little effect on the central value. In such a case, we agree with the PDG’s recommendation that, to mitigate this problem, data be excluded which have an error larger than some (arbitrary) limit, specifically  $3\delta\sqrt{N}$ , where  $N$  is the number of measurements and  $\delta$  is the unscaled error on the mean. However, applying this exclusion criterion may not be adequate to resolve this difficulty in all cases.

While the IFM makes no assumptions about the reasons for discrepant data, in actual applications it may be apparent that not all data sets are equally reliable. In such cases judgment is necessary, and data selection is appropriate. Data should be discarded if the error analysis is poorly documented or inadequate. Data may be discarded if the procedure used to generate them involves questionable assumptions, or if corrections were not made

for effects now known to be important. Data errors may be modified (e.g. increased) if such new information is available.

### C. Application of the inflation factor method

The following is based on the discussion in the Introduction of the PDG compilation of Amsler *et al.* (2008):

1. In general, statistical and systematic data errors should be identified and specified separately. Systematic errors should be subdivided into varying (random) and common-mode (normalization) errors. For a single data set, normally the statistical and *varying* systematic errors should be combined in quadrature and used as data errors in a  $\chi^2$  minimization to determine unknown parameters. The resulting fit error(s) should be multiplied by the inflation factor (see below). The common-mode error is then folded in quadrature with the inflated fit error to determine the overall normalization error.

For multiple data sets, the systematic errors should be examined to determine if they are independent among the different data sets. Parameters determined from multiple, independent data sets may be combined in a separate  $\chi^2$  minimization in which each parameter value is characterized by its total error determined by combining statistical and systematic (normalization) errors in quadrature. Again, this fit error should be multiplied by the inflation factor. If the systematic errors in different data sets are correlated, then this correlation must be taken into account in the fitting. A convenient method for handling correlations is described in the 2008 PDG compilation.

2. Whenever  $\chi^2 > \chi^2(P = 0.5)$  the fit errors should be increased by the multiplicative inflation factor  $\sqrt{\chi^2/\chi^2(P = 0.5)}$ , where  $\chi^2(P = 0.5)$  is the  $\chi^2$  corresponding to a  $P$  value of 0.5 for  $\nu$  degrees of freedom. The  $\chi^2$  and  $\nu$  should be stated, along with the inflation factor when it is larger than unity. Large reported inflation factors serve to alert the reader to potential problems.
3. Data with uncertainties larger than  $3\sqrt{N}\delta$ , where  $N$  is the number of measurements and  $\delta$  is the (unscaled) error on the mean should be excluded. One should be aware of possible error underestimation in certain cases as mentioned above. The resolution of such situations may require additional judgment.

### D. Other methods

Other error analysis methods follow somewhat different strategies. The cost function methods used in CO-DATA analyses (Cohen and Taylor, 1987) are designed

to reduce the  $\chi^2$  by selective re-weighting of data; i.e. by increasing the errors nonuniformly on the data, in such a manner as to minimize the “cost”, i.e. the error on the mean. Alternatively, D’Agostini (1994) has advocated a procedure for fitting multiple data sets in which one minimizes the sum of a data  $\chi^2$  and a normalization  $\chi^2$ .

One method that has been applied to the analysis of solar fusion cross section is that of Cyburt (2004) (see also Cyburt and Davids (2008)). This approach introduces a “discrepancy error”,  $\sigma_{\text{disc}}$ , that is added in quadrature with the normalization errors of individual experiments when fitting mixed data sets. Effectively this procedure distributes the unexplained discrepancy equally over the data sets, regardless of their stated accuracy, in contrast to the PDG procedure, which assigns the discrepancy in way that preserves the relative stated accuracy of data sets. The Cyburt (2004) method leads, in cases where there is excess dispersion, to increased de-weighting of the more precise data points, compared to the IFM. In addition, the contribution of  $\sigma_{\text{disc}}$  to the error of the mean does not decrease as the number of measurements  $N$  increases.

The Cyburt (2004) and IFM methods reflect two limits in how one apportions an unexplained discrepancy among data sets: one could construct other models that interpolate between these two limits (equal vs. proportionate allocation of the discrepancy error). The argument for the IFM procedure has been stated previously: it is easier to miss a large systematic error within a low-quality data set than within a high-quality one. In addition, it avoids a situation where archival data of poor quality, containing an unidentified systematic error, unduly impact the weight that would otherwise be accorded a new experiment of exceptional quality – thereby inappropriately diluting the impact of the best results. Alternatives to the IFM tend to produce roughly equivalent results unless the discrepancies among data sets are large. We are fortunate in this paper to be dealing with discrepancies that are modest.

### References

- Adelberger, E. G., *et al.*, 1998, Rev. Mod. Phys. **70**, 1265.  
 Aharmim, B., *et al.*, 2008, Phys. Rev. Lett. **101**, 111301.  
 Aharmim, B., *et al.*, 2006, Ap. J. **653**, 1545.  
 Ahmad, Q. R., *et al.*, 2001, Phys. Rev. Lett. **87**, 071301.  
 Ajzenberg-Selove, F., 1991, Nucl. Phys. A **523**, 1.  
 Aliotta, M., 2009, <http://www.fnuc.es/workshop/Presentaciones/Aliotta.pdf>.  
 Aliotta, M., *et al.*, 2001, Nucl. Phys. A **690**, 790.  
 Alt, E. O., B. F. Irgaziev, and A. M. Mukhamedzhanov, 2003, Phys. Rev. Lett. **90**, 122701.  
 Alt, E. O., B. F. Irgaziev, and A. M. Mukhamedzhanov, 2005, Phys. Rev. C **71**, 024605.  
 Amsler, C., *et al.* (Particle Data Group), 2008, Phys. Lett. B **667**, 1.  
 Andersen, H., and J. F. Ziegler, 1977, *The Stopping and Ranges of Ions in Matter* (Pergamon (N.Y.)).

- Ando, S., T. S. Park, K. Kubodera, and F. Myhrer, 2002, Phys. Lett. B **533**, 25.
- Ando, S., *et al.*, 2008, Phys. Lett. B **668**, 187.
- Andreev, V. A., *et al.* (MuSun Collaboration), 2008, <http://www.npl.uiuc.edu/exp/musun>.
- Angulo, C., and P. Descouvemont, 2000, Phys. Rev. C **61**, 064611.
- Angulo, C., and P. Descouvemont, 2001, Nucl. Phys. A **690**, 755.
- Angulo, C., *et al.*, 1993, Z. Phys. A **345**, 231.
- Angulo, C., *et al.*, 1999, Nucl. Phys. A **656**, 3.
- Angulo, C., *et al.*, 2003, Nucl. Phys. A **716**, 211.
- Arpesella, C., *et al.*, 1996, Phys. Lett. B **389**, 452.
- Asplund, M., N. Grevesse, and A. J. Sauval, 2005, in *Conference Proceedings Vol. 336, Cosmic Abundances as Records of Stellar Evolution and Nucleosynthesis*, edited by T. G. Barnes, III and F. N. Bash (Astronomical Society of the Pacific), p. 25.
- Assenbaum, H. J. K., K. Langanke, and C. Rolfs, 1987, Z. Phys. A **327**, 461.
- Aurdal, A., 1970, Nucl. Phys. A **146**, 385.
- Azhari, A., *et al.*, 1999a, Phys. Rev. Lett. **82**, 3960.
- Azhari, A., *et al.*, 1999b, Phys. Rev. C **60**, 055803.
- Azhari, A., *et al.*, 2001, Phys. Rev. C **63**, 055803.
- Azuma, R. E., *et al.*, 2010, Phys. Rev. C **81**, 045805.
- Baby, L. T., *et al.*, 2003a, Phys. Rev. Lett. **90**, 022501.
- Baby, L. T., *et al.*, 2003b, Phys. Rev. C **67**, 065805.
- Bacher, A. D., and T. A. Tombrello, 1965, Rev. Mod. Phys. **37**, 433.
- Bacrania, M. K., N. M. Boyd, R. G. H. Robertson, and D. W. Storm, 2007, Phys. Rev. C **76**, 055806.
- Bahcall, J. N., 1962, Phys. Rev. **128**, 1297.
- Bahcall, J. N., 1989, *Neutrino Astrophysics* (Cambridge University Press).
- Bahcall, J. N., 1990, Phys. Rev. D **41**, 2964.
- Bahcall, J. N., 1991, Phys. Rev. D **44**, 1644.
- Bahcall, J. N., 1994, Phys. Rev. D **49**, 3923.
- Bahcall, J. N., S. Basu, M. Pinsonneault, and A. M. Serenelli, 2005, Ap. J. **618**, 1049.
- Bahcall, J. N., L. S. Brown, A. V. Gruzinov, and R. F. Sawyer, 2002, A.&A. **388**, 660.
- Bahcall, J. N., and R. Davis Jr., 1982, in *Essays in Nuclear Astrophysics*, edited by C. A. Barnes, D. D. Clayton, and D. Schramm (Cambridge University Press), p. 243.
- Bahcall, J. N., and R. M. May, 1968, Ap. J. **152**, L17.
- Bahcall, J. N., and R. M. May, 1969, Ap. J. **155**, 501.
- Bahcall, J. N., and C. P. Moeller, 1969, Ap. J. **155**, 511.
- Bahcall, J. N., and M. H. Pinsonneault, 1992, Rev. Mod. Phys. **64**, 885.
- Bahcall, J. N., M. H. Pinsonneault, and S. Basu, 2001, Ap. J. **555**, 990.
- Bahcall, J. N., A. M. Serenelli, and S. Basu, 2006, Ap. J. Suppl. **165**, 400.
- Bahcall, J. N., and R. K. Ulrich, 1988, Rev. Mod. Phys. **60**, 297.
- Bahcall, J. N., *et al.*, 1996, Phys. Rev. C **54**, 411.
- Bailey, G. M., *et al.*, 1970, Can. J. Phys. **48**, 3059.
- Baimbetov, B. F., K. T. Nurekenov, and T. S. Ramazanov, 1995, Phys. Lett. A **202**, 211.
- Balamuth, D. P., *et al.*, 1983, Phys. Rev. C **27**, 1724.
- Balantekin, A. B., C. A. Bertulani, and M. S. Hussein, 1997, Nucl. Phys. A **627**, 324.
- Bang, J. M., L. S. Ferreira, E. Maglione, and J. M. Hansteen, 1996, Phys. Rev. C **53**, R18.
- Bardayan, D. W., *et al.*, 2009, Eur. Phys. J. A **42**, 457.
- Barker, F. C., 1971, Aust. J. Phys. **24**, 777.
- Barker, F. C., 1980, Aust. J. Phys. **33**, 177.
- Barker, F. C., 1983, Phys. Rev. C **28**, 1407.
- Barker, F. C., 1989, Aust. J. Phys. **42**, 25.
- Barker, F. C., 1995, Nucl. Phys. A **588**, 693.
- Barker, F. C., 2008a, Phys. Rev. C **78**, 044611.
- Barker, F. C., 2008b, Phys. Rev. C **78**, 044612.
- Barker, F. C., and T. Kajino, 1991, Aust. J. Phys. **44**, 369.
- Barker, F. C., and A. M. Mukhamedzhanov, 2000, Nucl. Phys. A **673**, 526.
- Batkin, I. S., and M. K. Sundaresan, 1995, Phys. Rev. D **52**, 5362.
- Baur, G., 1986, Phys. Lett. B **178**, 135.
- Baur, G., C. A. Bertulani, and H. Rebel, 1986, Nucl. Phys. A **458**, 188.
- Baye, D., 2000, Phys. Rev. C **62**, 065803.
- Baye, D., 2004, Phys. Rev. C **70**, 015801.
- Baye, D., 2005, Nucl. Phys. A **758**, 114.
- Baye, D., and E. Brainis, 2000, Phys. Rev. C **61**, 025801.
- Baye, D., and P. Descouvemont, 1985, Ann. Phys. **165**, 115.
- Baye, D., P. Descouvemont, and M. Hesse, 1998, Phys. Rev. C **58**, 545.
- Becker, H. W., *et al.*, 1982, Z. Phys. A **305**, 319.
- Bedaque, P. F., H. W. Hammer, and U. van Kolck, 1999, Phys. Rev. Lett. **82**, 463.
- Belyaev, V. B., M. Tater, and E. Truhlik, 2007, Phys. Rev. C **75**, 034608.
- Bemmerer, D., *et al.*, 2005, Eur. Phys. J. A **24**, 313.
- Bemmerer, D., *et al.*, 2006a, Phys. Rev. Lett. **97**, 122502.
- Bemmerer, D., *et al.*, 2006b, Nucl. Phys. A **779**, 297.
- Bemmerer, D., *et al.*, 2009, J. Phys. G **36**, 045202.
- Bennaceur, K., F. Nowacki, J. Okolowicz, and M. Pł Oszajczak, 1999, Nucl. Phys. A **651**, 289.
- Bertone, P. F., *et al.*, 2001, Phys. Rev. Lett. **87**, 152501.
- Bertone, P. F., *et al.*, 2002, Phys. Rev. C **66**, 055804.
- Bertulani, C. A., 1996, Z. Phys. A **356**, 293.
- Bertulani, C. A., 2004, Phys. Lett. B **585**, 35.
- Bertulani, C. A., 2005, Phys. Rev. Lett. **94**, 072701.
- Bertulani, C. A., and D. T. de Paula, 2000, Phys. Rev. C **62**, 045802.
- Bettini, S., 2009, <http://www.fnuc.es/workshop/Presentaciones/Bettini.pdf>.
- Bhattacharya, M., and E. G. Adelberger, 2002, Phys. Rev. C **65**, 055502.
- Bhattacharya, M., E. G. Adelberger, and H. E. Swanson, 2006, Phys. Rev. C **73**, 055802.
- Bonetti, R., *et al.*, 1999, Phys. Rev. Lett. **82**, 5205.
- Bowles, T. J., and G. T. Garvey, 1978, Phys. Rev. C **18**, 1447.
- Brown, L. S., and R. F. Sawyer, 1997, Ap. J. **489**, 968.
- Brown, T. A. D., *et al.*, 2007, Phys. Rev. C **76**, 055801.
- Brune, C. R., 2002, Phys. Rev. C **66**, 044611.
- Brune, C. R., R. W. Kavanagh, and C. E. Rolfs, 1994, Phys. Rev. C **50**, 2205.
- Buck, B., R. A. Baldock, and J. A. Rubio, 1985, J. Phys. G **11**, L11.
- Buck, B., and A. C. Merchant, 1988, J. Phys. G **14**, L211.
- Burbidge, E. M., G. R. Burbidge, W. A. Fowler, and F. Hoyle, 1957, Rev. Mod. Phys. **29**, 547.
- Burtebaev, N., S. B. Igamov, R. J. Peterson, R. Yarmukhamedov, and D. M. Zazulin, 2008, Phys. Rev. C **78**, 035802.
- Butler, M., and J.-W. Chen, 2001, Phys. Lett. B **520**, 87.
- Butler, M., J.-W. Chen, and X. Kong, 2001, Phys. Rev. C **63**, 035501.

- Butler, M., J.-W. Chen, and P. Vogel, 2002, Phys. Lett. B **549**, 26.
- Capel, P., and F. M. Nunes, 2006, Phys. Rev. C **73**, 014615.
- Carlson, J., D. O. Riska, R. Schiavilla, and R. B. Wiringa, 1991, Phys. Rev. C **44**, 619.
- Carmona, J. M., *et al.*, 2004, Astropart. Phys. **21**, 523.
- Carraro, C., A. Schaeffer, and S. E. Koonin, 1988, Ap. J. **331**, 565.
- Casella, C., *et al.*, 2002, Nucl. Phys. A **706**, 203.
- Caughlan, G. R., and W. A. Fowler, 1988, At. Data and Nucl. Data Tables **40**, 283.
- Chafa, A., *et al.*, 2005, Phys. Rev. Lett. **95**, 031101.
- Chafa, A., *et al.*, 2007, Phys. Rev. C **75**, 035810.
- Champagne, A. E., and M. L. Pitt, 1986, Nucl. Phys. A **457**, 367.
- Chen, J.-W., K. M. Heeger, and R. G. H. Robertson, 2003, Phys. Rev. C **67**, 025801.
- Chen, J.-W., T. Inoue, X. Ji, and Y. Li, 2005, Phys. Rev. C **72**, 061001(R).
- Chen, J.-W., G. Rupak, and M. J. Savage, 1999, Nucl. Phys. A **653**, 386.
- Christy, R., and I. Duck, 1961, Nucl. Phys. **24**, 89.
- Clayton, D. D., 1968, *Principles of Stellar Evolution and Nuclear Synthesis* (McGraw-Hill).
- Cohen, E. R., and B. N. Taylor, 1987, Rev. Mod. Phys. **59**, 1121.
- Confortola, F., *et al.*, 2007, Phys. Rev. C **75**, 065803.
- Costantini, H., *et al.*, 2008, Nucl. Phys. A **814**, 144.
- Costantini, H., *et al.*, 2009, Rep. Prog. Phys. **72**, 086301.
- Couder, M., *et al.*, 2008, Nucl. Inst. Meth. A **587**, 35.
- Couture, A., *et al.*, 2008, Phys. Rev. C **77**, 015802.
- Csoto, A., 1997, Phys. Lett. B **394**, 247.
- Csoto, A., and K. Langanke, 2000, Few-Body Syst. **29**, 121.
- Csoto, A., K. Langanke, S. E. Koonin, and T. D. Shoppa, 1995, Phys. Rev. C **52**, 1130.
- Cyburt, R. H., 2004, Phys. Rev. D **70**, 023505.
- Cyburt, R. H., and B. Davids, 2008, Phys. Rev. C **78**, 064614.
- Cyburt, R. H., B. Davids, and B. K. Jennings, 2004, Phys. Rev. C **70**, 045801.
- D'Agostini, G., 1994, Nucl. Inst. Meth. A **346**, 306.
- Das, P., and A. Ray, 2005, Phys. Rev. C **71**, 025801.
- Davids, B., A. V. Gruzinov, and B. K. Jennings, 2008, Phys. Rev. C **77**, 019801.
- Davids, B., and S. Typel, 2003, Phys. Rev. C **68**, 045802.
- Davids, B., *et al.*, 1998, Phys. Rev. Lett. **81**, 2209.
- Davids, B., *et al.*, 2001a, Phys. Rev. Lett. **86**, 2750.
- Davids, B., *et al.*, 2001b, Phys. Rev. C **63**, 065806.
- Davids, C. N., *et al.*, 1983, Phys. Rev. C **28**, 885.
- Davis Jr., R., 1994, Prog. Part. Nucl. Phys. **32**, 13.
- Davis Jr., R., D. S. Harmer, and K. C. Hoffman, 1968, Phys. Rev. Lett. **20**, 1205.
- De Braekeleer, L., *et al.*, 1995, Phys. Rev. C **51**, 2778.
- Descouvemont, P., 2004, Phys. Rev. C **70**, 065802.
- Descouvemont, P., and D. Baye, 1988, Nucl. Phys. A **487**, 420.
- Descouvemont, P., and D. Baye, 1994, Nucl. Phys. A **567**, 341.
- Descouvemont, P., and D. Baye, 2010, Rep. Prog. Phys. **73**, 036301.
- Descouvemont, P., *et al.*, 2004, At. Data and Nucl. Data Tables **88**, 203.
- Di Leva, A., *et al.*, 2008, Nucl. Inst. Meth. A **595**, 381.
- Di Leva, A., *et al.*, 2009, Phys. Rev. Lett. **102**, 232502.
- DIANA Collaboration, 2009, [http://ecrgroup.lbl.gov/Astro\\_DUSEL.htm](http://ecrgroup.lbl.gov/Astro_DUSEL.htm).
- Donoghue, T. R., *et al.*, 1983, Phys. Rev. C **28**, 875.
- Dubovichenko, S. B., and A. V. Dzhazairov-Kakhramanov, 1995, Phys. Atom. Nucl. **58**, 579.
- Dwarakanath, M. R., and H. Winkler, 1971, Phys. Rev. C **4**, 1532.
- Efros, V. D., W. Leidemann, G. Orlandini, and N. Barnea, 2007, J. Phys. G **34**, R459.
- Engstler, S. A., *et al.*, 1988, Phys. Lett. B **202**, 179.
- Engstler, S. A., *et al.*, 1992, Z. Phys. A **342**, 471.
- Epelbaum, E., 2006, Prog. Part. Nucl. Phys. **57**, 654.
- Esbensen, H., 2004, Phys. Rev. C **70**, 047603.
- Esbensen, H., 2009, Phys. Rev. C **80**, 024608.
- Esbensen, H., and G. F. Bertsch, 1996, Nucl. Phys. A **600**, 37.
- Esbensen, H., G. F. Bertsch, and K. A. Snover, 2005, Phys. Rev. Lett. **94**, 042502.
- Farmer, B. J., and C. M. Class, 1960, Nucl. Phys. **15**, 626.
- Fernandez, J. C., R. Crespo, and F. M. Nunes, 2000, Phys. Rev. C **61**, 064616.
- Fetisov, V. N., and Y. S. Kopysov, 1972, Phys. Lett. B **40**, 602.
- Filippone, B. W., A. J. Elwyn, C. N. Davids, and D. D. Koetke, 1983, Phys. Rev. C **28**, 2222.
- Fiorentini, G., C. Rolfs, F. L. Villante, and B. Ricci, 2003, Phys. Rev. C **67**, 014603.
- Fitzgerald, R., *et al.*, 2005, Nucl. Phys. A **748**, 351.
- Flambaum, V. V., and V. G. Zelevinsky, 1999, Phys. Rev. Lett. **83**, 3108.
- Formicola, A., *et al.*, 2003, Nucl. Inst. Meth. A **507**, 609.
- Formicola, A., *et al.*, 2004, Phys. Lett. B **591**, 61.
- Fowler, W. A., 1972, Nature **238**, 24.
- Fox, C., *et al.*, 2004, Phys. Rev. Lett. **93**, 081102.
- Fox, C., *et al.*, 2005, Phys. Rev. C **71**, 055801.
- Fukuda, S., *et al.*, 2001, Phys. Rev. Lett. **86**, 5651.
- Fukuda, Y., *et al.*, 1996, Phys. Rev. Lett. **77**, 1683.
- Gagliardi, C. A., *et al.*, 1999, Phys. Rev. C **59**, 1149.
- Gavrin, V. N., *et al.*, 2003, Nucl. Phys. B **118**, 39.
- Gazit, D., 2008, Phys. Lett. B **666**, 472.
- Gazit, D., S. Quaglioni, and P. Navratil, 2009, Phys. Rev. Lett. **103**, 102502.
- Gialanella, L., *et al.*, 2000, Eur. Phys. J. A **7**, 303.
- Goldstein, G., P. Capel, and D. Baye, 2007, Phys. Rev. C **76**, 024608.
- Golser, R., and D. Semrad, 1991, Phys. Rev. Lett. **66**, 1831.
- Greife, U., *et al.*, 1994, Nucl. Inst. Meth. A **350**, 327.
- Greife, U., *et al.*, 1995, Z. Phys. A **351**, 107.
- Griffiths, G. M., M. Lal, and C. D. Scarfe, 1963, Can. J. Phys. **41**, 724.
- Griffiths, G. M., E. A. Larson, and L. P. Robertson, 1962, Can. J. Phys. **40**, 402.
- Grineviciute, J., *et al.*, 2008, J. Phys. G **35**, 055201.
- Gruzinov, A. V., 1998, Ap. J. **469**, 503.
- Gruzinov, A. V., and J. N. Bahcall, 1998, Ap. J. **504**, 996.
- Gyurky, G., *et al.*, 2007, Phys. Rev. C **75**, 035805.
- Hagino, K., and A. B. Balantekin, 2002, Phys. Rev. C **66**, 055801.
- Halderson, D., 2006, Phys. Rev. C **73**, 024612.
- Hammache, F., *et al.*, 1998, Phys. Rev. Lett. **80**, 928.
- Hammache, F., *et al.*, 2001, Phys. Rev. Lett. **86**, 3985.
- Hardy, J. C., and I. S. Towner, 2009, Phys. Rev. C **79**, 055502.
- Hass, M., *et al.*, 1999, Phys. Lett. B **462**, 237.
- Haxton, W. C., P. D. Parker, and C. E. Rolfs, 2006, Nucl. Phys. A **777**, 226.

- Haxton, W. C., and A. M. Serenelli, 2008, *Ap. J.* **687**, 678.
- Haxton, W. C., *et al.*, 2007, *Nucl. Inst. Meth. A* **570**, 414.
- Hebbard, D. F., 1960, *Nucl. Phys.* **15**, 289.
- Holmgren, H. P., and R. Johnston, 1958, *Bull. Am. Phys. Soc.* II **3**, 26.
- Holmgren, H. P., and R. Johnston, 1959, *Phys. Rev.* **113**, 1556.
- Holt, R. J., H. E. Jackson, R. M. Laszewski, J. E. Monahan, and J. R. Specht, 1978, *Phys. Rev. C* **18**, 1962.
- Hutcheon, D. A., *et al.*, 2003, *Nucl. Inst. Meth. A* **498**, 190.
- Iben, Jr., I., K. Kalata, and J. Schwartz, 1967, *Ap. J.* **150**, 1001.
- Iliadis, C., C. Angulo, P. Descouvemont, M. Lugaro, and P. Mohr, 2008, *Phys. Rev. C* **77**, 045802.
- Imbriani, G., *et al.*, 2005, *Eur. Phys. J. A* **25**, 455.
- Israelian, G., *et al.*, 2009, *Nature* **462**, 189.
- Iwasa, N., *et al.*, 1996, *J. Phys. Soc. Japan* **65**, 1256.
- Iwasa, N., *et al.*, 1999, *Phys. Rev. Lett.* **83**, 2910.
- Jennings, B. K., S. Karataglidis, and T. D. Shoppa, 1998a, *Phys. Rev. C* **58**, 579.
- Jennings, B. K., S. Karataglidis, and T. D. Shoppa, 1998b, *Phys. Rev. C* **58**, 3711.
- Johnson, C. W., E. Kolbe, S. E. Koonin, and K. Langanke, 1992, *Ap. J.* **392**, 320.
- Junghans, A. R., K. A. Snover, E. C. Mohrmann, E. G. Adelberger, and L. Buchmann, 2010, *Phys. Rev. C* **81**, 012801(R).
- Junghans, A. R., *et al.*, 2002, *Phys. Rev. Lett.* **88**, 041101.
- Junghans, A. R., *et al.*, 2003, *Phys. Rev. C* **68**, 065803.
- Junker, M., *et al.*, 1998, *Phys. Rev. C* **57**, 2700.
- Kajino, T., 1986, *Nucl. Phys. A* **460**, 559.
- Kamionkowski, M., and J. N. Bahcall, 1994, *Ap. J.* **420**, 884.
- Kaplan, D. B., M. J. Savage, and M. B. Wise., 1996, *Nucl. Phys. B* **478**, 629.
- Kikuchi, T., *et al.*, 1997, *Phys. Lett. B* **391**, 261.
- Kikuchi, T., *et al.*, 1998, *Eur. Phys. J. A* **3**, 213.
- Kim, B. T., T. Izumoto, and K. Nagatani, 1981, *Phys. Rev. C* **23**, 33.
- Kim, K. H., M. H. Park, and B. T. Kim, 1987, *Phys. Rev. C* **35**, 363.
- Kirsten, T., *et al.*, 2003, *Nucl. Phys. B* **118**, 33.
- Kobzev, G. A., I. T. Iakubov, and M. M. Popovich, 1995, *Transport and Optical Properties of a Nonideal Plasma* (Plenum).
- Kolbe, E., K. Langanke, and H. J. Assenbaum, 1988, *Phys. Lett. B* **214**, 169.
- Kong, X., and F. Ravndal, 2001, *Phys. Rev. C* **64**, 044002.
- Krauss, A., *et al.*, 1987, *Nucl. Phys. A* **467**, 273.
- Krauss, H., K. Grün, T. Rauscher, and H. Oberhummer, 1993, *Annalen der Physik* **2**, 256.
- Kudomi, N., *et al.*, 2004, *Phys. Rev. C* **69**, 015802.
- Kurylov, A., M. J. Ramsey-Musolf, and P. Vogel, 2003, *Phys. Rev. C* **67**, 035502.
- La Cognata, M., V. Z. Goldberg, A. M. Mukhamedzhanov, C. Spitaleri, and R. E. Tribble, 2009, *Phys. Rev. C* **80**, 012801(R).
- La Cognata, M., *et al.*, 2007, *Phys. Rev. C* **76**, 065804.
- La Cognata, M., *et al.*, 2008, *Phys. Rev. Lett.* **101**, 152501.
- La Cognata, M., *et al.*, 2009, *Publ. Astron. Soc. Austral.* **26**, 237.
- La Cognata, M., *et al.*, 2010, *Ap. J.* **708**, 796.
- Lane, A. M., and R. G. Thomas, 1958, *Rev. Mod. Phys.* **30**, 257.
- Langanke, K., 1986, *Nucl. Phys. A* **457**, 351.
- Langanke, K., T. D. Shoppa, C. A. Barnes, and C. Rolfs, 1996, *Phys. Lett. B* **369**, 211.
- Lattuada, M., *et al.*, 2001, *Ap. J.* **562**, 1076.
- Laubenstein, M., *et al.*, 2004, *Appl. Rad. Iso.* **61**, 167.
- Lemut, A., *et al.*, 2006, *Phys. Lett. B* **634**, 483.
- Limata, B. N., *et al.*, 2006, *Eur. Phys. J. A* **27**, 193.
- Liu, W., *et al.*, 1996, *Phys. Rev. Lett.* **77**, 611.
- Lorentz-Wirzba, H., *et al.*, 1979, *Nucl. Phys. A* **313**, 346.
- Ma, L., *et al.*, 1997, *Phys. Rev. C* **55**, 588.
- Mao, D., K. Mussack, and W. Däppen, 2009, *Ap. J.* **701**, 1204.
- Marcucci, L. E., K. M. Nollett, R. Schiavilla, and R. B. Wiringa, 2006, *Nucl. Phys. A* **777**, 111.
- Marcucci, L. E., M. Pervin, S. C. Pieper, R. Schiavilla, and R. B. Wiringa, 2008, *Phys. Rev. C* **78**, 065501.
- Marcucci, L. E., R. Schiavilla, S. Rosati, A. Kievsky, and M. Viviani, 2002, *Phys. Rev. C* **66**, 054003.
- Marcucci, L. E., M. Viviani, R. Schiavilla, A. Kievsky, and S. Rosati, 2005, *Phys. Rev. C* **72**, 014001.
- Marcucci, L. E., *et al.*, 2000, *Phys. Rev. C* **63**, 015801.
- Marta, M., *et al.*, 2008, *Phys. Rev. C* **78**, 022802(R).
- Mathews, G. J., R. C. Haight, R. G. Lanier, and R. M. White, 1983, *Phys. Rev. C* **28**, 879.
- McKeown, R. D., G. T. Garvey, and C. A. Gagliardi, 1980, *Phys. Rev. C* **22**, 738.
- Mei, D.-M., and A. Hime, 2006, *Phys. Rev. D* **73**, 053004.
- Mertelmeier, T., and H. M. Hofmann, 1986, *Nucl. Phys. A* **459**, 387.
- Mitler, H. E., 1977, *Ap. J.* **212**, 513.
- Moazen, B. H., *et al.*, 2007, *Phys. Rev. C* **75**, 065801.
- Mohr, P., 2009, *Phys. Rev. C* **79**, 065804.
- Mohr, P., *et al.*, 1993, *Phys. Rev. C* **48**, 1420.
- Morlock, R., *et al.*, 1997, *Phys. Rev. Lett.* **79**, 3837.
- Moro, A. M., R. Crespo, F. M. Nunes, and I. J. Thompson, 2003, *Phys. Rev. C* **67**, 047602.
- Mosconi, B., P. Ricci, E. Truhlik, and P. Vogel, 2007, *Phys. Rev. C* **75**, 044610.
- Motobayashi, T., *et al.*, 1994, *Phys. Rev. Lett.* **73**, 2680.
- Mukhamedzhanov, A., *et al.*, 2003, *Phys. Rev. C* **67**, 065804.
- Mukhamedzhanov, A. M., C. A. Gagliardi, and R. E. Tribble, 2001, *Phys. Rev. C* **63**, 024612.
- Mukhamedzhanov, A. M., and F. M. Nunes, 2002, *Nucl. Phys. A* **708**, 437.
- Mukhamedzhanov, A. M., and N. K. Timofeyuk, 1990, *Yad. Fiz.* **51**, 679.
- Mukhamedzhanov, A. M., *et al.*, 1997, *Phys. Rev. C* **56**, 1302.
- Mukhamedzhanov, A. M., *et al.*, 2008, *Phys. Rev. C* **78**, 015804.
- Nakamura, T., *et al.*, 2009, *Phys. Rev. C* **79**, 035805.
- Napolitano, J., S. J. Freedman, and J. Camp, 1987, *Phys. Rev. C* **36**, 298.
- Nathan, A. M., G. T. Garvey, P. Paul, and A. K. Warburton, 1975, *Phys. Rev. Lett.* **35**, 1137.
- Navrátil, P., C. A. Bertulani, and E. Caurier, 2006a, *Phys. Lett. B* **634**, 191.
- Navrátil, P., C. A. Bertulani, and E. Caurier, 2006b, *Phys. Rev. C* **73**, 065801.
- Neff, T., and H. Feldmeier, 2008, *J. Phys. Conf. Ser.* **111**, 012007.
- Neff, T., H. Feldmeier, and K. Langanke, 2010, *Proceedings of Science: 11th Symposium on Nuclei in the Cosmos*.
- Nelson, S. O., *et al.*, 2003, *Phys. Rev. C* **68**, 065804.
- Newton, J. R., *et al.*, 2010, *Phys. Rev. C* **81**, 045801.
- Nir-El, Y., *et al.*, 2007, *Phys. Rev. C* **75**, 012801(R).



- Nogga, A., *et al.*, 2003, Phys. Rev. C **67**, 034004.
- Nollett, K. M., 2001, Phys. Rev. C **63**, 054002.
- Nollett, K. M., S. C. Pieper, R. B. Wiringa, J. Carlson, and G. M. Hale, 2007, Phys. Rev. Lett. **99**, 022502.
- Nollett, K. M., R. B. Wiringa, and R. Schiavilla, 2001, Phys. Rev. C **63**, 024003.
- Norman, E. B., *et al.*, 1983a, Phys. Rev. C **27**, 1728.
- Norman, E. B., *et al.*, 1983b, Phys. Rev. C **28**, 1409.
- Norman, E. B., *et al.*, 2001, Phys. Lett. B **519**, 15.
- Nunes, F. M., R. Crespo, and I. J. Thompson, 1997a, Nucl. Phys. A **615**, 69.
- Nunes, F. M., R. Crespo, and I. J. Thompson, 1997b, Nucl. Phys. A **627**, 747.
- Nunes, F. M., R. Crespo, and I. J. Thompson, 1998, Nucl. Phys. A **634**, 527.
- Ogata, K., and C. A. Bertulani, 2009, Prog. Theor. Phys. **121**, 1399.
- Ogata, K., S. Hashimoto, Y. Iseri, M. Kamimura, and M. Yahiro, 2006, Phys. Rev. C **73**, 024605.
- Ogata, K., M. Yahiro, Y. Iseri, and M. Kamimura, 2003, Phys. Rev. C **67**, 011602(R).
- Ohtsuki, T., H. Yuki, M. Muto, J. Kasagi, and K. Ohno, 2004, Phys. Rev. Lett. **93**, 112501.
- Ortiz, C. E., A. Garcia, R. A. Waltz, M. Bhattacharya, and A. K. Komives, 2000, Phys. Rev. Lett. **85**, 2909.
- Park, T.-S., K. Kubodera, D.-P. Min, and M. Rho, 1998, Ap. J. **507**, 443.
- Park, T. S., *et al.*, 2003, Phys. Rev. C **67**, 055206.
- Parker, P. D., and R. W. Kavanagh, 1963, Phys. Rev. **131**, 2578.
- Paul, P., M. Suffert, and P. Gorodetzky, 1977, Phys. Lett. B **71**, 71.
- Peña-Garay, C., and A. Serenelli, 2008, arXiv:0811.2424 .
- Pervin, M., S. C. Pieper, and R. B. Wiringa, 2007, Phys. Rev. C **76**, 064319.
- Pieper, S. C., 2008, in *Proceedings of the "Enrico Fermi" Summer School, Course CLXIX, Nuclear Structure far from Stability: New Physics and new Technology*, edited by A. Covello, F. Iachello, R. A. Ricci, and G. Maino (IOS Press, Amsterdam), p. 111.
- Pieper, S. C., V. R. Pandharipande, R. B. Wiringa, and J. Carlson, 2001, Phys. Rev. C **64**, 014001.
- Pieper, S. C., K. Varga, and R. B. Wiringa, 2002, Phys. Rev. C **66**, 044310.
- Pieper, S. C., R. B. Wiringa, and J. Carlson, 2004, Phys. Rev. C **70**, 054325.
- Pizzone, R. G., *et al.*, 2009, Phys. Rev. C **80**, 025807.
- Prati, P., *et al.*, 1994, Z. Phys. A **350**, 171.
- Prati, P., *et al.*, 2008, in *Frontiers in Nuclear Structure, Astrophysics, and Reactions*, edited by P. Demetriou, R. Julin, and S. V. Harissopoulos (AIP, Vol. 1012), p. 305.
- Pudliner, B. S., V. R. Pandharipande, J. Carlson, and R. B. Wiringa, 1995, Phys. Rev. Lett. **74**, 4396.
- Quaglioni, S., and P. Navrátil, 2009, Phys. Rev. C **79**, 044606.
- Quarati, P., and A. M. Scarfone, 2007, Ap. J. **666**, 1303.
- Quarati, P., and A. M. Scarfone, 2009, J. Phys. G **36**, 025203.
- Raiola, F., *et al.*, 2004, Eur. Phys. J. A **19**, 283.
- Ramírez, R., J. Meléndez, and M. Asplund, 2009, A.&A. **508**, L17.
- Ray, A., *et al.*, 1999, Phys. Lett. B **455**, 69.
- Ray, A., *et al.*, 2002, Phys. Lett. B **531**, 187.
- Ray, A., *et al.*, 2006, Phys. Rev. C **73**, 034323.
- Redder, A., *et al.*, 1982, Z. Phys. A **305**, 325.
- Reifarth, R., *et al.*, 2008, Phys. Rev. C **77**, 015804.
- Riisager, K., and A. S. Jensen, 1993, Phys. Lett. B **301**, 6.
- Riska, D. O., 1984, Phys. Scr. **31**, 471.
- Robertson, R. G. H., 1973, Phys. Rev. C **7**, 543.
- Rogalla, R., *et al.*, 2003, Nucl. Inst. Meth. A **513**, 573.
- Rolfs, C., 1973, Nucl. Phys. A **217**, 29.
- Rolfs, C., 2001, Prog. Part. Nucl. Phys. **46**, 23.
- Rolfs, C., and W. S. Rodney, 1974, Nucl. Phys. A **235**, 450.
- Rolfs, C., and E. Somorjai, 1995, Nucl. Inst. Meth. B **99**, 297.
- Rowland, C., C. Iliadis, and A. E. Champagne, 2002, Nucl. Inst. Meth. A **480**, 610.
- Runkle, R. C., *et al.*, 2005, Phys. Rev. Lett. **94**, 082503.
- Sagara, K., *et al.*, 2005, Nucl. Phys. A **758**, 427.
- Salpeter, E. E., 1954, Aust. J. Phys. **7**, 373.
- Schiavilla, R., R. B. Wiringa, V. R. Pandharipande, and J. Carlson, 1992, Phys. Rev. C **45**, 2628.
- Schiavilla, R., *et al.*, 1998, Phys. Rev. C **58**, 1263.
- Schmid, G. J., *et al.*, 1995, Phys. Rev. C **52**, R1732.
- Schmid, G. J., *et al.*, 1996, Phys. Rev. Lett. **76**, 3088.
- Schröder, U., *et al.*, 1987, Nucl. Phys. A **467**, 240.
- Schümann, F., *et al.*, 2003, Phys. Rev. Lett. **90**, 232501.
- Schümann, F., *et al.*, 2006, Phys. Rev. C **73**, 015806.
- Schürmann, D., *et al.*, 2008, Phys. Rev. C **77**, 055803.
- Segrè, E., 1947, Phys. Rev. **71**, 274.
- Serpico, P. D., *et al.*, 2004, J. Cosmology and Astro-Part. Phys. **12**, 10.
- Shoppa, T. D., S. E. Koonin, K. Langanke, and R. Seki, 1993, Phys. Rev. C **48**, 837.
- Singh, B. S. N., M. Hass, Y. Nir-El, and G. Haquin, 2004, Phys. Rev. Lett. **93**, 262503.
- Sirlin, A., 1967, Phys. Rev. **164**, 1767.
- Snover, K. A., and A. E. Hurd, 2003, Phys. Rev. C **67**, 055801.
- Spitaleri, C., *et al.*, 2001, Phys. Rev. C **63**, 055801.
- Spitaleri, C., *et al.*, 2004, Phys. Rev. C **69**, 055806.
- Stahler, S. W., 1988, Ap. J. **322**, 804.
- Stonehill, L. C., J. A. Formaggio, and R. G. H. Robertson, 2004, Phys. Rev. C **69**, 015801.
- Strieder, F., C. Rolfs, C. Spitaleri, and P. Corvisiero, 2001, Naturwissenschaften **88**, 461.
- Strieder, F., *et al.*, 1998, Eur. Phys. J. A **3**, 1.
- Strieder, F., *et al.*, 2001, Nucl. Phys. A **696**, 219.
- Summers, N. C., and F. M. Nunes, 2005, J. Phys. G **31**, 1437.
- Summers, N. C., and F. M. Nunes, 2008, Phys. Rev. C **78**, 011601(R).
- Tabacaru, G., *et al.*, 2006, Phys. Rev. C **73**, 025808.
- Tombrello, T., 1965, Nucl. Phys. **71**, 459.
- Tombrello, T. A., and P. D. Parker, 1963a, Phys. Rev. **131**, 2582.
- Tombrello, T. A., and P. D. Parker, 1963b, Phys. Rev. **130**, 1112.
- Trache, L., F. Carstoiu, C. A. Gagliardi, and R. E. Tribble, 2004, Phys. Rev. C **69**, 032802(R).
- Tribble, R. E., and G. T. Garvey, 1974, Phys. Rev. Lett. **32**, 314.
- Tribble, R. E., and G. T. Garvey, 1975, Phys. Rev. C **12**, 967.
- Tumino, A., *et al.*, 2003, Phys. Rev. C **67**, 065803.
- Typel, S., and G. Baur, 2005, Nucl. Phys. A **759**, 247.
- Typel, S., G. Blüge, K. Langanke, and W. A. Fowler, 1991, Z. Phys. A **339**, 249.
- Typel, S., H. H. Wolter, and G. Baur, 1997, Nucl. Phys. A **613**, 147.
- Viviani, M., A. Kievsky, and S. Rosati, 1995, Few-Body Syst. **18**, 25.
- Viviani, M., S. Rosati, and A. Kievsky, 1998, Phys. Rev. Lett. **81**, 1580.



- Voytas, P. A., *et al.*, 2001, Phys. Rev. Lett. **88**, 012501.
- Walliser, H., H. Kanada, and Y. C. Tang, 1984, Nucl. Phys. A **419**, 133.
- Walliser, H., Q. K. K. Liu, H. Kanada, and Y. C. Tang, 1983, Phys. Rev. C **28**, 57.
- Wang, B., *et al.*, 2006, Eur. Phys. J. A **28**, 375.
- Warburton, E. K., 1986, Phys. Rev. C **33**, 303.
- Weissman, L., *et al.*, 1998, Nucl. Phys. A **630**, 678.
- Wiescher, M., *et al.*, 1980, Nucl. Phys. A **349**, 165.
- Wiescher, M., *et al.*, 2010, Ann. Rev. Nucl. Part. Sci. **61**, in press.
- Wilkinson, D. H., and D. E. Alburger, 1971, Phys. Rev. Lett. **26**, 1127.
- Williams, R. D., and S. E. Koonin, 1981, Phys. Rev. C **23**, 2773.
- Winter, W. T., S. J. Freedman, K. E. Rehm, and J. P. Schiffer, 2006, Phys. Rev. C **73**, 025503.
- Winter, W. T., *et al.*, 2003, Phys. Rev. Lett. **91**, 252501.
- Wiringa, R. B., 1991, Phys. Rev. C **43**, 1585.
- Wiringa, R. B., R. A. Smith, and T. L. Ainsworth, 1984, Phys. Rev. C **29**, 1207.
- Wiringa, R. B., V. G. J. Stoks, and R. Schiavilla, 1995, Phys. Rev. C **51**, 38.
- Xu, H. M., C. A. Gagliardi, R. E. Tribble, A. M. Mukhamedzhanov, and N. K. Timofeyuk, 1994, Phys. Rev. Lett. **73**, 2027.
- Yamada, Y., *et al.*, 2004, Phys. Lett. B **579**, 265.
- Yamaguchi, H., *et al.*, 2009, Phys. Lett. B **672**, 230.
- Ziegler, J. F., *et al.*, 2008, SRIM program, version 2008, <http://www.srim.org>.
- Zyskind, J., and P. D. Parker, 1979, Nucl. Phys. A **320**, 404.